DEPARTMENT OF THE AIR FORCE

AIR UNIVERSITY

AIR FORCE INSTITUTE OF TECHNOLOGY

Wright-Patterson Air Force Base, Ohio

AFIT/GE/ENG/89D-32

EXPERIMENTAL EVALUATION OF IMPEDANCE CONTROL FOR ROBOTIC AIRCRAFT REFUELING

THESIS

Vernon Wade Milholen
Captain, USAF

AFIT/GE/ENG/89D-32

AFIT/GE/ENG/89D-32

Experimental Evaluation of Impedance Control for Robotic Aircraft Refueling

THESIS

Presented to the Faculty of the School of Engineering
of the Air Force Institute of Technology
Air University
In Partial Fulfillment of the
Requirements for the Degree of
Master of Science in Electrical Engineering

Vernon Wade Milholen, BSEE
Captain, USAF

December 14, 1989

Preface

The robotics program at AFIT is quite advanced in the areas of interest to the Air Force such as human arm emulation and robotic assisted aircraft turnaround. Compliant motion is an enabling technology for these efforts that will prove useful in other applications as well. The refueling task provided the impetus for future development that may soon be used in grasping operations and of course, the completion of the impedance control algorithm implementation.

The goals of this thesis were essentially to build on the foundation laid in previous work by Capt David Duvall and advance the development he began. Specifically, two things were sought: a refueling demonstration, and a more user friendly environment for future progress. Thanks to considerable effort and the assistance of many people, these goals were accomplished very effectively. Tools have been forged for continued efforts in force sensing control laws and a refueling demonstration was very successful. Many loose ends still exist though and should be tied off.

Acknowledgements are due for several people. First, Thanks to Dr. Chawla for providing the problem originally and the backing for development. Considerable thanks and recognition must be afforded Capt Duvall for his meticulous record keeping and thorough research. Without his documentation, I would have been completely lost. To Capt Le[illegible]y, for endless hours of patient explanations and helpful hints, thank you for continuing when it appeared for nought. And for the friendly help of the ISL folks; Dan Zambon and Dick Wager, many thanks and may you always have one like me around to keep things interesting.

Thanks go to all my colleagues as they provided intellectual stimulation and support throughout our shared experience at AFIT. Special thanks go to Capt Sam Sablan who always seemed to have a life preserver handy, and also Capt Mark

Johnson for particularly stimulating conversations. Many others contributed to my enrichment, edification, and education while at AFIT, too many to mention here.

The most appreciated and neglected of those to whom I am indebted are my loving wife, Vivian and our two beautiful children, Matthew and Traci, who suffered through the long hours and inattentiveness that accompanied my AFIT experience. Without them I would never have made it. With their help, and more importantly, the help of One mightier than any man, this task was accomplished.

Vernon Wade Milholen

Table of Contents

List of Figures

List of Tables

Abstract

The Air Force is seeking to enhance maintenance operations using robotic assistance in hazardous environments and for possible autonomous operations. One task identified for developmental research is aircraft refueling. An approach under investigation at AFIT combines visual servoing and compliant motion control. This thesis addresses the compliant motion developments. During this research, a PUMA-560 was used to simulate the refueling operation. An existing compliant motion evaluation environment was reorganized and enhanced to support implementation of the improved impedance controller used for the simulation. Improvements to the PUMA control system provided more flexible timing control and faster sampling rates for control law operation. An impedance control law was applied to the second and third links of the PUMA. Trajectory tracking was used as a measurement of performance for unconstrained motion and the results were superior to previous implementations. Constrained motion performance was evaluated by measuring stability, maximum force build up, and continued trajectory tracking with large position errors. Effective use of the active compliance of the impedance control law for the refueling demonstration provides the impetus for future developments for robotic refueling of aircraft. The enhanced evaluation environment provides the means for continuing compliant motion research at AFIT.

Experimental Evaluation of Impedance Control for Robotic Aircraft Refueling

I. Introduction

1.1 Motivation

Robotic manipulators are very useful in certain circumstances such as hazardous or volatile environments. Autonomous or remotely controlled robotic manipulators greatly decrease the number of personnel required for a particular operation. Because the Air Force may have occasion to perform combat operations in environments contaminated by nerve agents or similar hazards and with fewer skilled personnel available, robotic aircraft turnaround has been studied [10,5]. Automated or robotic assisted turnaround would allow operators or supervisors to remain in relative safety while accomplishing mission objectives efficiently. This scenario has several advantages, such as lower personnel requirements, successful operations in normally impossible conditions, and less fatigue and danger for personnel. However, many technical advances are necessary before such an operation can become a reality. Refueling is a very good example. If the aircraft position is precisely known and the aerial refueling port (on top of the A/C usually) is used, then the task is well defined and fixtured. Even so, some portions of the refueling task are not well suited to current technology, and new solutions must be developed if refueling (or any other turnaround functions) are to be accomplished on the flightline using robotics. To prevent damage to the aircraft structure from manipulator contact, a stable, force sensitive motion control law is mandatory for the heavy manipulator required to connect to the refueling port and carry the

hose for fuel. Autonomous service operations and those accomplished through telepresence both require the assurance of damage prevention provided through compliant motion control. A compliant motion controller also has many applications in manufacturing and hazardous material handling or any other operation requiring continuous manipulator to environment contact.

An initiative of the AFIT robotics research group is to evaluate enabling technologies required for ground based robotic refueling. An immediate goal of that research project was to demonstrate a refueling concept that employs visual servoing and pattern recognition techniques to locate the port and place the nozzle on (or very near) the slipway. From that point on, a compliant control algorithm would be employed to complete the insertion. This thesis addressed the compliant control aspects of that project. A separate thesis effort investigated visual servoing and pattern recognition concurrently [37]. A secondary objective of this research was to extend the results of the concept demonstration to future applications and provide a comprehensive environment for force control studies in the robotic systems laboratory at the Air Force Institute of Technology (AFIT).

1.2 Objective

The primary objective of this work was to accomplish a simulated refueling port connection between a refueling nozzle and the UARRI receptacle using the PUMA-560 robot controlled with an active compliance control law using force feedback. The approach for accomplishing that objective is to refine a particular implementation of a compliant motion control law previously accomplished on the AFIT PUMA manipulator by Capt David Duvall [10]. This application met basic stability requirements and successfully demonstrated effective motion control during the very sensitive transition from free motion to contact with the environment. However, testing of the control law revealed large tracking errors and a tendency to lose contact with the constraint surface. Duvall's investigation revealed three

specific problems, for which solutions were selected as most likely to increase performance.

1.3 Problem Statement

Several approaches to compliant motion have been developed: e.g. stiffness control where the stiffness of the environment and the manipulator are considered as a controlled input [35]; impedance control where a linear inverse relationship between compliance and stiffness is used to control both applied force and position; and hybrid control where some axes are controlled by force feedback and others by position feedback. The scope of this research was intentionally limited to improving the performance of an impedance controller previously implemented on a PUMA robot by Capt David Duvall [10]. The theoretical basis for Duvall's research is from an experimental application of impedance control accomplished by Hogan [16]. Hogan used a circular motion path with a constraint to demonstrate smooth motion through an interrupted trajectory. He used a specially designed manipulator exhibiting very low friction characteristics and a trajectory in the horizontal plane so gravity was not a concern. In preparation for a practical trajectory for the refueling scenario, Duvall used a similarly constrained circular path in the vertical plane, with the added difficulties of overcoming the friction effects of a heavy, geared manipulator [10, p 5-10], thereby requiring continuously varying gravity compensation. Initial testing with this vertical circular trajectory resulted in unanticipated errors; specifically, at low velocities, tracking was jerky and generally followed a stick-slip pattern. While Duvall's research did provide a great deal of insight on impedance control, he was not not able to demonstrate compliant tracking and nozzle insertion.

Three specific problems were identified as the most likely causes of performance degradation. These were:

- slow computation rate,

- no velocity feedback, and
- insufficient friction compensation.

The computation rate of Duvall's control law was 14 milliseconds (msec) [10]. This rate was dictated by two system requirements. The source of timing for servo control in the old PUMA control evaluation system was a 7 msec clock; consequently, any servo rate must be timed in multiples of 7 msecs [30]. Computation of the compliant motion control law required nearly 10 msecs [10, p5-5], so the minimum sampling time for the process was 14 msec. Another 10 msec restriction was the force sensor operation rate. If the 7 msec restriction could be removed and force sensor sampling matched into the higher sampling rate, control law performance should improve on at least two counts. First, the sampling effect necessary for a digital control system appears as a delay that causes phase lag to the point of instability. Faster sampling causes less lag, hence, less instability [8, p 293-294]. Secondly, Duvall's control law was a continuous time implementation of desired dynamics (a model) for the manipulator, and the validity of using continuous time techniques on a digital control law is improved by higher sampling rates. More precise information concerning these errors will be presented in later sections and can be found in [10, p5-7]. Unfortunately, higher sampling rates will result in smaller error terms and possibly more sensitivity to friction effects. Even so, increased sampling is considered necessary to achieve the desired performance.

Duvall's control law implementation assumed a zero commanded velocity input. This assumption simplified implementation and was considered valid as long as motion was kept slow [10]. His assumption caused all velocity feedback to be considered error. Stated otherwise, velocity tracking is not possible since a continuous error exists and that error is always opposed to the motion in progress. Duvall claimed this was an excellent candidate for performance improvements since the necessary algorithmic variation required only minor modifications [10, p 5-24].

Accurate trajectory tracking through the combined trajectory (through constraints) was hampered by the friction effect labeled 'stiction.' Duvall described this as "the case where static friction does not equal sliding friction [10]." A reasonably complete discussion of the stiction effect will be presented in the literature review. A system with high stiction characteristics will operate through a stick-slip cycle when velocity becomes small (a requirement for the assumptions in Duvall's implementation) causing stiction to overcome the commanded torque until a sufficient position error builds up to increase the commanded torque to a level that will 'break loose.' [10,38]

1.4 Method of Approach

The plan of attack for each of the three problems described in the previous section will be presented here in identical order. First, computation rates, then commanded velocity effects and finally, the stiction/friction problem. To simplify the conceptual development of the control law, Duvall restricted the control law to two degrees of freedom. Joints 1,4,5, and 6 were controlled by a standard proportional plus derivative law with weak position gains to provide some compliance. Implementation details for these joints can be found in [10]. Compliant control was applied only to joints 2 and 3 of the PUMA since this was the minimum system necessary to demonstrate the refueling concept. This restriction also allows easier conceptualization of force and motion interactions in the workspace.

Sampling a feedback variable effectively inserts transport lag into the control system which reduces the phase margin and therefore, stability [8, p 293-294]. To increase the sampling rate of the control law, and thereby minimize transport lag, a new source of timing was provided. A KWV-11C programmable clock source was installed in the VAXStation III that controls the PUMA. This device can generate alternative clock signals for the servo control timing.

In the control law developed by Hogan, the commanded velocity v_0, is a

significant part of the damping terms [15]. This value is a vector of the joint velocity values and was simply removed from the control law in Duvall's implementation. A dummy trajectory was generated and stored in the trajectory files but never used in the control law [11, p 27]. To apply velocity control, the velocity trajectory file for each path was reaccomplished to contain computed velocities for the desired trajectory. The subroutine SLCTTJ (select trajectory) was modified to compute velocity information as the position trajectory is computed, both in cartesian space. Additional software modifications were necessary to track cartesian trajectories rather than joint trajectories. To examine performance improvements, plots of position errors and interface force were compared to similar plots from Duvall's research.

The friction compensation problem is more involved than the previous two. The PUMA is a gear driven manipulator and the two links being controlled by the impedance control law (links 2&3) [10] are not massless so there is significant stiction in the system. A significant study of low velocity friction was accomplished to lend insights into solutions for this problem. Several compensation schemes were considered, including adaptive techniques and some of these were shown in the literature to effectively reduce stiction problems such as those observed by Duvall [4,6,10]. Duvall's friction compensation scheme did not include viscous effects, but present implementations of various control laws on the AFIT Robotic Control Algorithm Development and evaluation Environment (ARCADE) system employ friction compensation that includes static friction, coulomb friction, and viscous friction. Because this scheme is effective in other experimental control laws on the PUMA, it is considered an excellent choice to improve performance of the impedance control law.

One primary task in this effort was the rehosting of the control law. Duvall's implementation was primarily at the assembly code level in the hierarchial control system and used diverse functions with significant parameter passing. To provide

an environment for force feedback testing that is easily accessible and generally compatible with ARCADE, all possible functions were translated from VAX assembly to FORTRAN and implemented on the VAXStation III. Many routines were easily translated and all data files were unchanged, but some functions required complete rethinking and new coding. Once all force feedback environmental functions and control law operations were translated, a variety of trajectories were generated and used to test the impedance control law improvements.

After rehosting and all improvements were completed, a simulated refueling connection was performed. This included free motion onto the slipway, continuous contact throughout constrained motion on the slipway and successful reorientation based on force minimization to accomplish the actual insertion.

1.5 Contribution and Summary of Results

The primary contributions of this research effort are itemized below.

- Successful demonstration of:
  - two degree of freedom refueling simulation,
  - interface force reduction under constrained motion, and
  - continuous surface contact during constrained trajectory.
- Improved compliant control environment:
  - minimized differences in force feedback control law and other control laws tested in the ARCADE,
  - most functions translated to high level language for easier access,
  - cartesian trajectory generator accomplished, and
  - inverse kinematics routine accomplished.
- Improved force feedback compliant motion control:

- increased flexibility and range for sampling rates in the AFIT robotic control system,
- increased operation rate for the 6 degree of freedom force sensor,
- inclusion of desired velocity tracking in impedance control law, and
- inclusion of both viscous and static friction compensation.

1.6 Organization

This thesis is organized into five chapters. Chapter two is a review of significant historical developments as well as an extensive discussion of recent advances in two particular subjects; compliant motion control and modeling, and compensation of friction effects. Chapter three presents the impedance control law implementation, including assumptions, justifications, hardware developments, and software modifications. Chapter four contains test descriptions as well as experimental results and analysis. Chapter five draws conclusions and provides recommendations for future compliant motion control research.

II. Literature Review

2.1 Motivation and Scope

Robotic manipulators hold the promise of greatly increased productivity and safety developments for industrial tasks. Many tasks that are dangerous and repetitive could be performed much more effectively by a robot. Unfortunately, many of those same tasks require the dexterity and adaptiveness of a human operator. Contact with the environment is the limiting scenario of many control systems since small errors can produce disastrous results when large forces are involved. To overcome this problem designers have proposed control systems that explicitly or implicitly control force through use of a force sensing system and/or knowledge of the environment. Rigorous experimental verification of these techniques has been sparse. Compliant control algorithms produce poor high speed gross motion tracking and as a class, are not as mature as position control. The natural solution is to control force when in contact and position when not, but this requires essentially two control systems in parallel and a logical, sensitive switching scheme to change controllers. Considerable research has been accomplished to characterize this problem and develop stable, implementable solutions. Any effort to develop a new approach or implement an existing one should be prefaced with a reasonable study of current ideas. Two of the major areas of interest are compliant motion control and compensation of nonlinear friction effects. This review will concentrate on the most recent developments in compliant control with a specific emphasis on impedance controllers and on the compensation of the nonlinear friction effect called stiction. The intention was to thoroughly review the appropriate background material and obtain guidance for selecting the most appropriate solution for this specific application.

2.2 *Compliant Motion Control*

Motion control of robotic manipulators is traditionally a position feedback control problem. The controller commands a particular position which is then converted to the corresponding joint torques, causing the arm to move to the new position. Arm position is monitored and fedback to determine any adjustments necessary to the original motion plan. If an obstacle is encountered, the control system will simply attempt to force through the obstacle, and motion may cease, depending on the orientation and rigidity of both the manipulator and obstacle. Any task requiring motion on or near an environment surface presents such a problem. Many tasks such as finishing, require specific contact forces to be maintained continuously. The basic idea of compliant control is to allow a manipulator to contact the environment, exerting minimal (controlled) force, and still achieve the desired movements. In general, compliant control is completely task dependent. For the refueling scenario, compliance is necessary to prevent aircraft damage as the refueling probe moves to connect with the port and after connection to assure continued contact. Compliance can be accomplished by passive means through physical spring and damper assemblies but this approach may allow unknown position errors [10, p 44]. For an example of passive compliant control, see [10, p 15]. Compliance can also be achieved by active means, i.e. by controlling position and force at the end effector through actuator commands [41]. This method generally uses a force sensor to feedback contact force information but may instead use sensed torque feedback [41] or knowledge of the task and environment [42, p.35] to control the amount of force applied by the manipulator. An excellent review of several force control schemes was accomplished by Whitney [41]. The two broad classes of force controlling schemes are hybrid control where some motion axes are force controlled and some position controlled, and impedance control where the compliance of the manipulator is controlled by selecting velocity and position feedback gains to give the manipulator a specific stiffness in each axis. A summary

review of hybrid control techniques is given in [10]. An overview of impedance control concepts will be presented here.

An explanation of the concept of impedance is appropriate. For a mechanical system with linear characteristics, two variables can be used to describe system behavior with respect to time. These two variables are effort (F) and flow (v) (where $v = \dot{x}$) and x is the displacement. A force (or torque) is then an effort while a linear (or angular) velocity is a flow [3]. Proportional, derivative, and integral relationships between these two basic elements have been formulated and used to describe impedance as:

$$Z(s) = \frac{F(s)}{v(s)}$$

i.e. impedance is the ratio of Laplace transforms of the effort to the flow. The concept of impedance implies a dual value known as admittance. Figure 2.1 shows the concept of mechanical impedance in terms of physical action. An impedance will control an effort generated by a flow applied to the impedance,

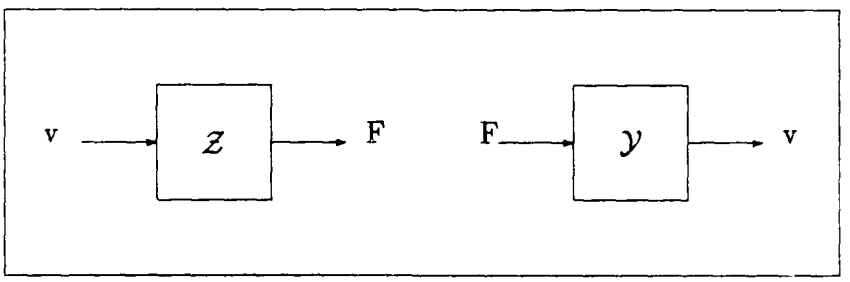

Figure 2.1. Mechanical Impedance and Admittance

while an admittance will control the flow resulting from an applied effort [42, p36,37]. Since the environment can generally be considered an admittance a manipulator should be controlled as an impedance to take advantage of the dual

relationship. A more detailed discussion of this dual relationship and its ramifications is found in [3]. For a given environment, the damping(B), stiffness(K), and inertia(I) determine the impedance (admittance) and hence the most effective manipulator impedance to maintain during trajectory tracking. Impedance gains can be made adaptive in order to maintain the same impedance throughout changing conditions. Also, impedance values of the environment and the force values fedback from contacts are more easily described in the world coordinates than in joint space, therefore many force control laws compute control variables in the world frame. Such transformations require use of the manipulator inverse Jacobian which is mathematically unstable due to singularities. Finally, impedance control is useful in modeling nonlinear mechanical systems when the model is linearized about an operating point.

2.3 Survey of Some Recent Developments in Compliant Motion Control

2.3.1 Force Control Several approaches to compliant motion have been developed, e.g. stiffness control where the stiffness of the environment and the manipulator are considered as a controllable input [35]; impedance control where the stiffness and compliance are defined as inverse values in linear systems [15]; and hybrid control where some axes are controlled by force feedback and the others by position feedback [34]. Limitations of these approaches have been studied and new developments continue. A recent publication by Liu, Mei-Hua, et.al. [31], summarizes several methods in a *unified* control law that includes all previously mentioned approaches as subsets. Results of tests using the controllers developed in [31] show instability and a tendency to lose surface contact. These problems were aggravated by nonlinear effects and gravity force [10,17,31]. Liu, et.al. developed and simulated two adaptive schemes using feedforward dynamics and estimating force control parameters. Simulation results indicated very good force tracking with the adaptive force controller but several limitations were noted. Environmental

stiffness was found to be a major stability issue; stiffer surfaces resulted in worse stability. This is a complication to the refueling task since the aircraft is certainly very stiff. High relative velocity between manipulator and environment was found to cause poor tracking. De Schutter considered a similar task and used an external force controller and state space methods to control a manipulator in contact with a moving object. A priori information of the object motion was fed forward when available and estimated by an observer when not. This feedforward method allowed higher approach speeds and reasonable force overshoots but requires very high peak torque values [9].

Another limitation of force sensing systems is the frequent requirement for different sampling rates of the force sensor and the position encoders. For Duvall's implementation, the control law required less than 10 msec and could have been trimmed more but the force sensor was fixed at an update rate of 10 msecs. Duvall considered using a second processor for force information and computation [10] and Ishikawa, et.al. did so in a hierarchial system using multiple microprocessors. Ishikawa also found the compliance of the force sensor had no effect on stability when the sensor's natural frequency was much higher than the control system's [20]. Duvall also considered sampling the force sensor at an integer multiple of the control law computation rate, thereby maintaining synchronous operation with the two different rates, but this approach was never successfully implemented.

2.3.2 Impedance Control An examination of some methods and specific control laws is appropriate here. The impedance control law described by Hogan [16] is:

$$\begin{aligned} \tau_{act} = & I(q)J^{-1}M^{-1}K[x_0 - L(q)] + S(q) \\ & + I(q)J^{-1}M^{-1}B[v_0 - J\dot{q}] + V(\dot{q}) \\ & - [J^T + I(q)J^{-1}M^{-1}]F_{int} \\ & - I(q)J^{-1}G(q,q) + C(q,\dot{q}) \end{aligned} \tag{2.1}$$

where:

q is the measured joint position

$\dot{q}$ is the computed joint velocities

I is the manipulator inertia matrix

J^{-1} is the inverse jacobian matrix

M^{-1} is the inverse desired mass matrix

K is the desired stiffness matrix

x_0 is the commanded position

L is the position from forward kinematics

S is the gravity compensation term

B is the desired damping matrix

v_0 is the commanded velocity

V is the friction compensation

J^T is the jacobian transpose

F_{int} is the interface force between constraint and manipulator

G and C are corriolis and centipetal terms

And the control law implemented by Duvall is

$$\begin{aligned} \tau_{act} = {} & I(q)J^{-1}M^{-1}K[x_0 - L(q)] + S(q) \\ & -I(q)J^{-1}M^{-1}BJ\dot{q} + V(\dot{q}) \\ & -[J^T + I(q)J^{-1}M^{-1}]F_{int} \end{aligned} \tag{2.2}$$

The first row of both Equation 2.1 and Equation 2.2 is the position dependent terms, the second row, the velocity terms, and the third row, the force term. The control law attributed to Duvall is the one modified in this research effort. Details

of that modification and the new control law are stated in the implementation chapter.

Impedance control methods have been applied to several robotic systems using various approaches. Mechanical impedance (defined in section above) has not been defined in terms of the nonlinearities that exist in any physical system and these nonlinearities (friction, stiction, motor characteristics) are significant. Friction and stiction will be considered in the next section. Anderson and Spong [3] have furthered the definition of mechanical impedance and applied electrical concepts of Thevinin's and Norton's equivalents as an aid to determine correct impedance for a manipulator in a particular environment. The impedance model was used in both position and force control loops with a classical switching matrix to determine which axes were controlled by force and which by position. Sharon, et.al. [36] introduced a design approach referred to as 'Design in the Physical Domain'. His method considers the entire physical system in designing an ideally controllable system and *then rearranges* control elements for valid implementation. The concept of impedance matching was used in the design process to assure maximum energy transferance. This application was unique in impedance concepts because the energy transference was between a macromanipulator and a micromanipulator in the same structure [36]. The effects of manipulator model accuracy were examined with a nonlinear analysis by Lawrence [23] using describing functions and including actuator torques and back EMF values. Lawrence indicated mechanical design should be done concurrently with electrical design and concluded that his technique provided basic information about performance limitations. Many of the performance limitations he witnessed are due to poorly modeled terms such as stiction and incomplete dynamics compensation. These problems are excerbated by the requirement for a very heavy manipulator that will be required for the refueling task. Recent investigations into adaptive techniques [32,22] to compensate friction effects present possible solutions.

2.3.3 Summary Force control in general and impedance control specifically are techniques under intense research that are being applied in conjunction with other control concepts. Robotic manipulators cannot work well with environmental restrictions. To accomplish autonomy or even telepresence with a manipulator system, stable compliant motion must be accomplished. Considerable research has been performed with several concurring opinions emerging. Some important points are:

- environmental stiffness is a critical parameter,
- control loop sampling should emulate continuous time systems,
- higher speed motion causes position tracking errors,
- high force requirements cause position tracking errors,
- nonlinear effects cause tracking errors and poor stability, and
- a unified approach to both force and position control is necessary for complicated tasks that will transition from free motion to constrained motion [31,10].

2.4 Friction, Stiction, and Approaches to Compensation

Many recent control law developments disregard nonlinear effects [32,22], or assume compensations are accomplished in an inner loop [3]. Task dependent nonlinear effects can be significant. A partial list of the known sources of nonlinearities would include:

- coulomb friction,
- stiction effect,
- viscous friction asymmetries,
- unmodeled mechanical imperfections,

- gear backlash,
- bearing dynamics, and
- unmodeled structural dynamics (assumptions of rigidity, etc.)

Two classes of solutions are readily apparent; mechanical and electrical. Mechanically, better models alter design practice to eliminate as many errors as possible. An example would be using a direct drive actuator system to eliminate backlash as an error source. For the refueling effort a direct drive system cannot be produced with available technology. The electrical solution is advanced control system design (and component quality increase) and is the presently pursued approach. Relatively small tracking inaccuracies can be overcome by adaptive compensation but the best controller will perform better with an accurate model, so both issues must be considered. If an accurate model of system dynamics is available, feedforward compensation can be used to overcome much of the error [29].

A *primary source of nonlinear* mechanical behavior and resulting instability is the stiction effect. Research into friction sources and compensation methods on robotic manipulators is significant and ongoing. Some recent efforts will be compared and contrasted as background for the selection of a preferred compensation procedure for the PUMA-560 manipulator in the Robotics System Laboratory at AFIT.

2.4.1 Modeling Friction Effects Exhaustive research pertaining to friction compensation has provided many friction models and compensation techniques. This section will first review sources and effects of frictions in servomechanisms and some developmental history. Dynamic joint frictions will be contrasted against end effector frictions, and several models for various circumstances will be presented.

Friction has long been known to cause limit cycles in steady state operation of servomechanisms [39,14,4]. Tustin performed a detailed analysis of various friction effects including coulomb and stiction (based on backlash studies) using

techniques similar to describing functions and an exponential model for friction near zero velocity [39]. Recent efforts have verified the exponential model [7,4] while developing other models for specific situations such as sliding friction [14]. A generalized model for friction might include terms for all the following effects:

- nonlinear velocity dependence (direction and rate) [39,6,7,14,4],
- mechanical asymmetries [7],
- position dependence [7,4,13], and
- temperature and lubricant dependence [4].

In general, mechanical systems will have these friction components but dominance of one friction source over the others is sometimes determined only from collected data [7]. The refueling task requires environmental contact (task friction) and smooth motion at low velocity; both are affected primarily by velocity for a heavy manipulator such as the PUMA-560. Walrath, working with a gimbal system constantly reversing directions (i.e. traversing the zero velocity portion of the friction characteristic) concluded "characterization of friction by the classical 'Coulomb/stiction' model has proven to be especially lacking in this regard [40]." Recent studies of friction in low velocity, geared manipulator motion have provided more complete friction models [4]. Models of the separate major friction components can be summed to describe a composite friction characteristic.

Figure 2.2 is a classical description of coulomb friction and stiction. Coulomb friction is defined as the total friction characteristic when static and kinetic frictions are equal in magnitude. The impulse of breakaway torque above kinetic friction is defined as stiction [38].

Viscous friction is ideally a linear function of velocity with a simple coefficient and zero offset as shown in Figure 2.3 but empirical data indicates a nonsymmetric form as in Figure 2.4 [6,4]. Similarly, empirical data from [4, p 1425] shows a

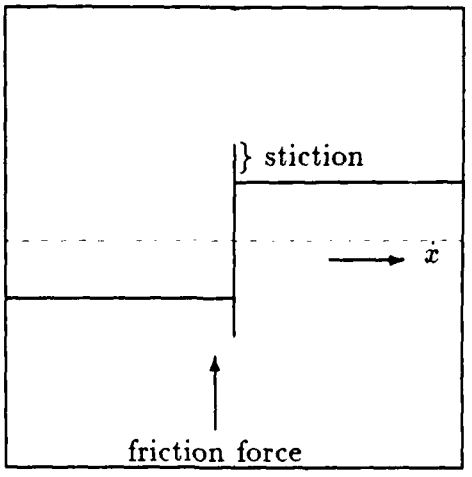

Figure 2.2. Classical Coulomb Friction and Stiction [38]

low velocity friction function (Figure 2.5) that approximates Tustin's original exponential model. Armstrong used acceleration feedback methods and a very stiff controller to achieve stable, smooth speeds as low as 0.012 rad/sec on the first joint of a PUMA-560 [4, p 1425].

Figure 2.5 is a composite of Coulomb, stiction, and viscous forces in the velocity range shown. This model has been used by other researchers in force control and friction compensation [14,7,13]. Armstrong explained the negative velocity dependence in terms of the boundary layer lubrication in the gear train. At low velocities, poor lubrication means gear meshing is essentially metal to metal and the backlash effect (well described by Tustin) is dominant; but at higher rates, full fluid lubrication causes viscous friction to dominate. For a system that reverses direction periodically such as a robotic manipulator, simple friction compensation is not possible since the model changes thru negative viscous, negative exponential, stiction, positive exponential, and finally positive viscous ranges. Control systems based on simple models such as Figure 2.2 result in limit cycle operation and stick-slip movement [8,7,4]. Townsend and Salisbury modelled stiction (joint or contact)

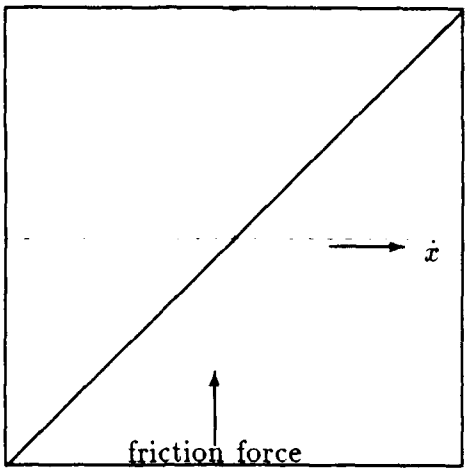

Figure 2.3. Ideal Viscous (Velocity Dependent) Friction [38]

in a force controlled system. Figure 2.6 is a physical representation of that system and Figure 2.7 shows the limit cycle behavior that might result from a step input. Duvall observed this effect and attributed it to stiction [10]. A more accurate model of the mechanical system will allow better physical design of the mechanism, and minor imperfections can be controlled by a sensitive, adaptive controller. A composite of the individual friction effects such as that shown in Figure 2.8 provides a model that allows adaptive and precomputed torque techniques to effectively compensate friction.

2.4.2 Control of Friction Effects Using the composite friction model presented (Figure 2.8) or similar models, very effective controllers have been implemented [6,13,7,40]. Controller designs will be reviewed with specific emphasis on adaptive techniques, both feedforward and feedback, that have proven successful against nonlinear effects, particularly friction.

Friction compensation is one aspect of the control system. The controllers discussed here are mostly compliant motion forms with force as an implicit or explicit input variable. Issues discussed previously: nonlinear effects, poor models,

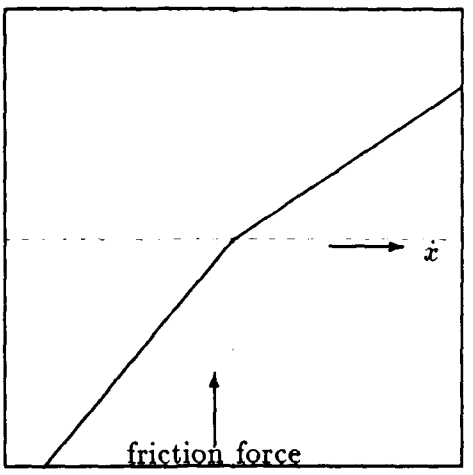

Figure 2.4. NonSymmetric Viscous Friction

etc., cause stability to be a major concern when designing compliant robotic motion controllers. The simple force feedback controller shown in Figure 2.8 was tested by An and Hollerbach on the MIT Serial Link Direct Drive Arm (manipulator frictions are minimal) for stability when in contact with different environments [1]. In a separate study [2], a more sophisticated controller by Raibert and Craig [34] shown in Figure 2.9 was proven unstable for application to revolute manipulators.

Other causes of instability include singularities in the Jacobian and computational delays. Overcompensation of friction effects has even been shown to cause limit cycles [7, p 1354]. Additional, 'outer loop' sensors (see Figure 2.10) have been successfully applied to impedance control [3] and position control [4].

While investigating friction compensation using acceleration feedback, Armstrong concluded," The region ...where friction diminishes with increasing speed is mechanically unstable, so much so that that stabilization by feedback without extraordinary sensors may be impossible [4]." Since a force controlling scenario such as refueling requires a transition from free motion thru contact to sliding motion **at slow speeds**, effective friction compensation is required. Acceptable

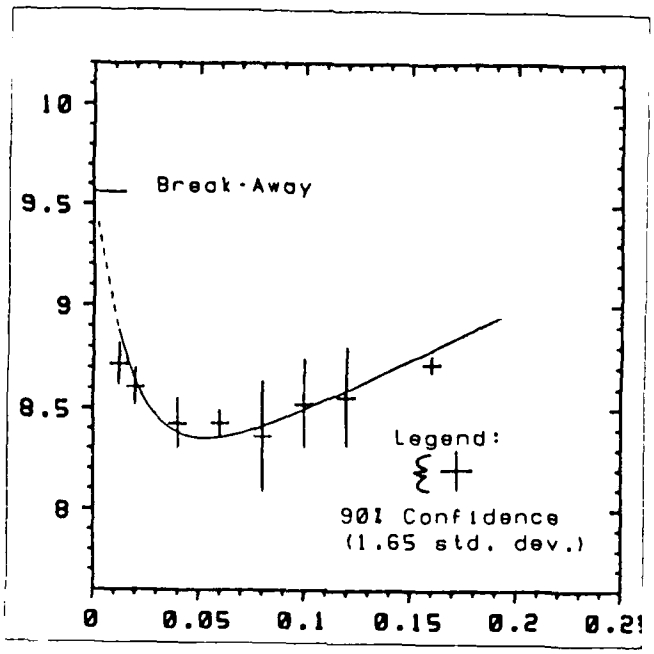

Figure 2.5. Low Velocity Friction Characteristic Vertical scale: newtons horizontal scale: velocitiy (rad/sec) [4, p 1425]

performance **in free motion** was demonstrated using adaptive control and the composite friction model of Figure 2.11 [7].

One common friction compensation model is [28]:

$$\tau_f = \begin{cases} \tau_c sgn(\dot{q}) & (|\dot{q}|) > d \\ \tau_c sgn(\tau_m) & (|\dot{q}|) \leq d \end{cases}$$

where:

τ_c is the compensation torque (90 % of experimentally determined value for stiction)

sgn$(\cdot)$ is the function returning the sign of its argument

$\dot{q}$ is the joint velocity in rad/sec

τ_m is the torque supplied to the motor

d is a velocity threshold also determined experimentally

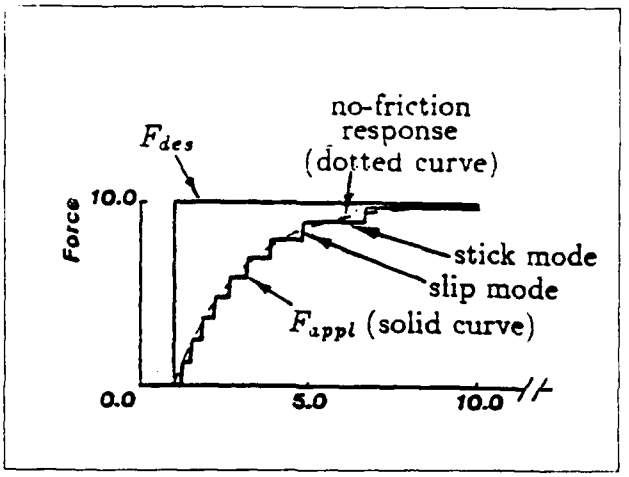

Figure 2.6. Stiction effect. Vertical scale: force (N) Horizontal scale:time (sec) [38]

In Duvall's impedance control law, no compensation was made for friction effects other than this kinetic velocity dependent term; consequently, Armstrong's over-compensation warning may apply at low velocities [4]. A more thorough model would include *coulomb*, *viscous*, and *stiction*. Canudas, et.al. [7] developed models for these:

$$\tau_f(\dot{q}) = \alpha sgn(\dot{q}) \tag{2.3}$$

$$\tau_f(\dot{q}) = \alpha_i sgn(\dot{q}) + \beta_i \dot{q} \tag{2.4}$$

$$\tau_f(\dot{q}) = [\alpha_0 + \alpha_1 e^{-\beta|\dot{q}|}] sgn(\dot{q}) \tag{2.5}$$

where:

τ_f is the torque required to compensate the friction effect

α in the first statement is the kinetic friction constant

α_i is the kinetic friction constant with

β_i is for the viscous term

α_0 and α_1 summed, are the stiction level with

β time constant of decay from $\alpha_0 + \alpha_1$

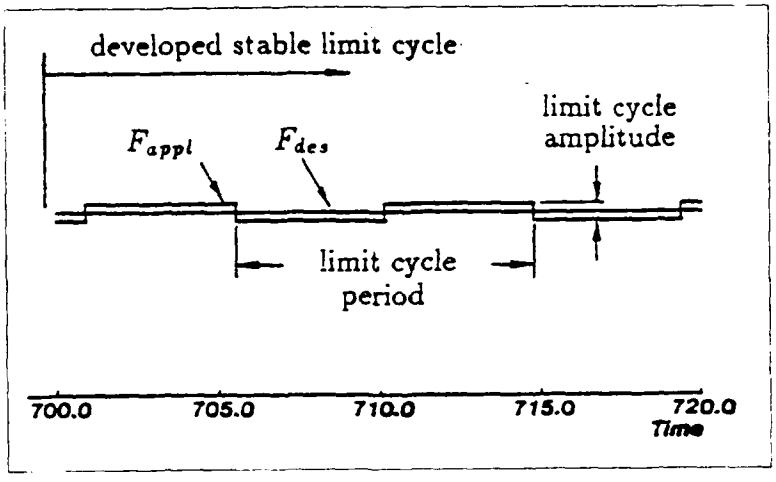

Figure 2.7. Example of Limit Cycle Operation Vertical scale: force (N) Horizontal scale: time (sec) [38]

Position dependence could also be considered but its effect was assumed small relative to velocity dependent terms. Equation 2.3 is the expression representing coulomb friction. Equation 2.4 models both coulomb and viscous friction effects, and Equation 2.5 is a composite law designed to also include the stiction effect using a model similar to Tustin's [39].

Except in the low velocity regions, Equation 2.4 is the friction compensation now in general use with other experimental control laws functioning through the AFIT Robotic Algorithm Development and Evaluation Environment (ARCADE).

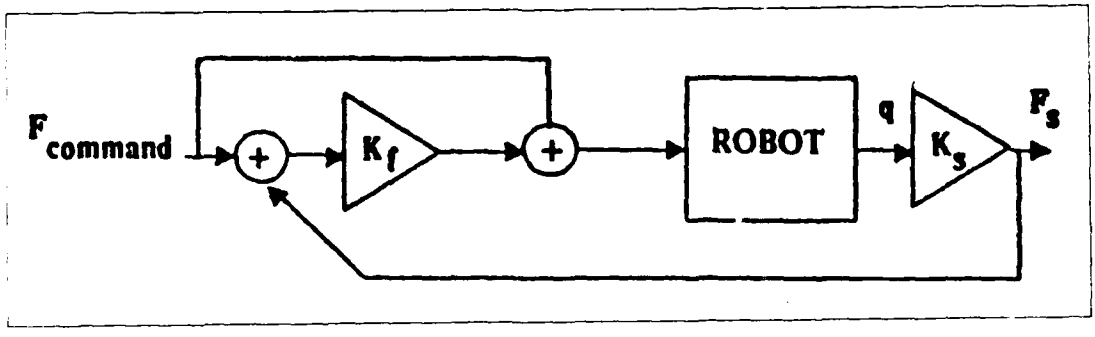

Figure 2.8. Simple Force Feedback Control System [1, p 892]

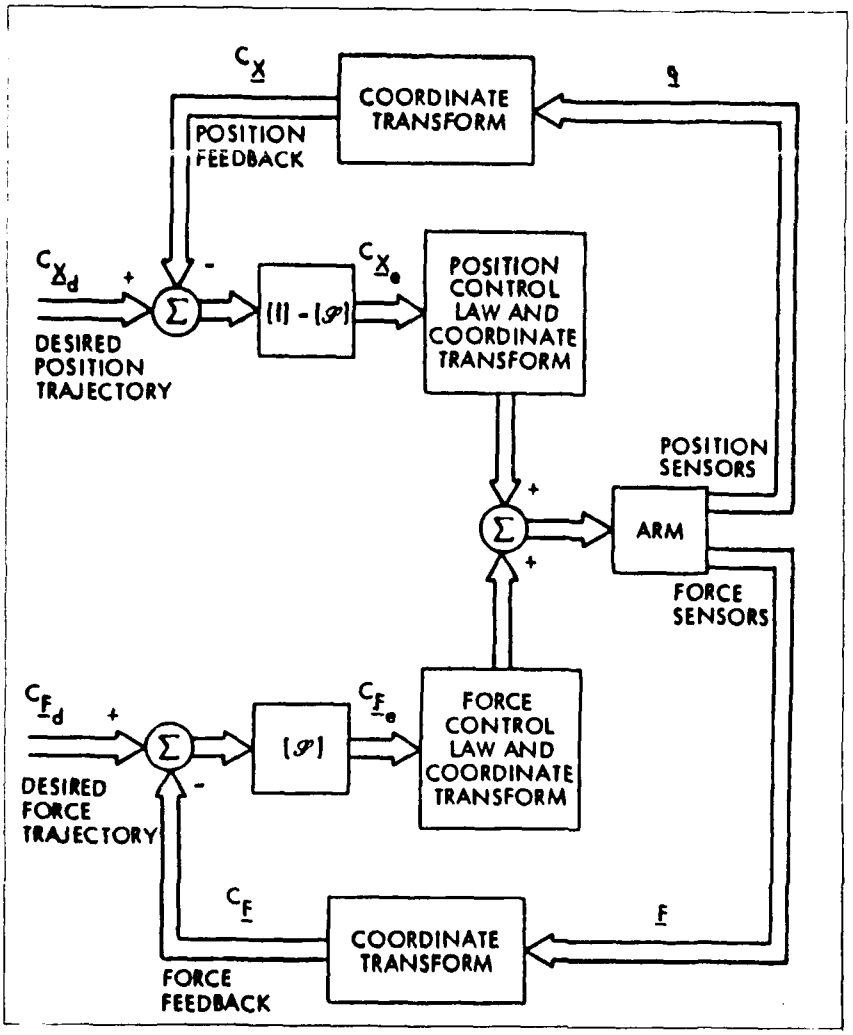

Figure 2.9. Hybrid Position/Force Feedback Control System [34, p 131]

Various schemes have been used successfully to eliminate the effects of the low velocity friction characteristic. Canudas [7] recommended an adaptive law with both feedback and feedforward compensation, but the applicability of his work to the friction compensation necessary for constrained motion is questionable since he was not researching constrained motion. Measurement noise for the position feedback may cause compensation to actually be the exact opposite of what is needed so calculations in this range are made using the q_d instead of q_a. This would allow off-line computation of compensation for those trajectory ranges. Leahy [29] used

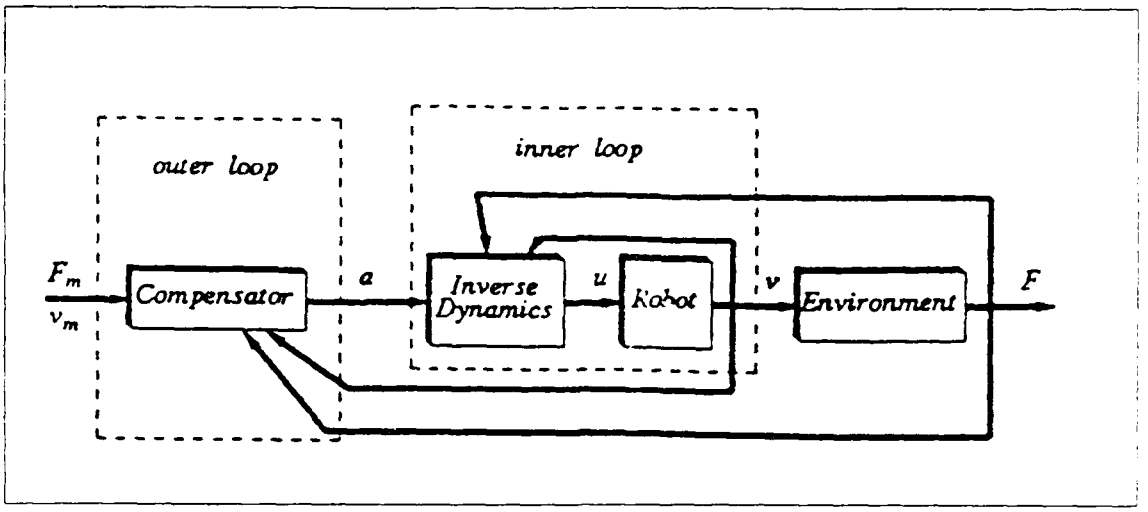

Figure 2.10. Example System Using an Outer Loop Feedback [3, p 549]

such an approach very effectively as early as 1986. Walrath [40] also selected both feedforward and feedback with adaptive friction coefficients. Armstrong was researching specifically for a low velocity friction model (in a non-contact role again) and precise compensation so he used an *open loop* correction, resulting in worst case endpoint error of 4.1 % and best case results of 0.14% [4]. Nearly all sources reviewed recommended adaptive control of friction compensation even though various implementations were suggested. It is important to note that essentially all sources reviewed did not consider compensation of friction while in contact with a constraining surface. This is an area of extreme uncertainty and a very necessary part of the refueling scenario.

2.5 Summary and Conclusions

Recent developments in compliant motion techniques were reviewed. Advances in impedance control methods and hybrid impedance control were examined. Problems resulting in instability for force controllers were reviewed, including friction. Some background and recent developments in friction modeling and compensation were discussed.

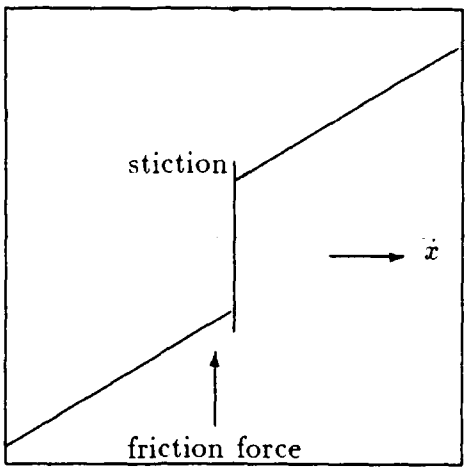

Figure 2.11. Composite Friction Model

No recent research efforts have described a better method for controlling a manipulator for refueling an aircraft than an impedance type force controller, whether a hybrid scheme or not. Specific problems with an impedance control law implemented on a heavy manipulator have been described and verified. The friction effects resulting in stick-slip operation for Duvall [10] have been detected and studied by others. The problem of stable compliant motion at slow velocities is still a significant challenge but progress has been made in both physical modelling and adaptive control of torque correction methods. For the refueling task, solutions were developed for the three problems selected as most likely candidates for improvement. In the next chapter, details of the implementation of those solutions will be presented.

III. Impedance Control Environment Development

3.1 Overview

The implementation of refinements to Duvall's impedance control law [10] began with an understanding of the hardware and software components used in his research. Figure 3.1 is a block diagram representation of the AFIT Hierarchial Control System (AHCS) hardware used by Duvall.

A detailed description of that system is found in [10, p 4-17]. Since the basic structure of the new system (Figure 3.2) remains unchanged, discussion will focus on modifications. The AHCS offered the speed of assembly code at the coordinator level and the flexibility of FORTRAN at the organizer level. This hierarchial structure allowed tasks to be performed at the most appropriate level but did not fully utilize that capability.

The general testing environment supported by the AHCS is the AFIT Robotic Control Algorithm Development Environment (ARCADE). ARCADE provides serial and parallel communications between the VAXstation III (organizer level) and the LSI-11/73 (coordinator level) [27]. These communication connections allow the organizer to command basic functions of the manipulator such as calibration and repositioning.

The remainder of this chapter describes the efforts to upgrade the impedance control evaluation environment in the AFIT robotic systems laboratory. Details of changes and derived controller improvements will be presented with an overview of the impedance control law for background. First, equipment used in this research effort will be briefly presented. Then architectural changes to the AHCS will be discussed including control law structure. Specific functions of the environment, i.e. the timing system improvements, will be presented in some detail. Finally,

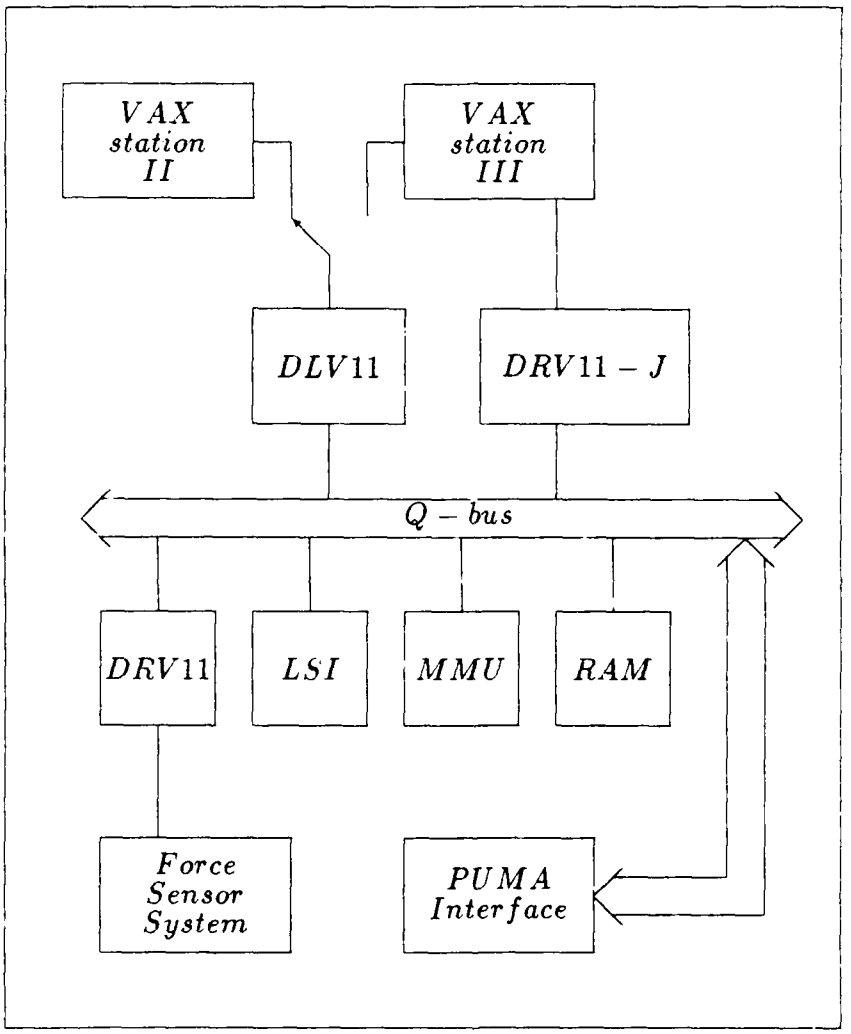

Figure 3.1. Block Diagram of Hierarchial Control System as Used By Duvall For Impedance Control Research

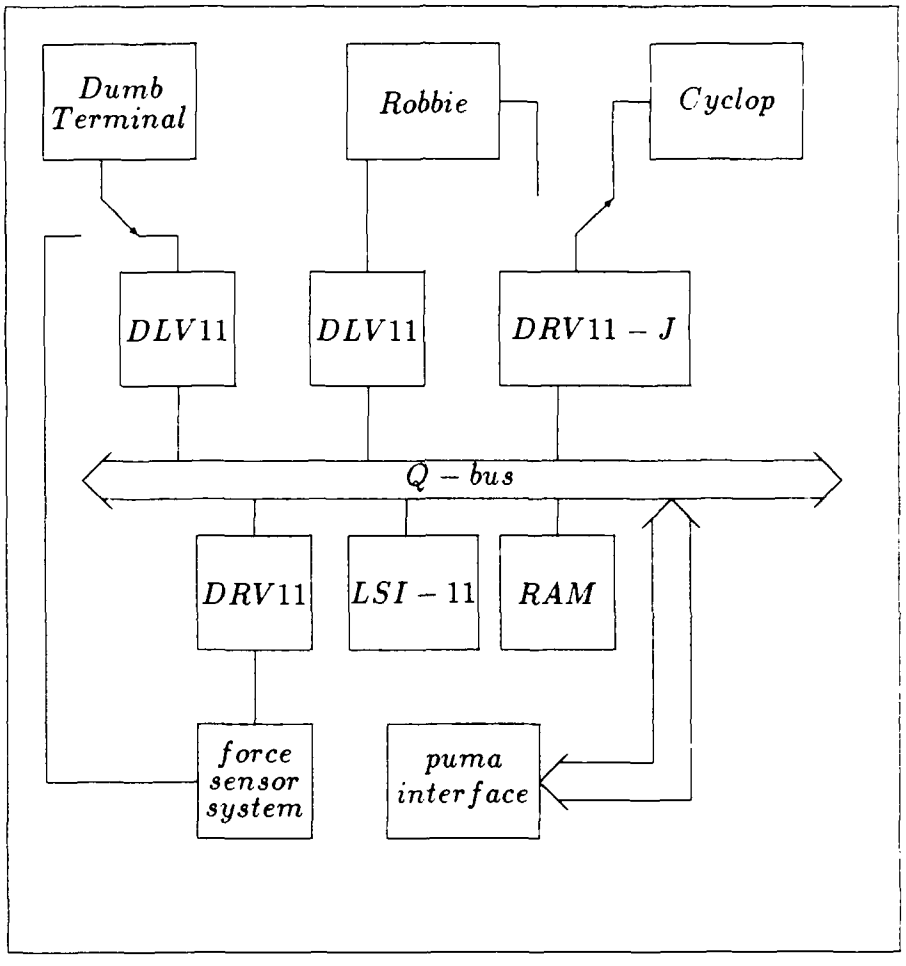

Figure 3.2. Hierarchial Control System with upgrades. Robbie and Cyclop are both VAXStation IIIs. The timing system is split between Robbie and the puma interface.

functions required to operate the algorithm exerciser but not necessarily required for the impedance controller will be discussed.

3.2 Equipment of the Algorithm Evaluation Environment

3.2.1 Manipulator The manipulator used in this thesis was a PUMA-560, which is a vertically articulated 6 DOF industrial robot. Figure 3.3 shows the PUMA and the coordinate frame assignments used for the Denavit-Hartenburg parameter calculation. The six degrees of freedom consist of three heavy links in a serial configuration and three lighter links in a roll-bend-roll wrist.

The manipulator is platform mounted in a permanent installation in the AFIT robotics systems laboratory. In the heavy links, drive power is transmitted from electric motors through gear trains to the joints. The system weight requires that torque values be computed and applied to the motors in addition to the desired dynamics model computed torques. The gear trains and bearings require similar compensation to overcome friction effects. Position data is supplied by optical encoders calibrated through a software routine downloaded to the coordinator from the organizer and force and moment values are returned through the sensor electronics to the organizer via the coordinator. Feedback variables will be detailed in Section 3.3.

3.2.2 Force Sensor The PUMA wrist is fitted with a six axis (3 forces, 3 moments) force sensor to provide force feedback. The force sensor is produced by JR^3, Inc. and is discussed in detail in Section 3.4.3.

3.2.3 Refueling Apparatus A special fixture simulating a refueling system hose and designed to attach to the force sensor was used to simulate a refueling port connection. The simulated refueling port is a half scale mockup of a standard Universal Aerial Refueling Receptacle Slipway Installation (UARRSI). These two pieces of refueling hardware were designed by Capt David Duvall from the original

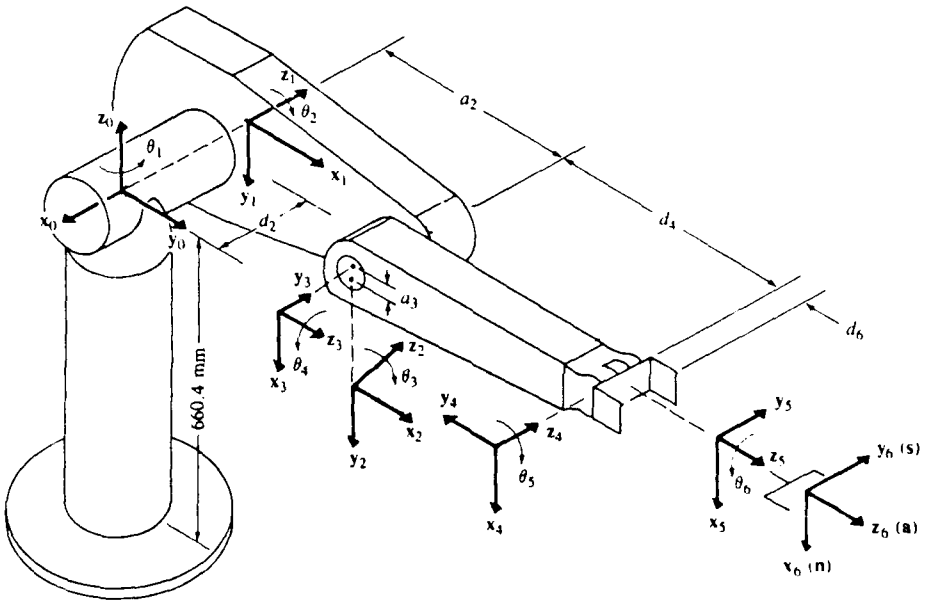

PUMA robot arm link coordinate parameters					
Joint i	θ_i	α_i	a_i	d_i	Joint range
1	90	−90	0	0	−160 to +160
2	0	0	431.8 mm	149.09 mm	−225 to 45
3	90	90	−20.32 mm	0	−45 to 225
4	0	−90	0	433.07 mm	−110 to 170
5	0	90	0	0	−100 to 100
6	0	0	0	56.25 mm	−266 to 266

Figure 3.3. PUMA-560 Robotic Manipulator with Rotation Axes and Denavit-Hartenburg Parameters Selected as Indicated.

specifications and produced in the AFIT models shop for Capt Duvall's thesis research in 1988 [10, p 4-11].

3.3 New Architecture

Most of Duvall's research was performed without the benefit of the parallel interface that now links the VAXStation III (organizer) and the LSI-11/73 (coordinator) as seen in Figure 3.2. This forced all realtime routines to be written in assembly language for coordinated execution. Consequently, a primary objective of this thesis effort was the translation and rehosting of most functions from the assembly language environment of the coordinator to the high level language of the organizer. Some changes in the ARCADE hardware were also necessary. The total refueling effort (including visual servoing) will more easily integrate now that most functions can be controlled from the higher level. Also, the force sensor subsystem is now more accessible for any future force feedback studies. Anticipated direct benefits of rehosting include:

- less fragmented coordination of various controller functions,
- the capability to easily attempt various adjustments to the controller,
- the capacity to develop more complicated subfunctions that otherwise would be tedious and unprofitable, and
- greater compatibility with other algorithms using ARCADE.

Another benefit of the high level language was the accessibility of collected data. More extensive data collection was possible since memory is not a limiting factor and the computations accomplished in the FORTRAN environment are easily captured. This same ease of access greatly expedited development of major software generation such as the cartesian trajectory generator (Section 3.4.4) and many minor adjustments to code.

The following sections will present the ARCADE as it is after modifications such as the new timing system and updates to the force sensor channel. Control law implementation and software translation of ARCADE functions will also be discussed.

3.4 ARCADE and AFIT Hierarchial Control System

3.4.1 Controlling Hardware The ARCADE consists of both software and hardware (Figure 3.2). In this section the hardware and and low level software functions will be discussed. Major software functions will be the subject of later sections. The hardware level includes 'primitive' functions such as collecting force values and joint positions and generating electrical currents from commanded torques. The coordinator level in this implementation is a data concentrator only and consists of the original PUMA LSI-11/73. This level handles conversion of joint positions and force scaling as well as communication tasks. The upper level of ARCADE is implemented on a VAXStation *III* running under the VMS operating system using a layered software package called VAXlab. VAXlab supplies constructs for communicating through the parallel and serial links between organizer and coordinator. Also, VAXlab provides interactive graphing functions to quickly display data taken during control algorithm tests. This capability has been invaluable for troubleshooting control law implementation errors.

3.4.2 Timing System Operations The PUMA pulses the BEVENT line of the LSI bus at a 7 msec rate. The manufacturer supplied operating system, VAL-II, uses this source for timing motion control of the manipulator. This 7 ms clock is derived from a source that times the reading of the encoder units used to feedback position information. This was the smallest increment of time available to Duvall and was identified as a possible source of performance limitations such as poor tracking. To provide a more finely discretized timing source, a KWV11-C clock card was installed in the VAXStation III and software written to operate it. The

fastest sampling possible is the rate at which all system functions can be completed. The most basic function, receiving information from the position encoders, was determined to be the limiting operation. This reading rate was selected as the smallest increment of time for the improved system timing. To implement the new timing system, several steps were necessary. First, minor modifications to the interface 'B' card in the Unimate controller provided a 1 Mhz clock from the same source as the encoder sampling operation. Then the KWV11-C clock card was installed in the VAXStation III and the 1 Mhz source was supplied to the card. Software was developed to control the KWV11-C and provide the desired integer multiples of the basic sampling time T_s. This new timing source was then injected back into the interface 'B' card in place of the original 7 msec signal. This system provides the operator with maximum flexibility in control loop rate selection, and was first used to evaluate the effect of different sampling rates on link vibrations at low velocity [26]. Slight hardware modifications provided a permanent system used by the ARCADE environment for all manipulator control. A block diagram (Figure 3.4) provides information concerning connections and signal flow. The T_s for the system is nominally .875 ms according to Unimate documentation but was found to be 0.9 ms on the AFIT Puma installation. All software is designed to operate with a clock that is a multiple of that basic rate. The software produced was a subroutine that attaches, initializes, and starts the KWV11-C with the requested operating parameters. The subroutine must be called by any program attempting control of the manipulator but is otherwise completely transparent to the user.

A significant problem encountered during development was the noise level on the transmission lines between the LSI-11 and the VAXStation III. The 1 Mhz clock going to the VAXStation III coupled to many other signals in the vicinity and caused a variety of errors. After some basic decoupling techniques were applied, the system seemed usable. Unfortunately, after many hours of operation, the force

sensor performance was found to be degraded and the cause was traced to noise on data transmission lines. The clock system was carefully reworked and improved so that the installation in Figure 3.4 is more reliable.

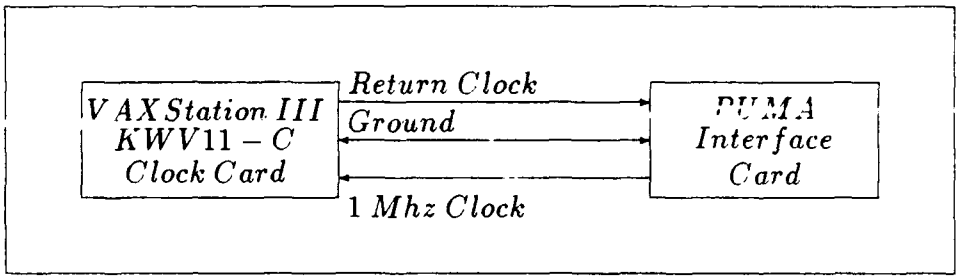

Figure 3.4. Timing System Modifications

Some of the benefits of increased sampling rates include but are not necessarily limited to:

- greater controller bandwidth,
- position dependent calculations (i.e. J, I) build less errors, and
- assumptions based on high speed sampling are better satisfied.

3.4.3 Force Sensor Operations

3.4.3.1 Overview A force sensor subsystem is necessary for any research with force feedback as a function. Duvall completely integrated the sensor into the ARCADE environment and noted that some of the sensor systems limitations could be corrected by future upgrades of the sensor's operating system. Update of the operating system was accomplished as part of this thesis and will be discussed in this section. Translation of some functions from the assembly code level to the FORTRAN level was also done to provide a more flexible interface to the force sensor channel. Figure 3.5 is a modified block diagram of the sensor channel from [10, p4-6] and will be referenced to throughout this discussion. Operation

of the force subsystem includes collection of raw data, transformation to world coordinates and correct scaling of the sensed forces and moments. Maximum force measurements must also be considered in order to prevent damage to the physical sensor.

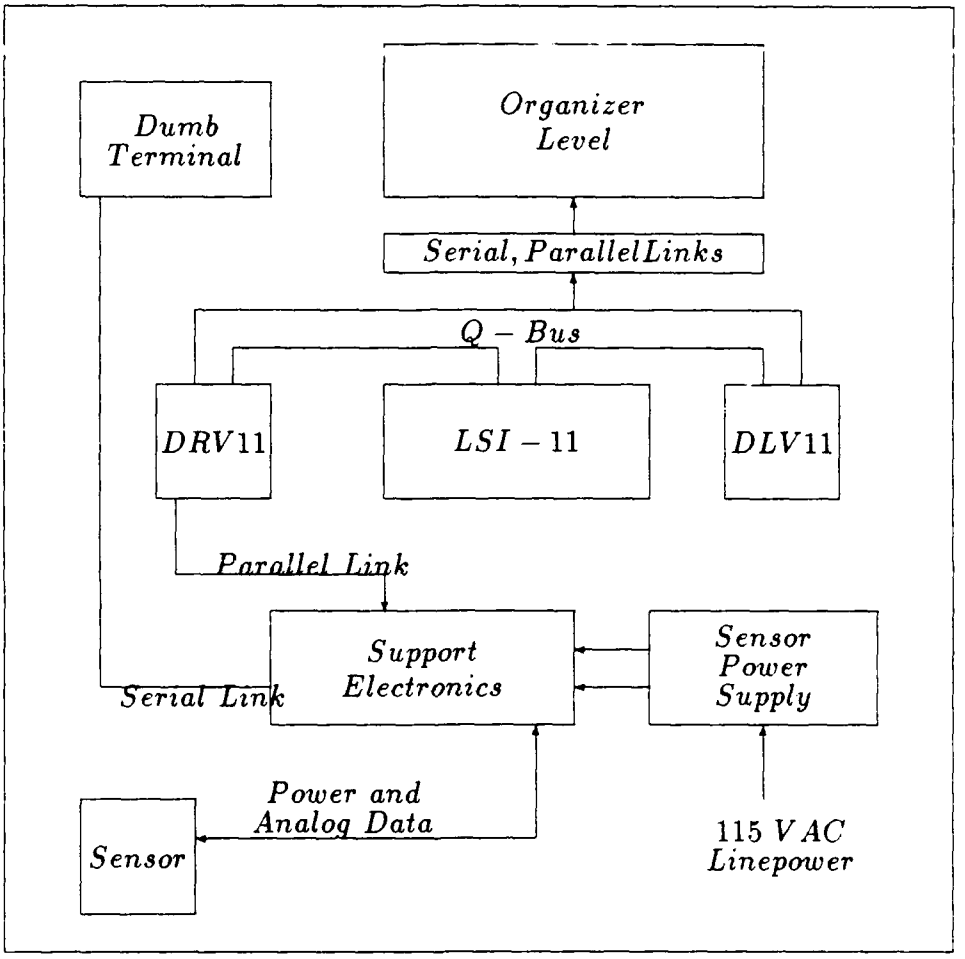

Figure 3.5. Sensor System Detailed Block Diagram

3.4.3.2 Raw Data Collection The sensor electronics (the operating system) is accessed through the serial port on the electronics package. Data is requested by an assembly code routine (when commanded by the coordinator) that operates the hardware of the sensor's parallel data port. The sensor system samples

the forces and moments at a rate controlled by its own operating system. With the earlier version of sensor software, the operation rate (10 msec) was the primary limit on control law sample rate for Duvall's implementation of the impedance control law. The sensor electronics package was returned to the manufacturer for installation of upgraded software that now provides force information at sample rates as fast as 1 ms (under restrictive circumstances) [21, p 4-11]. The timing system (Section 3.4.2) allows control law sampling rates in integer increments of 0.9 ms but the force sensor is not locked into this system. Sampling rate control for the sensor electronics must be set to a rate that is equal to or higher than the control law sample rate. Through trial and error, a balance between maximum control law sample rate and acceptable force sensor reliability was found at 5.4 ms for control law operation. Best sensor performance was seen with commanded sensor operation rate of 300 hertz, and noisy readings were seen with rates less than 200 hertz. This is expected since the sensor is operating asynchronously to the rest of the system. One hidden restriction on this operating rate is operating system requirements. The sensor's internal software requires some housekeeping time and consequently will limit data transfer rates, causing unexpected errors to occur during the first few operation cycles. The operating system will automatically adapt to best fit time sharing and provide the highest cycle rate possible if the requested rate can not be met, but a few cycles of operation are required to make adjustments and the output data is noticeably in error during those few cycles. Because of this potential hazard, it is recommended that all force collection operations be preceded with careful examination of the outputs of *all three forces and all three moments.*

3.4.3.3 Transformation of Data Duvall accomplished a unique method of accurately transforming the sensed forces and moments from the tool tip into properly scaled values in world coordinates [10, p 4-3]. Data supplied to the organizer from the coordinator is scaled only. Transformation to world coordinates is performed by a realtime routine at the organizer level. The transformation process

developed by Duvall [10, p 3-25] includes correction for gravity based on manipulator position and the masses of the test fixtures. Prior to transformation, data is scaled; and before outputs are valid, some sort of calibration must be accomplished. These operations are discussed in the next section.

3.4.3.4 Sensor Accuracy: Calibration, Scaling, and Repeatability Calibration of the sensor and electronics is crucial to valid operations. Electronic calibration procedures are provided in [21] but are not recommended unless a problem is confirmed. Removal of 'tare weight' is also provided through a keyboard command and this *is* recommended during pretesting warm up with the sensor in the upright position (F_z the only sensed force) to remove any electronic bias. The data scaling is also crucial to proper operation and is not easily changed. This operation is performed at the assembly code level and is 'hardwired' to fullscale force readings of 111.2 newtons for F_x and F_y and 222.4 newtons for the F_z direction. Interface moments M_x, M_y, M_z are similarly limited to 8.473 newton-meters. During the operation of the present impedance control law, calibration of the entire sensor channel is performed by standing the arm upright, translating the sensed forces into the world frame, and then saving the computed values as bias to be subtracted from subsequent readings. This procedure was developed by Duvall and has demonstrated acceptable performance. It is a 'single-point' calibration and therefore could be considered faulty.

Another condition affecting sensor reading accuracy is the position repeatability. To determine this effect, Duvall and Leahy performed tests to determine force sensor resolution when the arm is moved and then returned. Ideally, this would have been 2^{-12} of the full scale readings, for instance, resolution of the F_z channel would be:

$$F_{zresolution} = \frac{1}{2^{12}} F_{zfullscale}$$

$$F_{zresolution} = \frac{1}{4096} 222.4 = 0.0543\, newtons \tag{3.1}$$

Results of those tests indicated reposition inaccuracies causing repeatability errors for force measurements, resulting in conservative limits for resolution of ± 6.0 N for forces and ± 2.0 N-m for moments [10, p5-3]. This resolution error forces a deadband limiting function to be used around zero force input to prevent false readings. Unfortunately, deadband limiting is highly nonlinear and could contribute to instabilities in the control system.

3.4.3.5 Software Reorganization Several low level functions of the system were translated from assembly to FORTRAN in the process of rehosting. These include coordinate transformation, dead band limiting, and removal of calibration bias. The communication process was also modified to handle the passing of parameters. In the ARCADE environment, a new FORTRAN COMMON block was added to handle parameter passing between internal operations as well as between ARCADE levels such as force sensing. For operations between subroutines running in the organizer level (e.g. the trajectory generator), variables and arrays (e.g. initial conditions and trajectory points) are passed through the common block. For operations between ARCADE levels, VAXlab utilities acquire data from the parallel port for common variables to be used by the algorithm. ARCADE subroutines (PDPCOM, PDPINO) do the same for the serial port. All force function related variables were included in the new common block to encapsulate changes from the previous ARCADE as much as possible. In general, the translation of force sensor operations to FORTRAN (except actual data gathering) resulted in a system much easier to use and understand, thereby enhancing the capabilities of the force feedback testing environment.

3.4.3.6 Miscellaneous Modifications The force sensor channel was modified by addition of a dedicated power supply. Grounding problems were discovered in the original power supply system wiring. The 1 Mhz clock signal from the KWV11-C subsystem (see Section 3.4.2) was coupling onto the sensor power

supply lines through the grounding structure. Effects were not noticed immediately because performance appeared nominal, with occasional loss of response, but noise levels were measured on the signal lines from the sensor electronics that were as high as 400 millivolts peak to peak. The manufacturer (JR^3) recommended a dedicated power supply. This solution was very successful in dramatically reducing signal line noise and providing more reliable performance. Another modification to the system was the upgrade to the sensor operating system. This was discussed in Section 3.4.3.2.

A new software routine was written to provide access to the channel through the parallel interface. This routine is named READ_FORCE and will access, scale, and translate to the world coordinates all sensor outputs. Any user should become familiar with the whole system through this document, and references [10,21] before trusting control functions to the force feedback.

3.4.4 Cartesian Trajectory Generation The cartesian trajectory generation process was completely new. One objective of rehosting the impedance controller was to obtain greater compatibility with other algorithms using ARCADE to interface to the PUMA. Generation of trajectories is a common function that may be useful for any future cartesian space control laws. The cartesian trajectory generation routine developed was supplied in two formats, a subroutine for on-line generation in the initialization process, and an offline stand-alone generator to save trajectories for experimental evaluation.

Trajectories are usually generated in joint space for a revolute robot but force control systems function more naturally in cartesian space. Cartesian motion planning is more intuitive than joint trajectory planning, but it is difficult to do limit checking on cartesian trajectories since each point is a compound function of all joint angles and may be at a singular point or even unreachable. Because it performs no limit checking, the cartesian trajectory generator must be used

cautiously. The operator generates trajectories by supplying total time and nodes locations along the path. A node is considered a point where direction of motion changes. For instance, to describe a square trajectory would require: four corner positions, the total time, and sample rate to actually compute the values of position and velocity that would be saved as the desired position and velocity. The first node position is converted from cartesian position to joint position when being loaded into the control system just prior to execution of the trajectory. This operation provides accurate initial conditions in joint space. Inverse kinematics are performed by a newly developed routine INVKIN.FOR that is discussed in section 3.4.5. Generated trajectories are restricted to only 30 seconds in length and (arbitrarily) 20 nodes. Stored information includes; incremental positions and velocities, and the total requested time is shared equally in every segment of motion. Consequently, large differences in velocity can exist from segment to segment and no attempt to handle discontinuities at the nodes was made. This is a relatively minor error that is assumed small enough to ignore.

Because Duvall's algorithm was restricted to the LSI-11 for real time operations, trajectories were precomputed, stored in data files and downloaded to the LSI-11 just before testing. The LSI-11 has limited memory space which restricts trajectory storage in that space to approximately 1000 points. Duvall's assumption of v_0=0 required slow motion (lengthy trajectories) and with a sample rate of 14 msecs, 1000 points would last only 14 seconds. Duvall chose to use an interpolation scheme and thereby greatly increase the apparent number of points in the trajectory. Figure 3.6 illustrates the path computed between saved trajectory points.

Part (a) shows the approximation that occurs in a curve with only a few points and interpolation in between. Compare this against part (b) with the same number of points, but computed on the curve. This is the difference between the previous implementation at the coordinator level and the present implementation

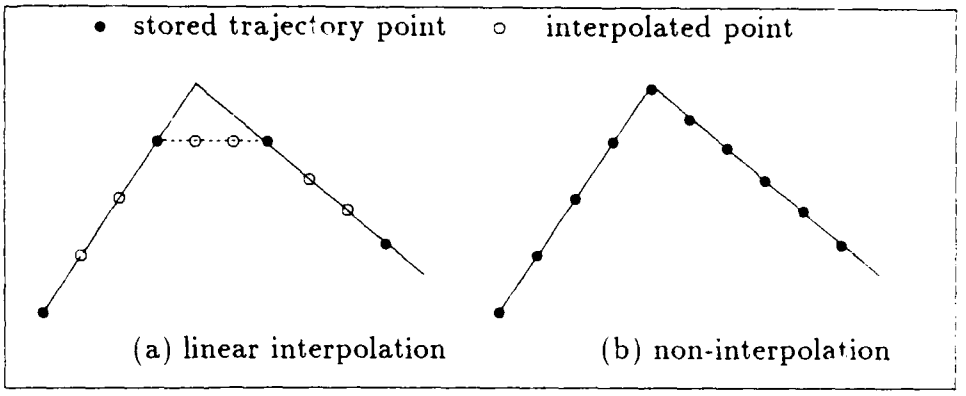

Figure 3.6. Comparison of trajectories: interpolated vs. non-interpolated.

at the organizer level. Analysis of benefits derived from this more accurate approximation was not accomplished but obviously the improved approximation will provide lower tracking errors and better performance. The new routine in FORTRAN on the VAXStation is designed to handle up to 6,000 points that each represent a value on the actual computed trajectory path.

3.4.5 Inverse Kinematics Routine Another new development is the inverse kinematics routine required by the trajectory generator to provide accurate initial conditions that match the first cartesian desired position point. The routine is an implementation of developments in Sectior 2.3 of [12] with the terms ARM and ELBOW both set equal to one. Restricting these two terms restricts the manipulator to operate in a subset of the full workspace and the further restriction to the xz plane limits operations substantially. This routine can be easily upgraded to three degrees of freedom by inserting ARM and ELBOW calculations.

3.5 Control Law Implementation

Any algorithm utilizing the ARCADE functions to operate the manipulator will contain a control law. This is the basic function of the ARCADE, to allow different control solutions to be implemented and hence tested on a standardized

interface using the same resources. The implementation of the various components of the impedance control law used in this thesis is presented next.

3.5.1 Control Law The control law implemented in this study is stated in Equation (3.2) and represented in block diagram form in Figure 3.7. This control law was translated from assembly code to FORTRAN and implemented on the VAXStation III in the form of a main routine and several subroutines. Functionality of the components of the algorithm will be discussed along with short development comments for completeness.

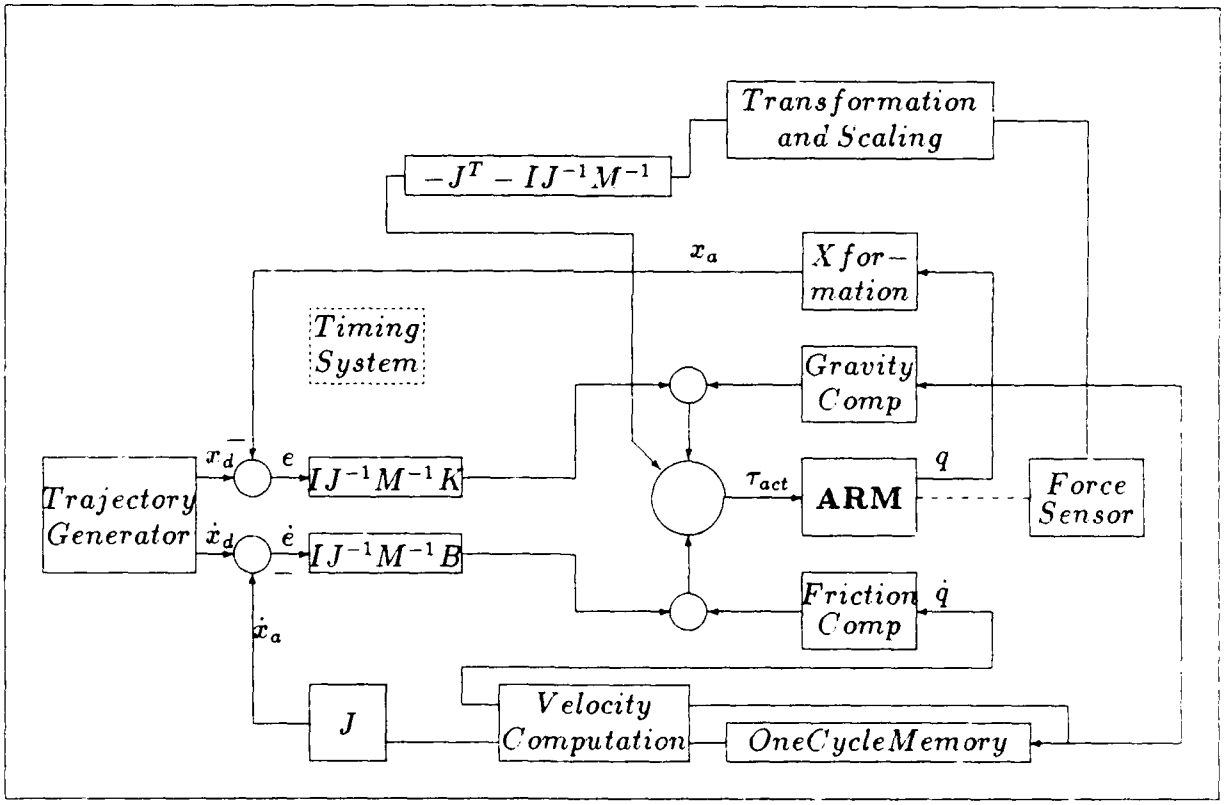

Figure 3.7. Control System in Block Diagram Form. System includes the Control Law and Parts of the Environment. All node inputs are summations except where indicated as subtractions.

$$\begin{aligned}\tau_{act} = \; & I(q)J^{-1}M^{-1}K[x_0 - L(q)] + S(q) \\ & + I(q)J^{-1}M^{-1}B[v_0 - J\dot{q}] + V(\dot{q}) \\ & - [J^T + I(q)J^{-1}M^{-1}]F_{int}\end{aligned} \tag{3.2}$$

A basic premise of the impedance control method, Figure 3.7, says a manipulator can be viewed as a second order system consisting of a spring, mass, and damper. This system is driven by an externally applied force and the measurement of system response is positional displacement resulting from applied forces and torques [15]. Hogan referred to this as the "desired dynamics" for the manipulator and Equation (3.3) is the mathematical statement of the desired dynamics model.

$$F_{int} = K(x_0 - x) + B(v_0 - v) + M\frac{dv}{dt} \tag{3.3}$$

This equation is implementable to any dimension but was restricted to the world xz plane as described previously. Later implementations should expand to at least three degrees of freedom to provide complete flexibility for the insertion task. Full details of the control law development are presented by Duvall [10, p3-6,appendix A] and are partially reproduced here as an aid to understanding. First, observe three error terms e, $\dot{e}$ and $\ddot{e}$ stated in the Equation (3.4).

$$\begin{aligned} e &= x_d - x_a \\ \dot{e} &= \dot{x}_d - \dot{x}_a \\ \ddot{e} &= \ddot{x}_d - \ddot{x}_a \end{aligned} \tag{3.4}$$

Using these error terms we can rewrite Equation (3.3) as:

$$F_{int} = Ke + B\dot{e} + M\ddot{e} \tag{3.5}$$

Applying the Laplace transform, and the knowledge that all three error terms are functions of time, we obtain the transfer function:

$$\frac{E(s)}{F_{int}(s)} = \frac{1}{s^2 + \frac{B}{M}s + \frac{K}{M}} \tag{3.6}$$

This transfer function has a characteristic equation of the form:

$$s^2 + 2\zeta\omega_n s + \omega_n^2 \tag{3.7}$$

or, substituting from the previous equation:

$$s^2 + \frac{B}{M}s + \frac{K}{M} \tag{3.8}$$

Using classic pole placement techniques [8] and the requirements of the task, we obtain the two poles of the closed loop system.

$$s = \sigma \pm j\omega_d \tag{3.9}$$

where

$$\sigma = -\zeta\omega_n \tag{3.10}$$

and

$$\omega_d = \omega_n\sqrt{1-\zeta^2} \tag{3.11}$$

Selection of B, K, and M provides particular parameters σ, ζ, and ω_n for a control system to handle task requirements. For this application, ζ was selected over-damped ($\zeta \geq 1$) to guard against overshoot and possible instabilities. This forces a relationship between M, B, and K, but not the exact values. Scaling of these values is the designer's degree of freedom for fitting control to the different task requirements. Selection of these values will be discussed in Chapter four.

3.5.2 Gravity Compensation Some terms of the torque computation are not modified by the impedance gains but use unique models for computing torque contributions. One of these, as seen in the block diagram of the control law in Figure 3.7, is gravity compensation ($S(q)$).

Gravity compensation for a two degree of freedom vertically articulated robot is:

$$\begin{aligned} S_1 &= S_2 - ga_2m_3cos(q_2)) + gm_2[y_2sin(q_2) - (x_2 + a_2)cos(q_2)] \\ S_2 &= -gm_3[(x_3 + a_3)cos(q_2 + q_3) - z_3sin(q_2 + q_3)] \end{aligned} \tag{3.12}$$

where:

g is gravity $= 9.8\ meters/sec^2$

a_2, a_3 are the D-H parameters for links 2 and 3

m_2, m_3 are the masses for links 2 and 3

x_3, z_3, y_2 are the first moments of those axes [10, p3-20]

This compensation development was taken from Duvall's original implementation since no changes in configuration have occurred. Duvall derived this form using MACSYMA to solve the equations [10, p 3-20].

3.5.3 Forward Kinematics The forward kinematics function is used to transform joint angles q to cartesian position x and orientation if there are more than three joints. The forward kinematics function was limited to the xz plane by Duvall and also for this thesis, but needs only minor modifications to be capable of 3-DOF operation. The forward kinematics equations can be found in [12, p45] and represent the terms in the homogenous transformation matrix:

$$\begin{bmatrix} n_x & s_x & a_x & p_x \\ n_y & s_y & a_y & p_y \\ n_z & s_z & a_z & p_z \\ 0 & 0 & 0 & 1 \end{bmatrix}$$

where n, s, and a are the normal, sliding and approach vectors as described in section 2.2.11 of Fu, Gonzalez, and Lee [12, p 41]. All terms must be computed for use later in transforming forces and moments into world coordinates from the sensor tool frame but the position terms (p_x, p_y, p_z) are computed to find x from q. These equations were determined under the assumption $q_1 = q_4 = q_5 = q_6 = 0$ and were:

$$p_x = d_{64}sin(q_2 + q_3) + a_3cos(q_2 + q_3) + a_2cos(q_2)$$

$$
\begin{aligned}
p_y &= d_2 \\
p_x &= d_{64}cos(q_2+q_3) - a_3sin(q_2+q_3) - a_2cos(q_2) \qquad (3.13)
\end{aligned}
$$

where d_{64} is the combined length of $d_6 + d_4+$ the tool length.

3.5.4 Jacobian and Inverse Jacobian The Jacobian operation translates torques in joint space into forces in cartesian space and joint velocities into cartesian velocities. It is obviously an integral part of the impedance controller and is a function of the position. A very complete discussion of the Jacobian is found in [12, appendix A]. For the restricted operations described in this thesis, the Jacobian is only 2x2 and is:

$$
\begin{bmatrix}
\frac{\partial p_x}{\partial q_2} & \frac{\partial p_x}{\partial q_3} \\
\frac{\partial p_z}{\partial q_2} & \frac{\partial p_z}{\partial q_3}
\end{bmatrix}
$$

Duvall derived an expression for the Jacobian by using MACSYMA and solving the kinematics equations symbolically [10, p 3-17]. The equations resulting from that derivation are:

$$
\begin{aligned}
J_{11} &= d_{64}cos(q_2+q_3) - a_3sin(q_2+q_3) - a2sin(q_2) \\
J_{12} &= d_{64}cos(q_2+q_3) - a_3sin(q_2+q_3) \\
J_{21} &= -d_{64}sin(q_2+q_3) - a_3cos(q_2+q_3) - a2cos(q_2) \\
J_{22} &= -d_{64}sin(q_2+q_3) - a_3cos(q_2+q_3) \qquad (3.14)
\end{aligned}
$$

The inverse Jacobian is also used in the control law and Duvall derived the inverse jacobian also using MACSYMA and the resulting equations are:

$$
\begin{aligned}
J_{11}^{-1} &= \frac{1}{\Delta}[d_{64}sin(q_2+q_3) + a_3cos(q_2+q_3)] \\
J_{12}^{-1} &= \frac{1}{\Delta}[-d_{64}cos(q_2+q_3) + a_3sin(q_2+q_3)] \\
J_{21}^{-1} &= \frac{1}{\Delta}[d_{64}sin(q_2+q_3) + a_3cos(q_2+q_3) + a_2cos(q_2)] \\
J_{22}^{-1} &= \frac{1}{\Delta}[-d_{64}cos(q_2+q_3) + a_3sin(q_2+q_3) + a_2sin(q_2] \qquad (3.15)
\end{aligned}
$$

where $\Delta = a_2[a_3sin(q_3) - d_{64}cos(q_3)]$ [10, p3-17].

3.5.5 Impedance Coefficients Used to enforce the desired dynamics on the control system, the impedance coefficients $(IJ^{-1}M^{-1})$, $(IJ^{-1}M^{-1}B)$, $(IJ^{-1}M^{-1}K)$, $(IJ^{-1}M^{-1}BJ)$, and $(J^T + IJ^{-1}M^{-1})$ are all computed in each cycle by an offline subroutine. The M, K, and B terms are all diagonal matrices and are input as control parameters for each unique application. The inversion of the mass matrix is a simple division since it is diagonal. All other terms are available from previous developments.

3.5.6 Inertia Tensor The inertia tensor matrix (I) is fully populated and describes the coupling of forces from each link of the manipulator to all others. Duvall [10, p3-18] derived this tensor using MACSYMA and under the same configuration assumptions stated previously.

3.5.7 Velocity Tracking A special point of interest here is the inclusion of velocity tracking. The velocity terms from Duvall's control law, [10, eq 3-20]

$$- IJ^{-1}M^{-1}BJ\dot{q} + V(\dot{q}) \tag{3.16}$$

became:

$$IJ^{-1}M^{-1}B[v_0 - J\dot{q}] + V(\dot{q}) \tag{3.17}$$

which is the same as Hogan's [16] original development. The values for v_0 were provided by the trajectory generator presented in Section 3.4.4.

3.5.8 Control of Other Joints Joints 1,4,5,and 6 are not controlled by the impedance control law but instead use a standard proportional derivative control law implemented in joint space. The computed torque is given by

$$\tau = K_p(q_d - q_a) + K_v(\dot{q}_d - \dot{q}_a) \tag{3.18}$$

and since:

$$q_d = \dot{q}_d = 0 \tag{3.19}$$

the control law becomes:

$$\tau = -K_p q_a - K_v \dot{q}_a \tag{3.20}$$

Values of K_p and K_v for joints 4,5, and 6 were selected to provide some stiffness but joint one K_p was selected relatively soft to allow for possible passive compliance in the refueling insertion task.

3.6 Friction Compensation

Friction compensation is absolutely necessary for smooth low velocity motion. To compensate for the friction of motion in the manipulator, that friction must be known or well estimated. Stated otherwise, a valid model must be formed. An accurate friction model is particularly difficult to accomplish but the general characteristic has been established through many studies [38,7,6,39,4,13,40,14]. Figure 3.8 represents such a characteristic that includes coulomb and viscous friction effects. The coulomb level is set at approximately 90% of the experimentally determined stiction level providing some stiction compensation.

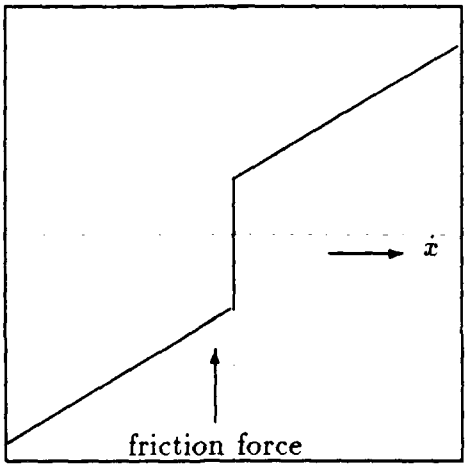

Figure 3.8. Composite Friction Model

As described in the Literature Review chapter, this model may have many distortions such as non symmetric viscous components, position and direction sensitivity, and higher order effects as yet unlabeled. The area most difficult to accurately examine is of course near zero velocity. This is especially true in the implementation of a compensation scheme. Many of the research efforts reviewed in the literature review were concerned with an implementable scheme and adjusted the models accordingly. Linear approximations of higher order equations can be used successfully if models are well chosen. To assure a good approximation, the important parameters of a friction model would include:

- slope of the viscous friction component,
- level of the coulomb friction component, and
- switching point for changing to viscous + coulomb from stiction.

This model represents the system now being used quite effectively in most algorithms running on ARCADE. It was chosen primarily because the parameters for this model were already available and success of the compensation was considered confirmation of acceptable accuracy. These parameters were experimentally determined in [29]. Equation (2.4.2) is repeated here so values can be matched with parameters used and to aid the explanation.

$$\tau_f = \begin{cases} \tau_c sgn(\dot{q}) & (|\dot{q}|) > d \\ \tau_c sgn(\tau_m) & (|\dot{q}|) \leq d \end{cases}$$

where:

τ_c is the compensation torque (90 % of experimentally determined value for stiction)

sgn($\cdot$) is the function returning the sign of its argument

$\dot{q}$ is the joint velocity in rad/sec

τ_m is the torque supplied to the motor

d is a velocity threshold also determined experimentally

Only two parameters were not selected. The first was the switching level and its source and the second was the velocity value to be used in the low velocity region. This second parameter is critical since it will determine the *direction* (but not magnitude) of the torque applied due to friction compensation. If this controlling function is not stable into and throughout the low velocity region between the switching limits, performance can actually be degraded, perhaps even to the point of limit cycles with the amplitude of the coulomb stiction. Because the impedance controller was expected to be used with relatively slow trajectories for validation tests, this parameter would be important throughout the trajectory. Several available velocity tracking terms were considered and computed velocity torque was selected. Computed velocity torque was discarded as a controlling value for the switching function after sharp transitions were observed in the friction torque characteristics. Joint velocities were tested in the switching controller role and found to provide smooth transitions. The threshold value of 0.01 was selected by experimentation.

3.7 Summary

The ARCADE environment used to test control algorithms has been modified and restructured to provide an environment for testing force feedback control laws and perform experiments in cartesian space. These modifications consisted of translating several basic functions from the coordinator level to the organizer level and generating several new functions to be used at the organizer level. Overall, the ability to develop, test, and adjust a control algorithm has been greatly enhanced. Duvall's impedance control law was translated to the FORTRAN level and improvements installed in preparation for testing. Results of translation, rehosting and improvements are presented in the next chapter.

IV. Results and Evaluation

4.1 Overview

A new compliant control architecture has been developed on the ARCADE system at AFIT. The purpose for development of this system was to develop compliant motion control laws for Air Force applications. The initial application was a two degree of freedom impedance control law developed by Hogan and modified by Duvall for a PUMA-560 robotic manipulator. The primary impetus for applying this control law to the PUMA was to demonstrate a refueling task. To accomplish this goal, modifications noted in the previous section were applied to the algorithm and/or the environment. In order to evaluate these corrections before attempting the refueling operation, controlled testing was necessary. Previous chapters have presented: the original control law, the required modifications, and the implementation of that modified control law. This chapter will present results of tests designed to verify equipment functionality, previous performance capabilities, and performance improvements. To provide a valid comparison, many operating parameters from Duvall's implementation were held constant during initial verification tests. After performance verification was completed, the refueling demonstration was performed and results were analyzed.

4.2 System Verification

ARCADE underwent several modifications and some new capabilities such as cartesian trajectory generation were added to the system. These changes required functionality verification. This section covers those tests and briefly analyzes test results.

4.2.1 Force Sensor Testing A critical requirement for implementing the impedance control algorithm of this thesis is force feedback. The force sensor

channel must be sensitive, accurate, and reliable. Duvall tested the sensor system and derived deadband limits based on worst case repeatability performance [10, p 5-2]. Similar tests were not repeated but proper operation was verified after software modifications were accomplished. Sensor outputs are scaled and translated into world coordinates. Scaling and axis sensitivity were verified using several one kilogram masses and positioning the sensor in different orientations while measuring force outputs. A more formal procedure was not devised since calibration was accomplished in the previous effort. Load limit testing was not necessary.

4.2.2 Trajectory Generation Testing The cartesian trajectory generation did not require rigorous testing. Original development troubleshooting was accomplished using calculated positions for trajectory start and stop points. Position plots indicated no computed errors. One implementation error was the round off created by forcing each trajectory segment between two nodes into an integer number of control law sampling periods. This error is very small relative to the overall trajectory and was not examined extensively. Another error was in the velocity computations. No effort was made to smoothly compute velocity transients, and this effect was examined by sampling several generated trajectory files for velocity spikes. In both moving trajectories used for testing, the velocity plots were discontinuous at the node points.

4.2.3 Timing System Tests The timing system was tested upon installation and again after the system overhaul (see Section 3.4.2). Tests consisted of frequency measurements using a frequency counter and signal quality examination using an oscilloscope. Frequency was found to be within 1 μsec of the requested value using sample sizes of 1000 points. Signal quality was acceptable but contained low amplitude reflected wave effects.

4.3 Evaluation of Previous Tests

Control law parameters such as the impedance coefficients, gravity, and friction compensation were not tested independently but instead as a composite of the control law performance which was then compared against previous results obtained with this control law before improvements. This verification procedure was designed to assure the control law was performing at previous levels as a minimum.

4.3.1 Tests Performed Three tests were designed to duplicate (as much as possible) Duvall's tests. Two trajectories were selected (see Figure 4.1) with one being used twice. The terminal points of each trajectory are listed in Table 4.1. The stationary trajectory was selected to test the stability of the control law and was identical to Duvall's except for the length of time. The linear trajectory was chosen because it is the simplest motion possible that will excite all error modes of the control law. Also as a control on the experiment, the path of the new linear trajectory was made similar to Duvall's linear trajectory and control law parameters were kept the same. Because the tests done in this effort used a faster sampling rate and no trajectory interpolation, implementations were not completely identical.

Table 4.1. Endpoints of the generated trajectories. All values are in meters. Note only X and Z positions are given since Y position is fixed at 0.14909.

Trajectory		X position	Z position
Stationary	Start	-0.020320	1.2703700
	Stop	-0.020320	1.2703700
Linear	Start	-1.000000	0.0500000
	Stop	-1.000000	-0.299930

To best simulate Duvall's trajectories, a 30 second time interval was used.

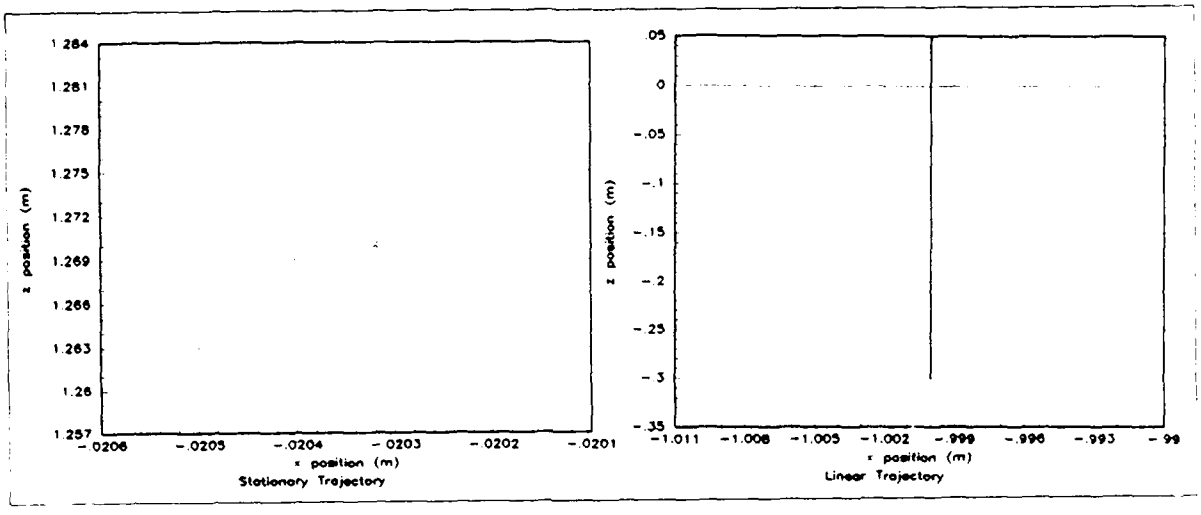

Figure 4.1. Trajectories used for testing improved control law performance. Both plots are in the XZ plane as seen from a positive Y viewpoint.

The new control law no longer required very slow motion to validate the assumption v_0=0, but fast rates do cause large transient forces at contact, a condition that might result in damage to the sensor, so fast motions were avoided for this implementation. Duvall's tests were somewhat longer than those in this research. He used times of 80 seconds for each track [10, p 5-12] and this research limited the time to 30 seconds per test because comparison of tests run at 60 seconds showed no perceptible performance degradation as compared to the 30 second trajectory. Therefore, the 30 second trajectory was used to shorten computation time and data storage.

4.3.2 Conditions for Test: Control Law Parameters Some parameters of the control law are fixed by task requirements or limits of theory. In Section 3.5.1, ζ was restricted by safety needs. Another restriction on these system parameters is the requirement to keep

$$\sigma \geq \frac{-0.1}{T_s} \tag{4.1}$$

where T_s is the sampling rate for the system, which was selected to be 5.4 msecs for all tests (Section 3.4.3.2). Solving this equation we have

$$\sigma \geq \frac{-0.1}{T_s} = \frac{-0.1}{5.4X10^{-3}} = -18.52\, rad/sec \tag{4.2}$$

This restriction is necessary to prevent pole warping caused by approximating a discrete time control system as a continuous time system for computing control parameters [19]. These restrictions were imposed during selection of control law parameters M, B, and K for trajectory tracking tests. Impedance coefficients are controlled by the desired dynamics model which is second order with selectable parameters. These parameters include the ζ and ω_n which provide M, B, and K, resulting in the desired settling times and overshoot. Many factors control the selection of these parameters. Performance comparison was considered critical to verification so ζ and ω_n were chosen to match the previous research even though the new sampling rate allows much higher bandwidth. Gain magnitudes are the only other selection since the relative magnitude of gains is fixed by the control law definition. This is the mechanism by which 'stiffer' and 'more compliant' gains were selected. Gains were adjusted in stiffness to examine the amount of force applied. No empirical data was taken in this process, but in general, stiffer gains tracked better and maintained higher interface force than softer gains. Of course to assure stable, well damped responses, the limit $\zeta \geq 1$ was observed. Table 4.2 presents the parameters used for each test trajectory.

4.3.3 Results and Analysis Actual tracking results indicate significant performance improvements. Table 4.3 indicates the maximum and terminal errors for both trajectories in free motion and compares the original control law's performance values against the updated control law's. Performance improvement was measured by observing trajectory tracking errors of the improved control law versus tracking errors recorded by Duvall under similar conditions. Also important were

stability, continuous surface contact when constrained, and no excessive build up of interface forces. Sufficient detail of collected data is presented here to illustrate desired performance while more complete data sets are provided in appendix A. Stability was demonstrated by the convergent nature of the position errors for both the stationary and the unconstrained linear trajectories. For the constrained linear routine, controlled motion is maintained even while large position errors build up.

4.3.3.1 Stationary It was considered an essential baseline that the manipulator could remain stationary under the most benign of conditions and this trajectory represents those conditions. In the fully vertical position (0,-90,90,0,0,0 joint angles), gravity is nulled and there is no interface force to contribute to calculated torques. If the impedance model is stable, only friction compensation will not reach a steady state value since it is *designed* to never null. Errors in the plane are plotted in Figure 4.2 and are seen to reach steady state values quickly and are very small. These steady state values were: in the x direction, 1.1 millimeter and the z direction, 0.026 millimeter. Of course, with an effective arm length of 1270.37 millimeters, that is equivalent to approximately 0.1 degrees of total angular error. Furthermore, the arm held steady at the commanded position without any motion and errors never changed after reaching steady state. Interface force value were not involved since no contact occurred. Other stationary tests were performed

Table 4.2. Critical control parameters selected for each test. Note the selected values are for both joints, i.e. K is the value used for both K_{11} and K_{22}. Likewise for all other values.

Test	Trajectory	ζ	ω_n	M	B	K	F_{int} threshold
T1	Stationary	1.2	7.0	10.204	171.43	500.0	Forces ±6 n
T2	Linear	1.2	7.0	10.204	171.43	500.0	Moments ±2 nm
T3	Linear	1.2	7.0	10.204	171.43	500.0	for all cases.

in different attitudes with similar results. The stationary case was found to be very stable in all positions. Steady state errors are normal in a PD loop, but in this case some error may have been due to numerical accuracy of the forward kinematics routine. This steady state error problem occurred in all stationary tests conducted but never produced values significantly larger than recorded here.

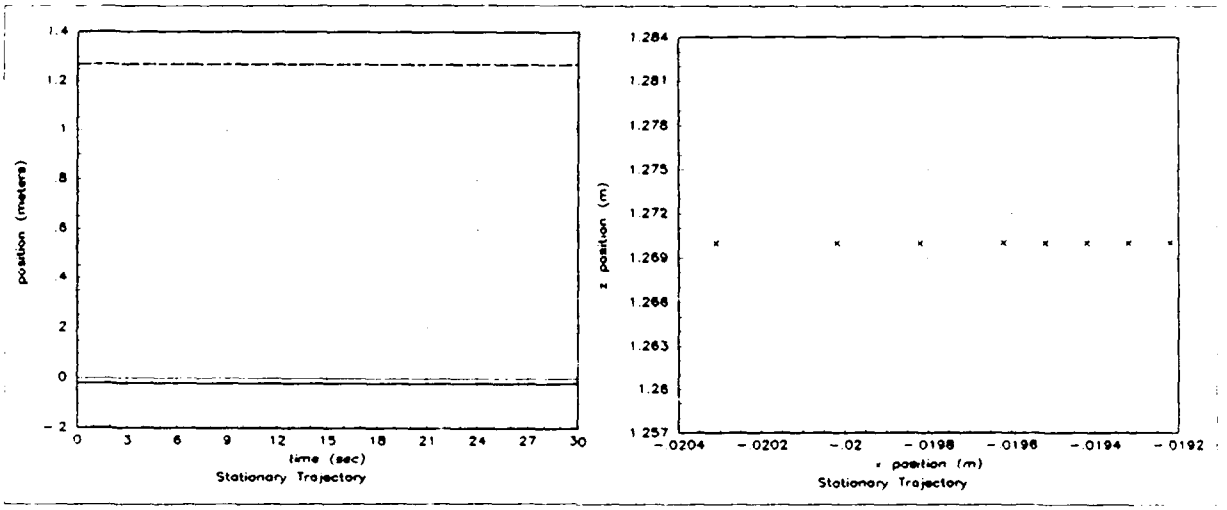

Figure 4.2. Stationary trajectory tracking. Left: X and Z against time. X is solid, Z is dashed. Right: X and Z in a spatial representation of the workspace.

4.3.3.2 Linear The linear trajectory was tested in free motion first. Free motion requires coordinated movement of the two joints under compliant control. This is a difficult tracking test since the motion is contrary to the natural motion of a revolute system. Results are displayed in Figure 4.3 and tabulated in Table 4.3. Cartesian position tracks the trajectory very well. The manipulator exhibited jerky motions even though the magnitude of variations was reduced from the original implementation. The jerky motion is attributed to the gear backlash of the heavy links of the robot. This backlash effect was pronounced because the PUMA was in need of adjustment. The system was stable and no contact forces were generated.

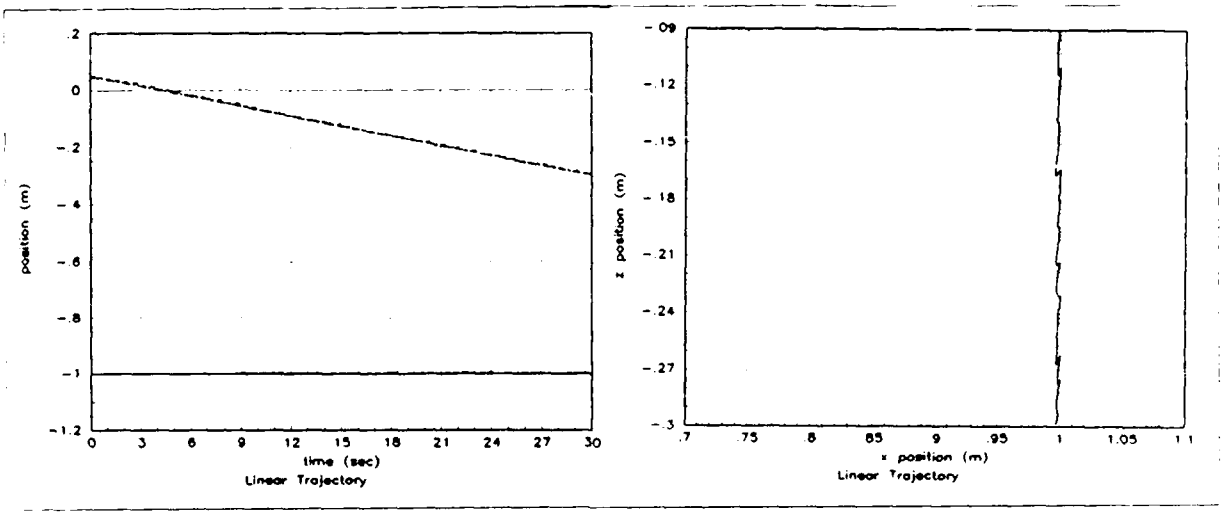

Figure 4.3. Unconstrained linear trajectory tracking. Left: X and Z against time. Right: X and Z in a spatial representation of the workspace.

To perform the constrained linear motion test, a constraint (refueling mockup) was placed in the trajectory path so that it was encountered at about 22 seconds into the 30 second trajectory. Results of the constrained linear test are plotted in Figure 4.4. For this trajectory, it is important to note the system remained stable as position errors built up. Interface force also accumulated and did not cause instability.

The x axis error seems to be well controlled throughout all three parts of the constrained trajectory. In free motion, it only develops about 4 millimeters of error at maximum. Contact was smoothly engaged and constrained motion errors build up smoothly during the constrained portion of the trajectory. In general, the x axis seems well controlled. Because there is no commanded motion in the x axis this could be misleading. The z axis shows a definite oscillation pattern of low amplitude error during free motion that is quelled out during constrained motion. This oscillation may be caused by a nonlinear friction effect, resulting in a stable limit cycle. Plots of joint velocities indicate a cyclic variation between

Table 4.3. Tracking errors from free motion tests. All values are in meters. Two left columns are from Duvall's results [10], two right columns from the upgraded control law. The two entries (n/a) were not available but estimated to be 0.001 m from plots.

	Original			Improved	
Trajectory	X errors	Z errors		X errors	Z errors
Stationary	0.0150	n/a	Maximum	-0.0011	-2.599E-5
	0.0150	n/a	Terminal	-0.0011	-2.599E-5
Linear	0.0270	-0.0680	Maximum	-0.0041	-0.0077
	0.0060	-0.0280	Terminal	-0.0026	-0.0012

the friction compensation formats above and below the switching point defined in the friction model. A high correlation between spikes of joint velocity and position errors also exists. The cause of this limit cycle is not fully understood but some attributes of the effect were observed. Note the increase in amplitude and frequency of the error after contact even though position error has smoothed out. The position error may only be smooth because of the physical constraint. Another characteristic of this constrained trajectory is the shared position error after contact. Position error after contact should ideally all be in the z direction for this trajectory. Plots indicate this is not so. Joint five is driven with soft gains and allows some displacement which in turn causes a sliding motion of the entire structure producing the displacement seen in the plots.

Torque plots of the constrained linear trajectory (Figure 4.5) show how the force feedback generates torques to prevent excessive force buildup. As position errors build up, position torque increases. Concurrently, building displacement results in increased sensed force. The torque generated by the sensed force is opposite the position torque so the force tends to cancel the increase in position torque. This is the active compliance effect of the impedance control law which results in a total

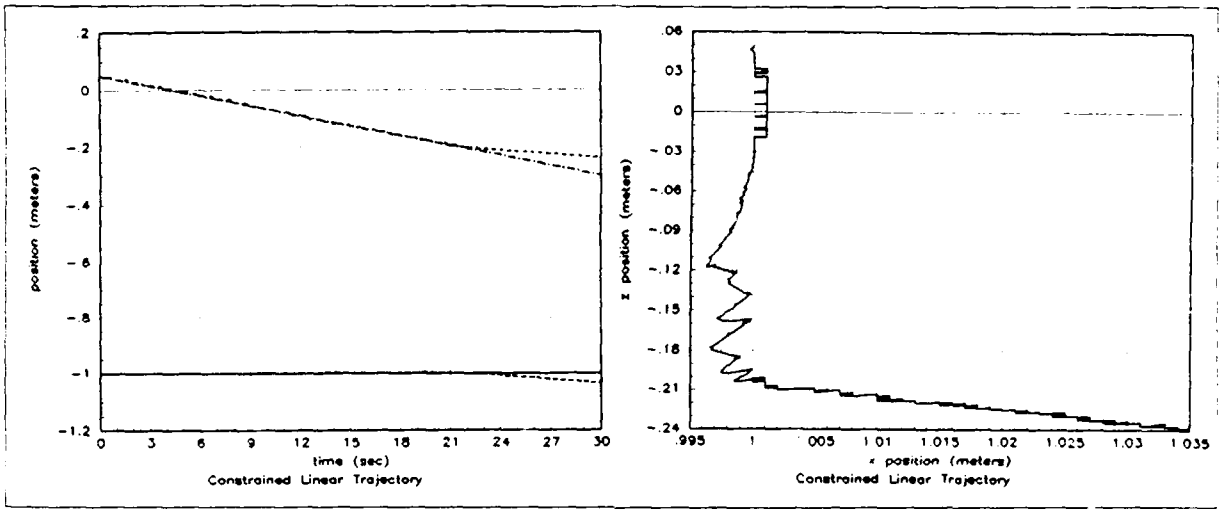

Figure 4.4. Constrained linear trajectory tracking. Left: X and Z against time. Right: X and Z in a spatial representation of the workspace.

torque that smoothly maintains interface force within an acceptable limit.

All three verification tests displayed marked performance improvements over the original control law developed by Duvall. All were stable in free motion, tracked more accurately than the original control law, and the constrained motion test demonstrated the ability of the control law to accept large position errors and remain stable. Therefore, the control law has been verified and the improvements have been successful in increasing performance. The only measurements of performance available for comparative analysis were the position tracking errors which have been significantly reduced from the original implementation. These results clearly validate the positive effect of system improvements to the AFIT compliant control environment and demonstrate the potential of impedance control concepts.

4.4 Refueling Demonstration Tests

The need to effectively implement impedance control on a heavy industrial manipulator was derived from the refueling task description. All functions of the

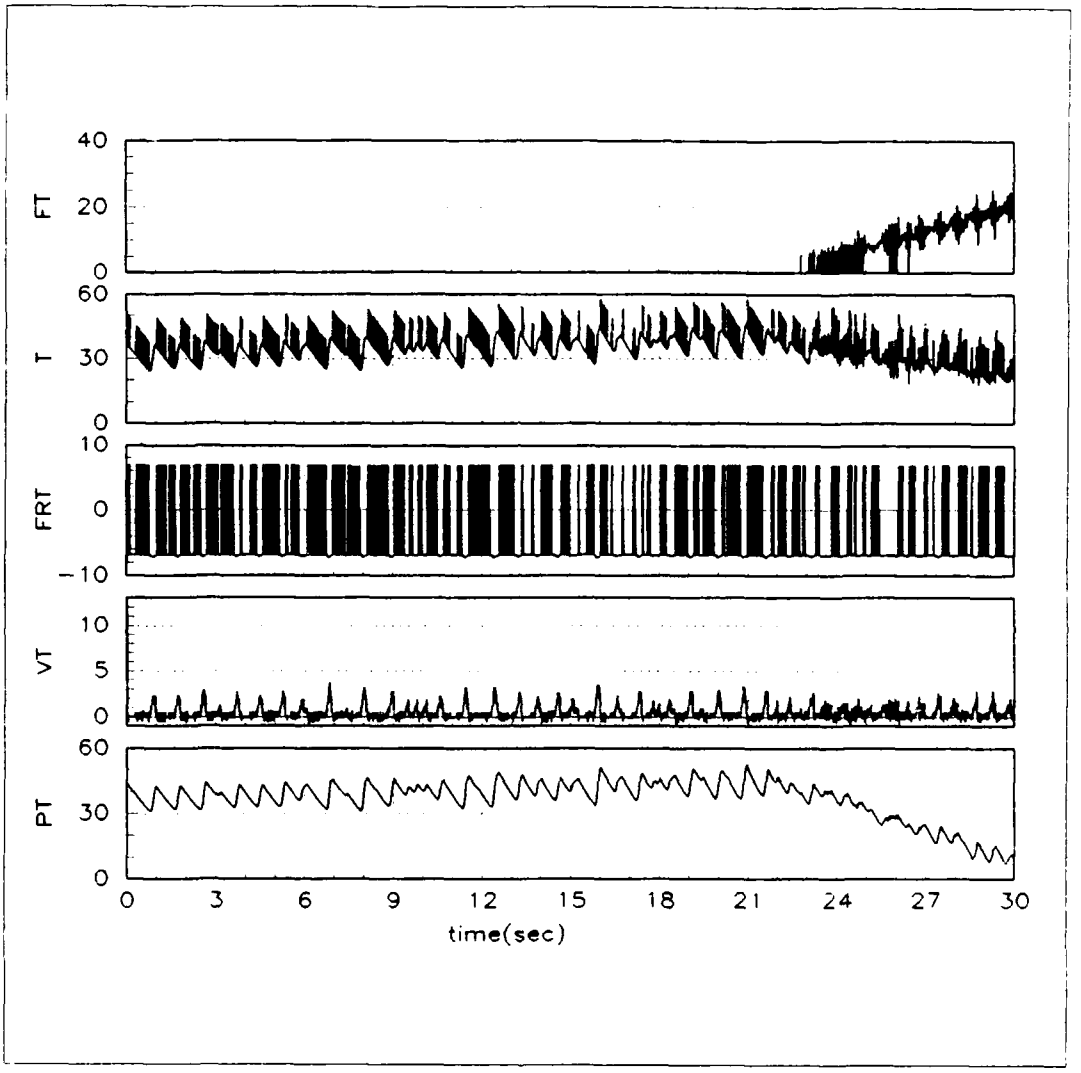

Figure 4.5. Various computed torque contributions and the summation for Joint 2 during the constrained linear trajectory. See text for explanation of terms.

control law, compliant motion testing environment, and various compensations were prepared to accomplish this one operation of performing a refueling connection demonstration. Control law validation through baseline tests showed performance gains over previous AFIT research [10]. The remainder of this section is the report and analysis of the refueling demonstration results.

4.4.1 Tests Performed The basic requirement of the trajectory was the three portions of any compliant task: free space motion, surface contact, and constrained motion. The simplest trajectory to accomplish these requirements consists of two segments, a vertical drop and a forward sweep. This trajectory was designed to drop onto the refueling port slipway with commanded position going *below* the slipway surface and then moving forward into the refueling receptacle. This motion provided continuous contact with the environment in the constrained case. Figure 4.6 provides more detailed information concerning this path. Note that only position is considered and not orientation. The trajectory was tailored to have the correct orientation since two degrees of freedom will not overcome misalignments that are out of the xz plane. Also, times for each stage of the process are not established since the position of the refueling port is not fixed. The trajectory was traced without the port first to test the freespace tracking and align the refueling port. Manual alignment is necessary for a planar controller. Extension of the controller to a third axis is the subject of future research.

4.4.2 Conditions for Test The refueling trajectory tested performance of the intended purpose by testing the component parts of the process. In chronological order these parts included:

- gain contact with the slipway,
- enter the refueling receptacle,
- maintain surface contact,

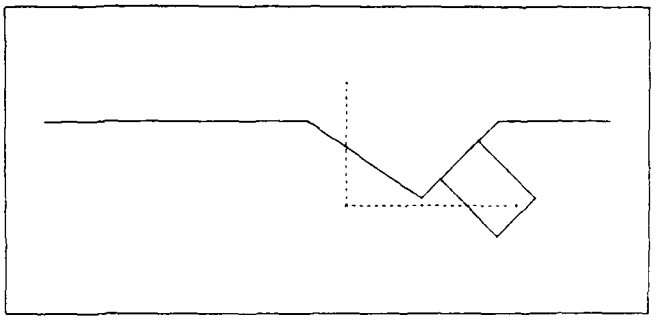

Figure 4.6. Refueling trajectory from positive Y viewpoint into the XZ plane. Note the track is *beneath* the refueling port.

- overcome jamming at the receptacle, and
- apply minimal force to the surface.

The values for M, B, and K displayed in Table 4.4 were selected by trial and error with a sequence of gains used to determine a set of values that would indeed minimize interface force and still maintain contact. The values selected provided very satisfactory performance of both requirements.

Table 4.4. Critical control parameters selected for refueling trajectory tests. Note the selected values are for both joints, i.e. K is the value used for both K_{11} and K_{22}. Likewise for all other values.

Test	Trajectory	ζ	ω_n	M	B	K
T4	Refueling	1.2	7.0	10.204	171.43	500.0
T5	Refueling	1.2	7.0	2.041	34.29	100.0

4.4.3 Results and Analysis The unconstrained refueling test reaffirmed the freespace trajectory tracking capabilities of the impedance control law and demon-

Table 4.5. Tracking errors from the unconstrained refueling trajectory test. All values are in meters.

Trajectory		X errors	Z errors
Refueling	Maximum	-0.0345	-0.0606
	Terminal	-0.0345	-0.0604

strated stability. Proper force sensor operation resulted in no interface force being generated. The path of the probe through the trajectory is displayed in Figure 4.7. Table 4.5 enumerates values of maximum and terminal position errors for the unconstrained case. Tracking errors are very acceptable but motion is not as smooth as was anticipated even though significantly smoother than before the improvements were made.

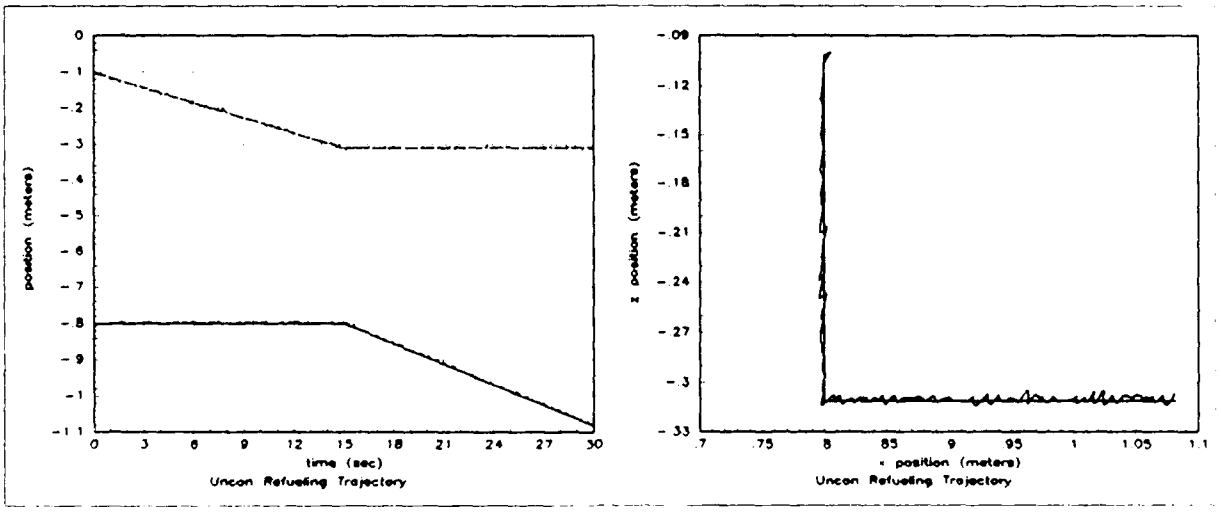

Figure 4.7. Unconstrained Refueling trajectory tracking. All values are in meters. Left: X and Z positions plotted as a function of time. X is on the lower half of the plot, Z the upper. Right: Same values plotted against each other.

The constrained refueling trajectory was successfully followed and force feedback successfully maneuvered the refueling probe to accomplish a smooth peg-in-the-hole operation and demonstrate the refueling concept. Position errors form the test of this trajectory (i.e. a refueling demonstration) are plotted in Figure 4.8. Several important points in the trajectory are easily seen from these plots. Three points in time will be identified for reference. At approximately 10 seconds, the probe first contacts the slipway. Once contact begins, it is never lost. At the 15 second point (half way through the trajectory), the trajectory changes from vertical motion to horizontal motion. At approximately 28 seconds, the refueling probe steps over the entry lip and enters the refueling receptacle. These three transitions are quite distinctive in some data streams such as cartesian position errors and interface forces. All data plots are available in the Appendix, but a representative sample will be reproduced here for clarity in presentation.

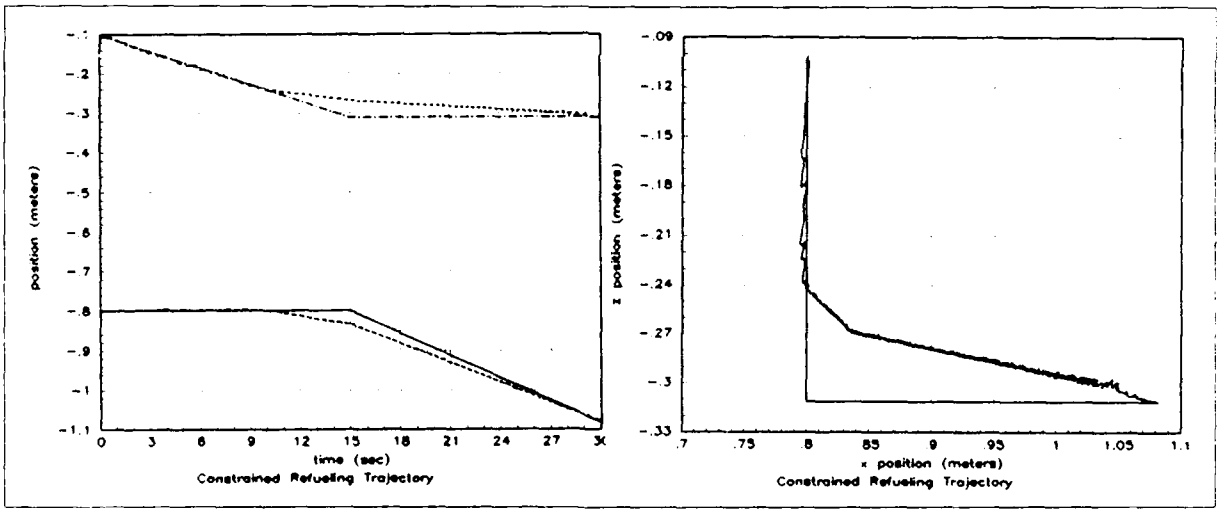

Figure 4.8. Constrained refueling trajectory tracking. Left: X and Z against time. Dotted traces are actual trajectories, X on lower half of plot, Z on upper. Right: X and Z in a spatial representation of the workspace.

The plot of cartesian position errors (Figure 4.9) is very revealing for this trajectory. Prior to contact, the characteristics of the tracking errors are seen to

be different for the two joints. Frequency content and amplitude of these two error streams are significantly different. This could be caused by using the same control law for the two very different physical links. If so, improved performance might be gained by adjusting the control law to account for the physical differences. Once contact is made the position errors begin to build up rapidly. Commanded motion is in the vertical direction only until the 15 second point so the expected error is only in the z direction. Actually, the error is shared almost equally between the x and z directions as shown in Figure 4.9.

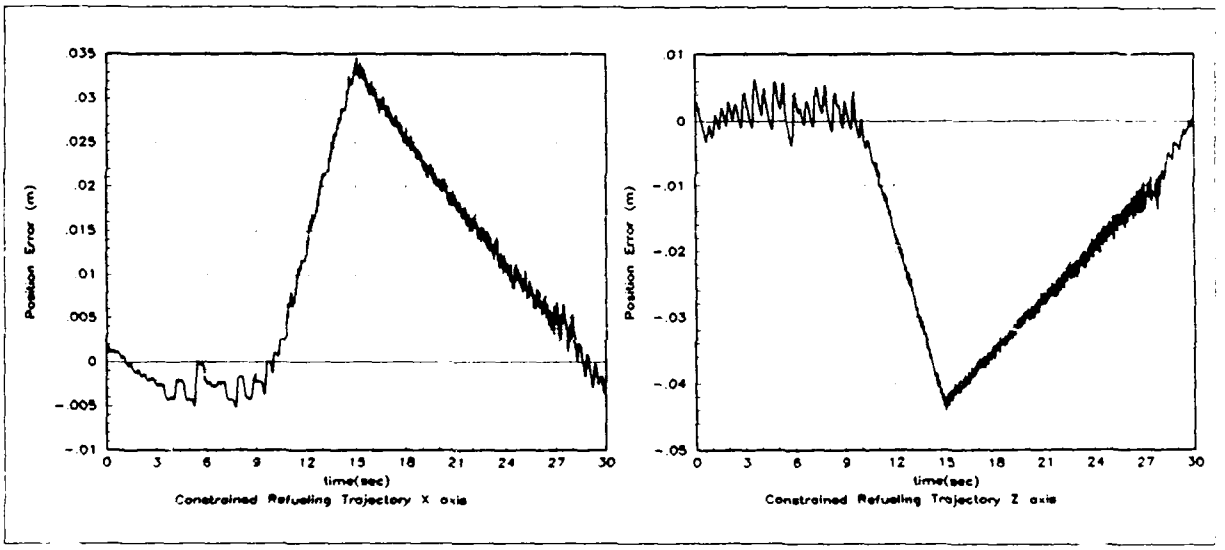

Figure 4.9. Cartesian position errors for the constrained refueling trajectory. Left: X axis Right: Z axis

The force generated (see Figure 4.10) is all in the z direction as expected. The control law will split this input into two torques based on the impedance coefficients. This force splitting is seen in the plot of force torques in Figure 4.11, which shows similar torque profiles being applied to both joints 2 and 3 to counteract the continually increasing position tor ue (Figure 4.12) developed from the position error. The results of these operations are seen in the total torque in Figure 4.13. Total torque is the value converted to motor currents. Figure 4.13 shows

a characteristic that is relatively flat over the entire test. This active compliance capability is the reason impedance control is ideal for application to the refueling task.

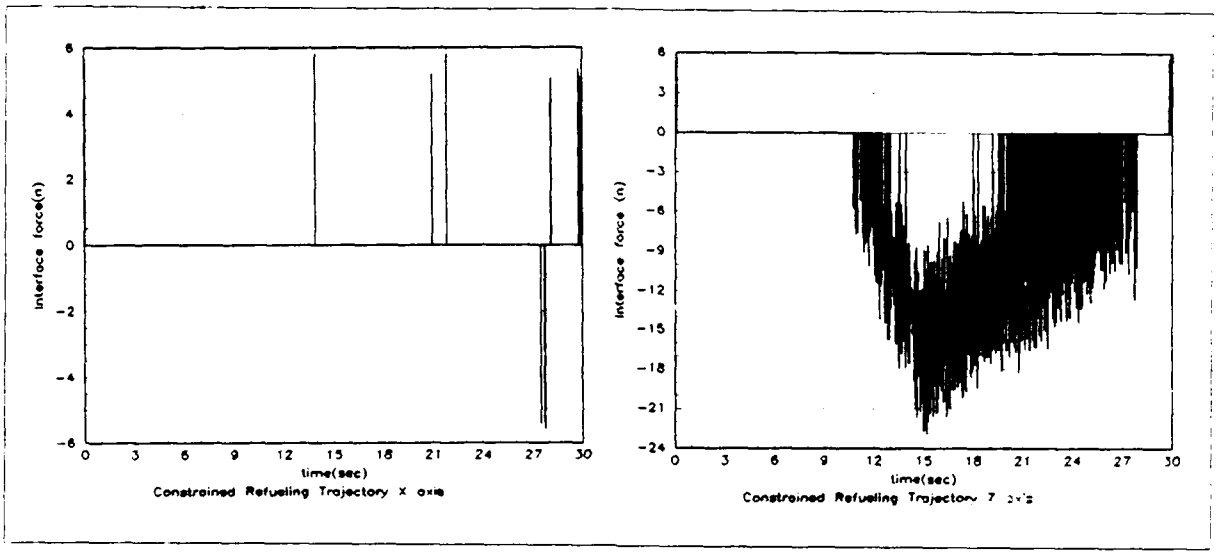

Figure 4.10. Interface Force for the Constrained Refueling Trajectory. Left: X axis Right: Z axis

As the probe moved down the slope, position errors decreased and likewise interface forces lessened. This trend continued until the probe encountered the metal housing around the receptacle. The lip at the bottom of the slipway was an obstacle that was detected and compensated for. The probe slipped into the receptacle and the nature of the motion changed. Obviously, motion was much more restricted once a connection was completed, and data plots show more damped operation once the probe is connected to the receptacle.

It is important to note that trajectory tracking was never lost even when position error was greatest. The full trajectory was completed, resulting in a valid refueling scenario demonstration. This test was very repeatable, but terminal position was also somewhat depend on the calibration point. For this reason, adjustment of the refueling receptacle was sometimes necessary for correct posi-

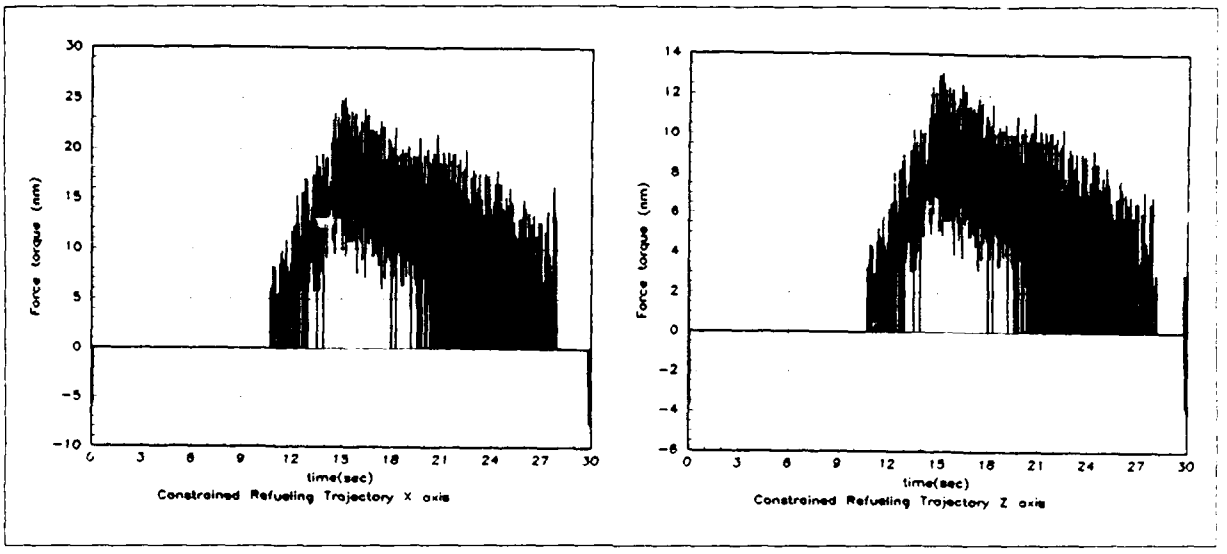

Figure 4.11. Force Torques for the constrained refueling trajectory.
Left: joint 2 Right: joint 3

tioning before constrained tests were performed. As stated earlier, this is a normal consequence of a two degree of freedom system and will be the subject of future research.

4.5 Summary

ARCADE was tested after modifications in order to establish functionality and performance improvements. Improvements in the force sensor channel provided significant sampling rate increases and better accessibility for further research. A newly developed function, cartesian trajectory generation, was tested and found acceptable, but limited in capacity. Another new development was the timing system applied to the ARCADE environment. It was tested at the hardware level and found superior to original equipment in terms of stability and flexibility of timing control.

Trajectory tracking tests were used to test the effectiveness of improvements to the control law and the environment. Results of a stationary trajectory and a

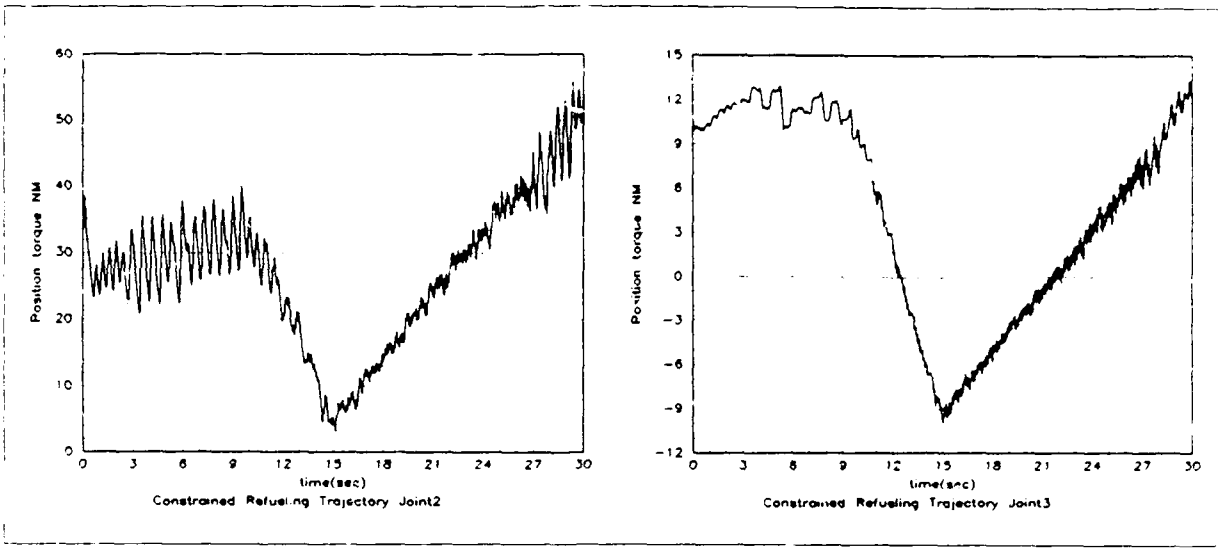

Figure 4.12. Position Torques for the constrained refueling trajectory. Left: joint 2 Right: joint 3

linear trajectory were found superior to the performance of a prior implementation. Constrained motion trajectory tests were conducted to verify the control law's ability to allow large position errors and maintain stability and tracking.

The final portion of testing was the previously untried refueling trajectory used to demonstrate compliant motion and continuous tracking applied to the task of inserting a refueling probe into a receptacle. This test was very successful in demonstrating the refueling concept and proving the applicability of the control law to this task. All phases of the operation were completed effectively. Free space tracking was acceptable and greatly improved over previous results. The cross over to constrained motion was very well damped with no oscillations or bouncing effects. Position tracking and force control during constrained motion were also very effective. Finally, sensed forces were used to adjust position in order to overcome obstacles. Such an operation had not been accomplished previously

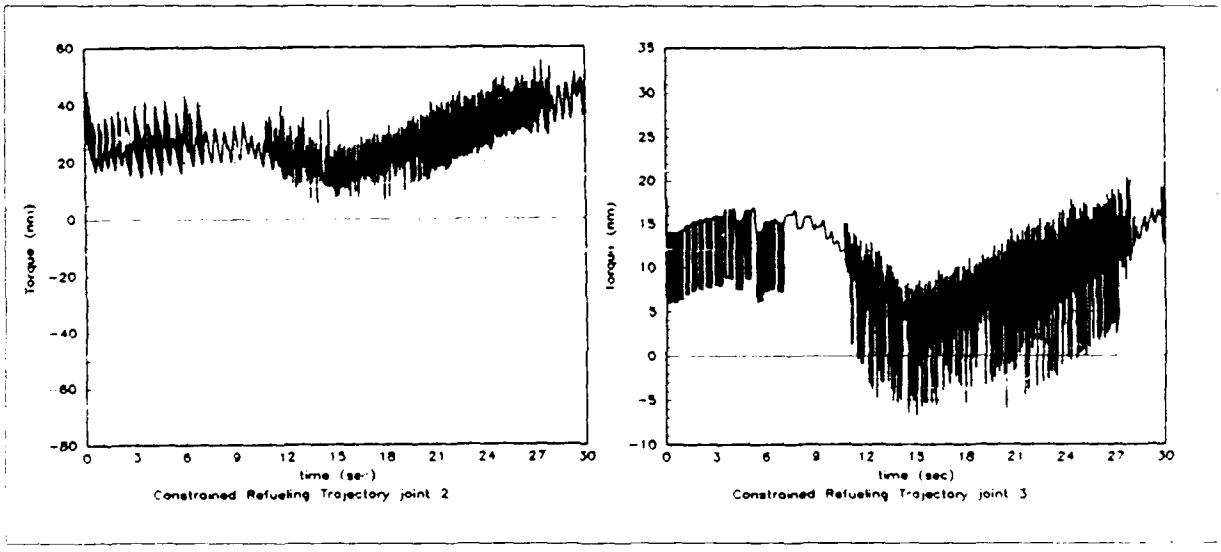

Figure 4.13. Total Torques for the constrained refueling trajectory.
Left: joint 2 Right: joint 3

V. Conclusions and Recommendations

5.1 Conclusions

The compliant motion research platform established at AFIT has been extended and improved. An impedance controller for a PUMA-560 was developed, experimentally evaluated, and then successfully applied to demonstrate a robotic refueling scenario. The refueling demonstration is significant because it is proof of concept and shows effective use of the applied technology for the specific task. The environment for evaluating compliant control with force feedback was significantly improved in three areas: accessibility, loop timing, and force sensing. The rehosting of the system and control law from assembly language to FORTRAN provides much greater accessibility for modifications or design of new algorithms. The loop timing system developed to operate the PUMA is effective for all evaluation of control laws, not just compliant motion controllers. This innovative improvement will be useful for all future tests on the PUMA test platform. The force sensor channel was rehosted to the higher level language and the sensor electronics operating system was upgraded for more flexibility. Of the many benefits derived from upgrading, one particularly useful improvement was the higher force sensor sampling rates. Force readings are now available at the same rate as control law computations. Compliant control can operate at the same servo rates as position control resulting in improved accuracy and simpler operations. Another improvement in the environment was a cartesian trajectory generator, which can produce the trajectories necessary for compliant motion research.

Velocity tracking was included in computations and proved to be effective in decreasing trajectory tracking errors. The full benefits of velocity tracking will be realized as trajectory speeds increase. Friction compensation was improved in two ways: accessibility and function. The function was improved through inclusion of viscous friction compensation, and the operation was made more accessible

through rehosting. Friction effects were not eliminated but results were improved over the previous implementation. Limitations on control law parameters were loosened by the timing system improvements providing greater selection of response characteristics and controller bandwidth for future tests.

5.2 Recommendations

This thesis effort has enhanced the compliant motion evaluation environment and provided easier access to the system. Improvements in the environment and control law implementation provided performance that culminated in a two degree of freedom, half scale refueling demonstration. Tracking performance was sufficient. Primary recommendations for most profitable approach to obtaining improved performance would include:

- expand algorithm to three degrees of freedom,
- adaptive friction compensation, and
- better selection of control law parameters.

Improvements in these areas should provide trajectory tracking results superior to those accomplished here and further the goal of successful robotic refueling of aircraft.

At least three degrees of freedom will be required to accomplish the refueling task. This is not a difficult improvement, requiring only expansion of the control law and some functions of the environment. Several of these functions have already included the third degree of freedom during development (i.e. cartesian trajectory generation). The Force sensor channel might be improved in two aspects. The calibration procedure is 'single point' and consequently may have some errors. A more comprehensive calibration procedure should be developed using multiple points and an averaging routine. Another problem in the force sensor channel is the occasional loss of communications. This effect results from transmission error

or shutdown due to sensor overload and should be eliminated in software. Finally, a force sensing limitation that is introducing significant nonlinear effect is the need to bandlimit the outputs. The reposition inaccuracies which require this limiting severly restrict force reading accuracy. A study similar to that done by Duvall and Leahy [10] but more extensive might provide operating ranges for more accurate positioning, thereby providing narrower ranges for force sensing repeatability.

The control law implementation should be examined in two areas: friction compensation and selection of parameters. Friction compensation applied in this thesis was not as effective as hoped even though improvements were observed. Poorly chosen switching parameters or inadequate knowledge of the friction levels were likely causes of this problem. The literature review covered several adaptive techniques that proved very effective under similar circumstances. The conslusion of that review was that such an adaptive approach would be effective in reducing friction effects on the PUMA. A low velocity model should be implemented with on line parameter estimation and an off line routine to determine friction coefficients of position dependence as well as velocity dependence. Another control law improvement strongly recommended is a detailed study of parameter selections. The parameters that determine the desired dynamics model are less restricted as a result of the new timing system and may yield systems providing higher performance. These parameters have been selected in previous efforts as well as this one as if the links of the robot were the same in physical characteristics. This assumption is now a point for likely performance improvements. Duvall implied an eigenvalue study was necessary to generate non-diagonal matrices for the model. More generally, a study of the complex plane activity of the control law during operation would be helpful in tuning for best stability, tracking, and force limiting.

Appendix A. *Representative Experimental Data*

This appendix contains data plots of one of the three tests performed to validate the test environment and the control law improvements. Also, the data sets for both the unconstrained and the constrained refueling tests are filed here. All plots will be displayed with only enough information to assure identification of information. Explanations are provided throughout the text as to operations repesented here. These plots are retained only for reference for future research, particularly on the development system in the AFIT Robotics Systems Laboratory.

The block diagram of the control system is repeated here with points indicated for the source of different plots shown in this appendix.

Test data from the constrained linear trajectory will be presented first, then the unconstrained refueling results, and finally the constrained refueling results. The data files will be presented as follows:

- Cartesian position.
- Cartesian position error.
- Interface force.
- Interface moments.
- Position torques.
- Velocity torques.
- Total torques.
- Force torques.
- Friction torques.
- Joint velocities.
- Raw force values.

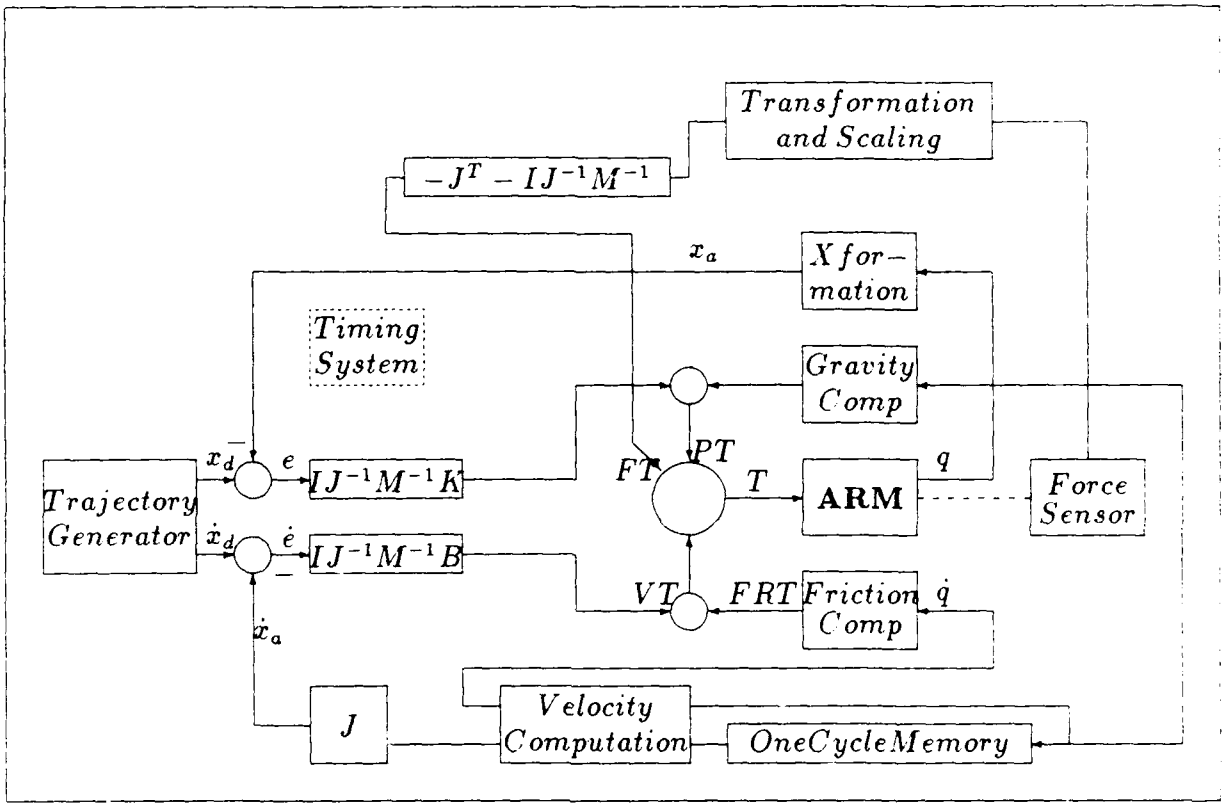

Figure A.1. Control System in Block Diagram Form. System includes the Control Law and Parts of the Environment. All node inputs are summations except where indicated as subtractions.

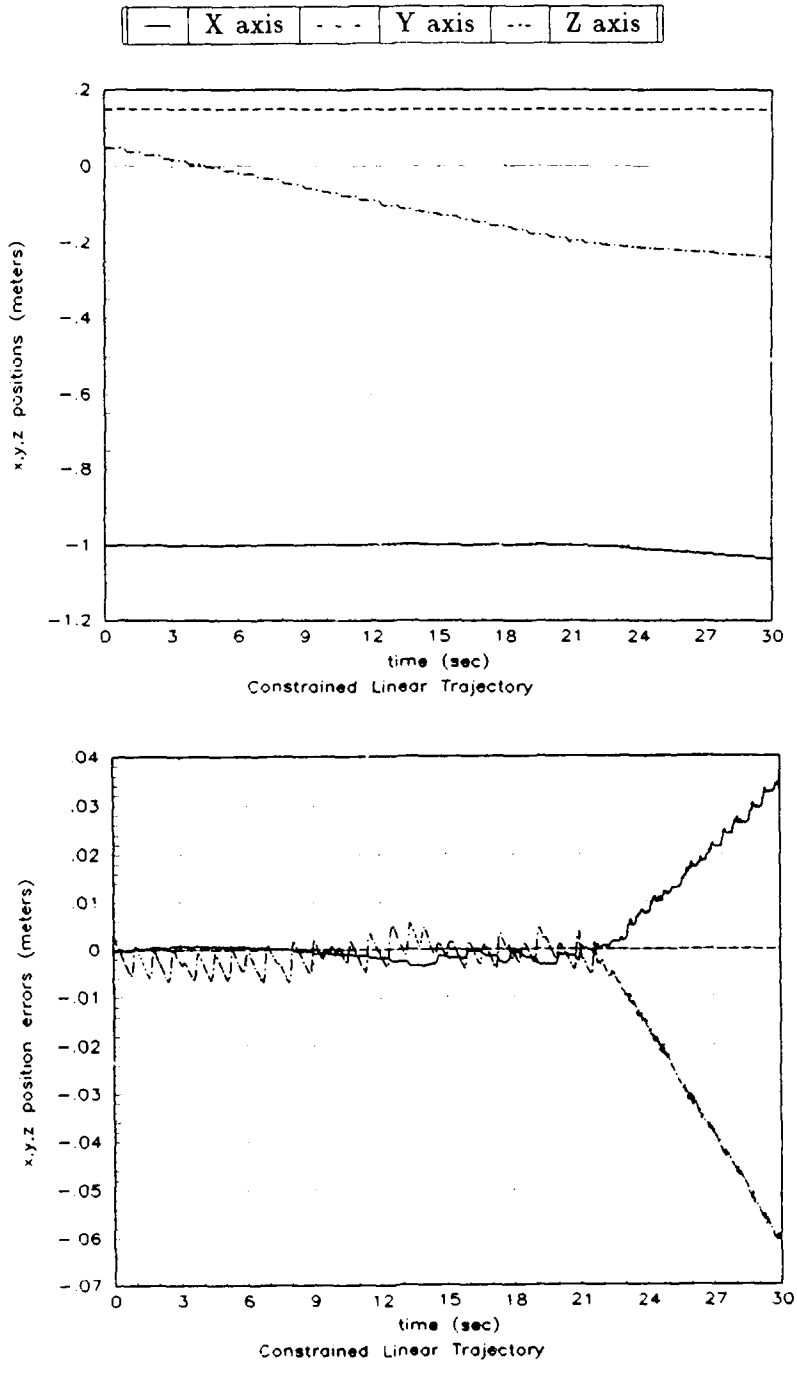

Figure A.2. Constrained Linear Trajectory
Top:Cartesian Position
Bottom: Cartesian Position Error

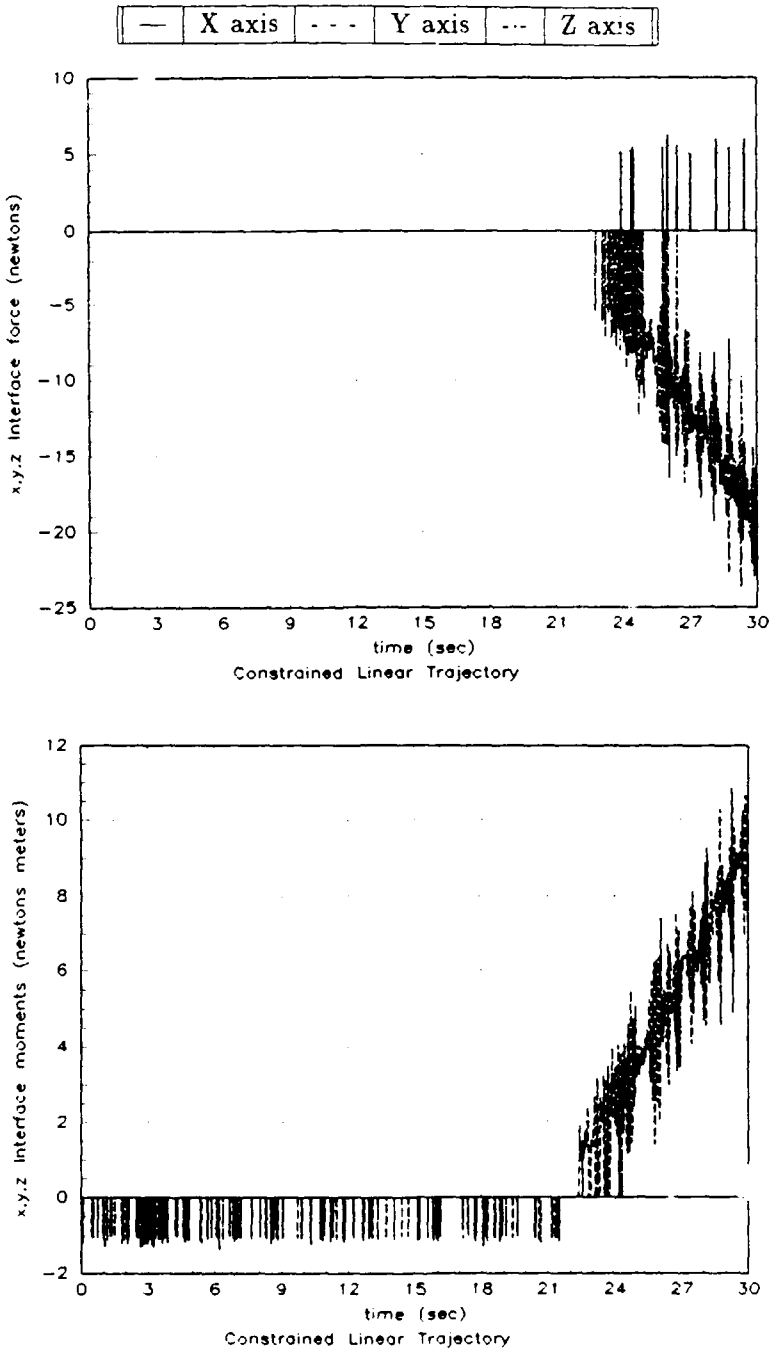

Figure A.3. Constrained Linear Trajectory
Top: Interface Forces
Bottom: Interface Moments

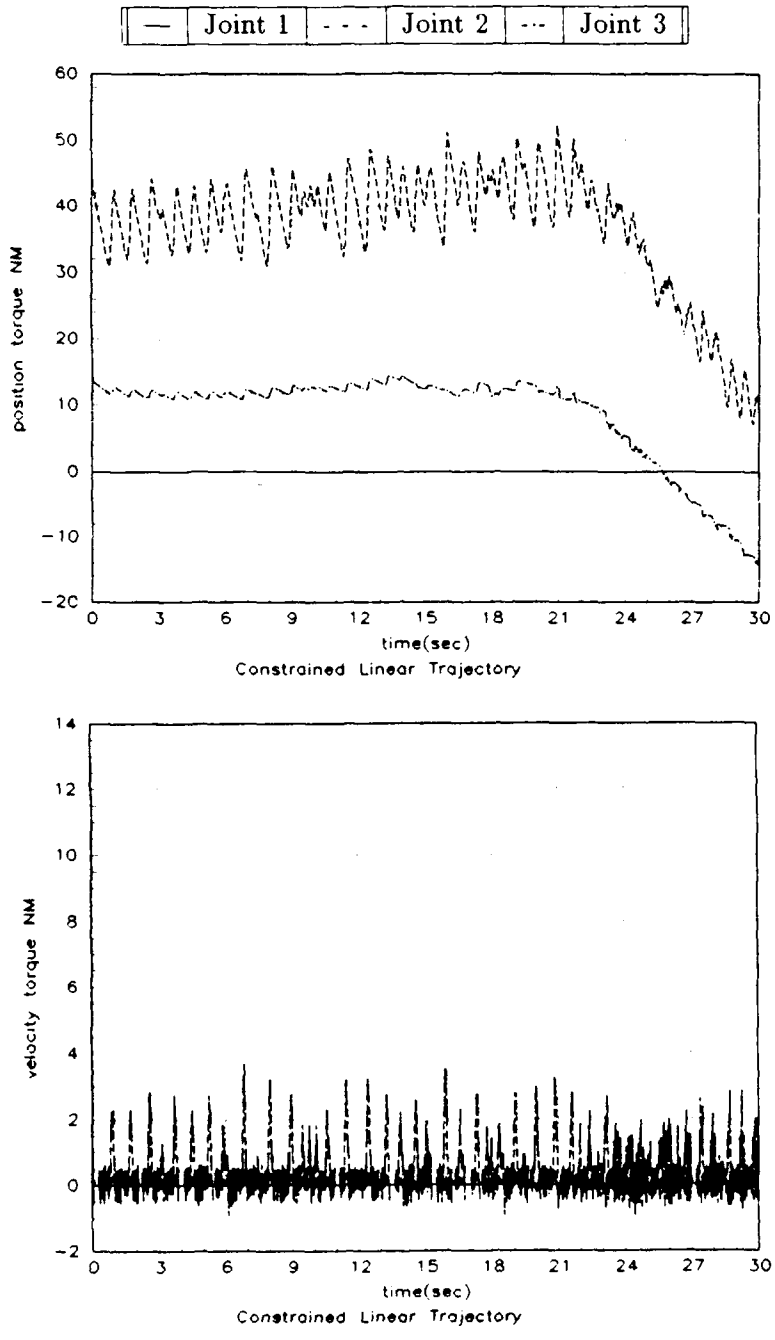

Figure A.4. Constrained Linear Trajectory
Top: Position torques
Bottom: Velocity torques

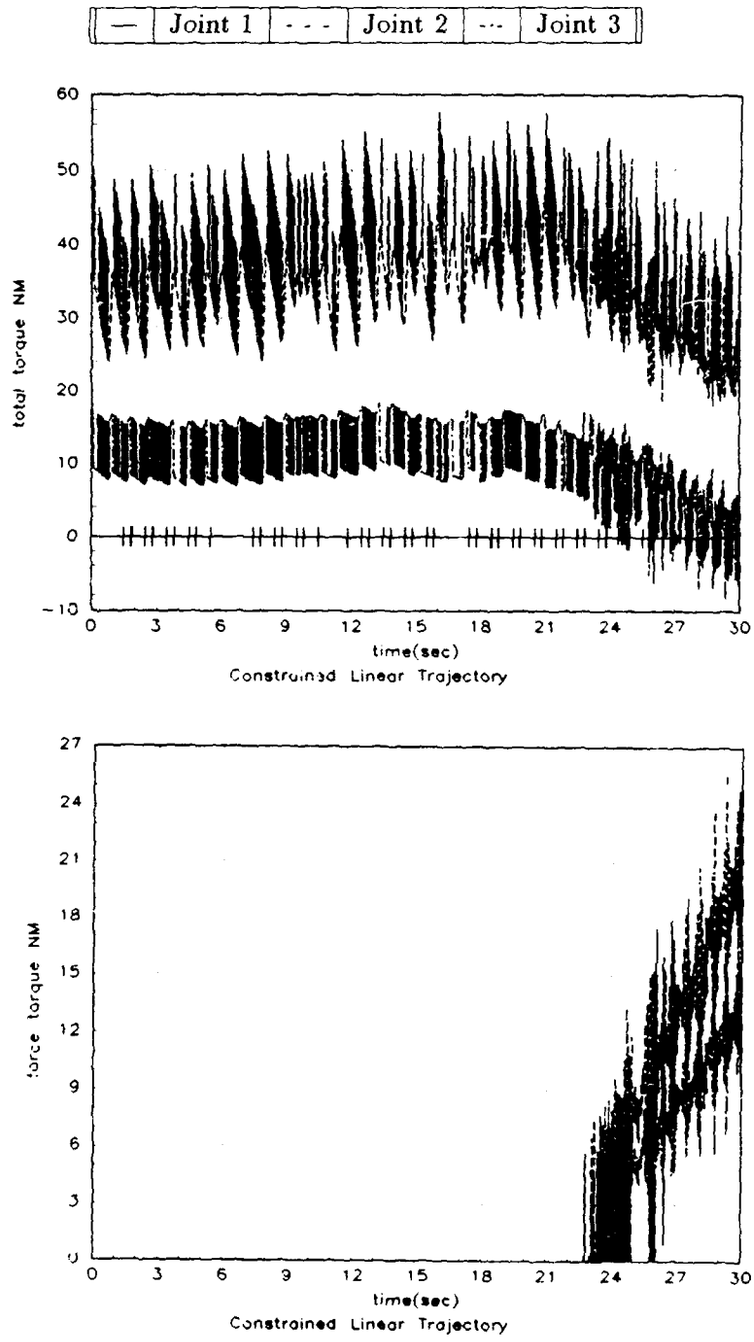

Figure A.5. Constrained Linear Trajectory
Top: Total torques
Bottom: Force torques

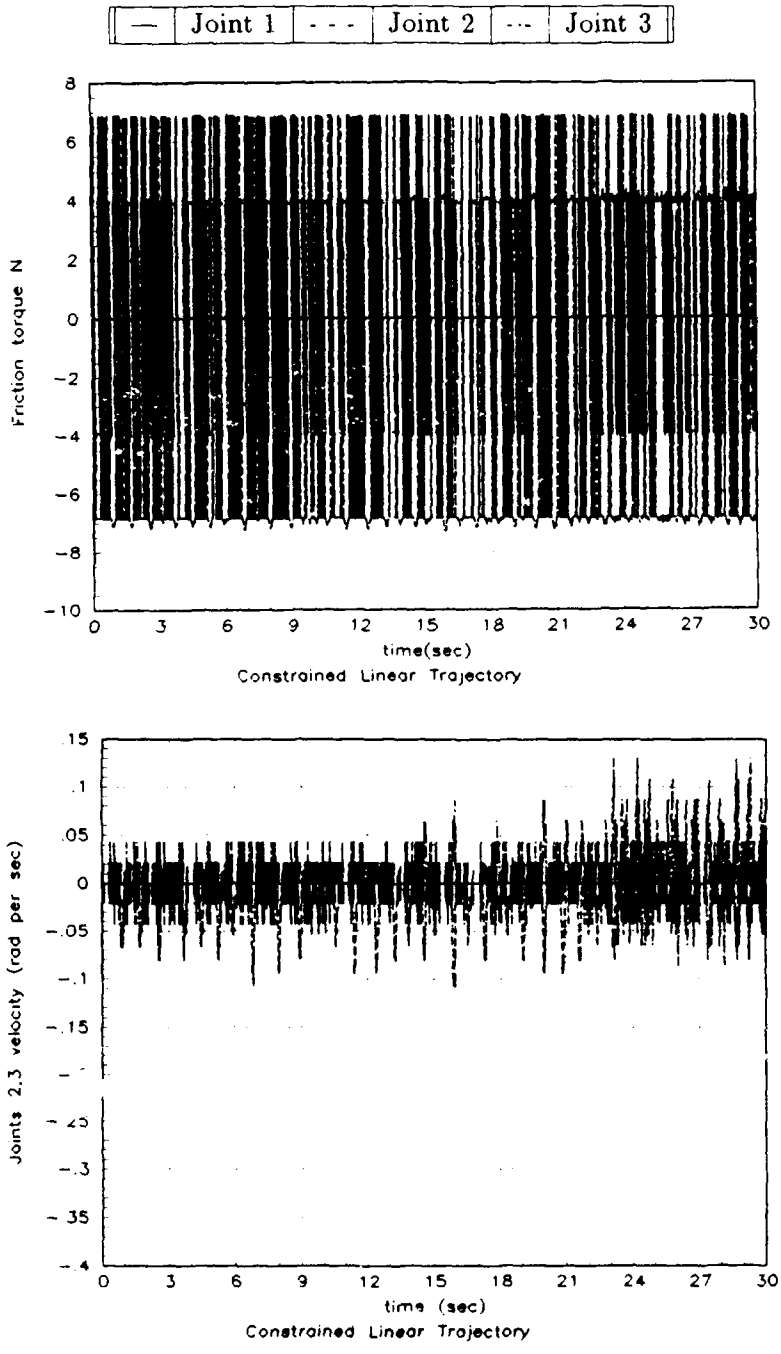

Figure A.6 Constrained Linear Trajectory
Top: Friction torques
Bottom: Joint velocities

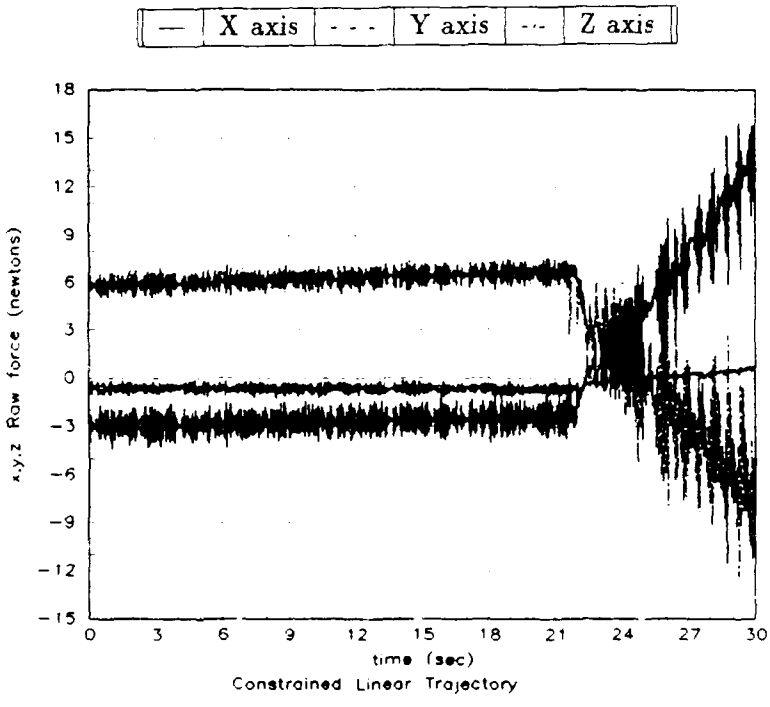

Figure A.7. Constrained Linear Trajectory, Raw Force Readings

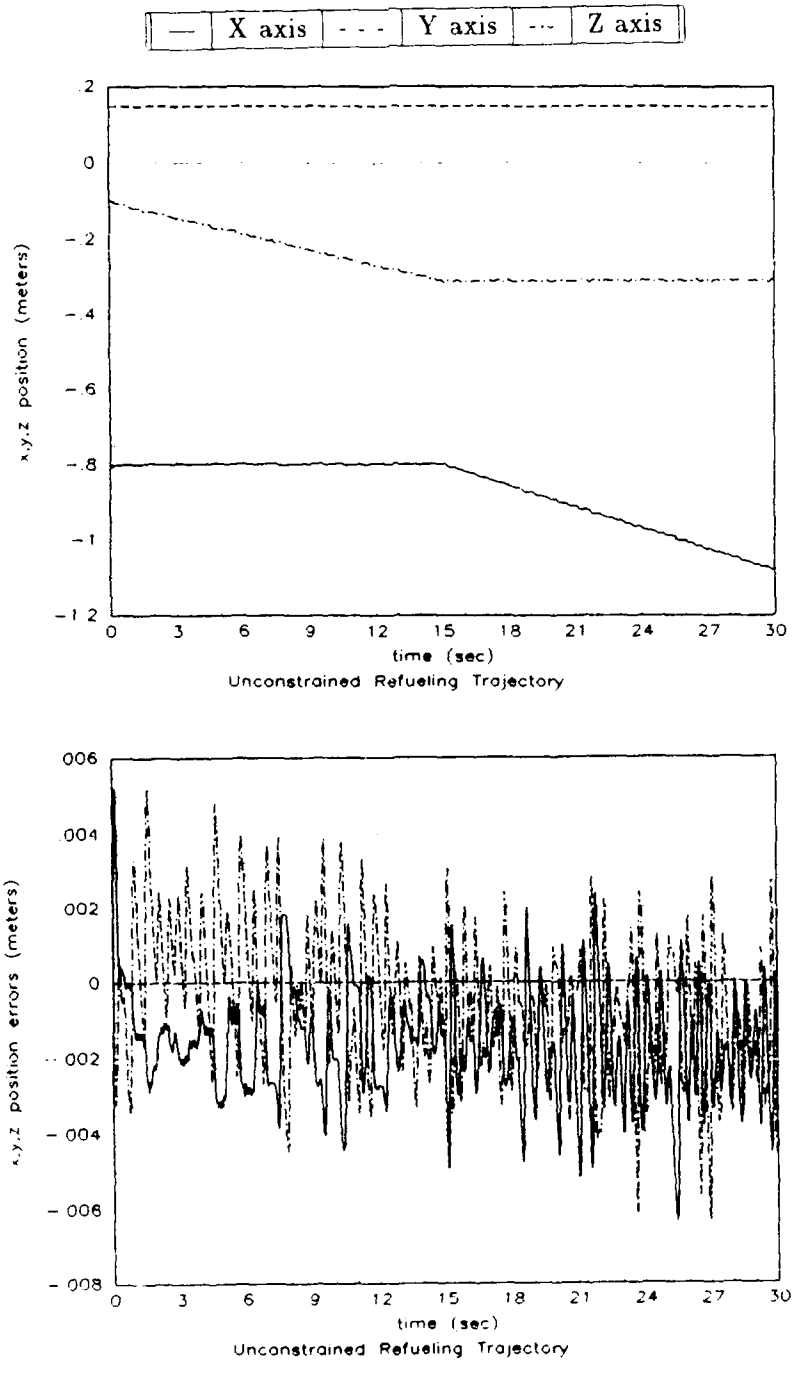

Figure A.8. Unconstrained Refueling Trajectory
Top:Cartesian Position
Bottom: Cartesian Position Error

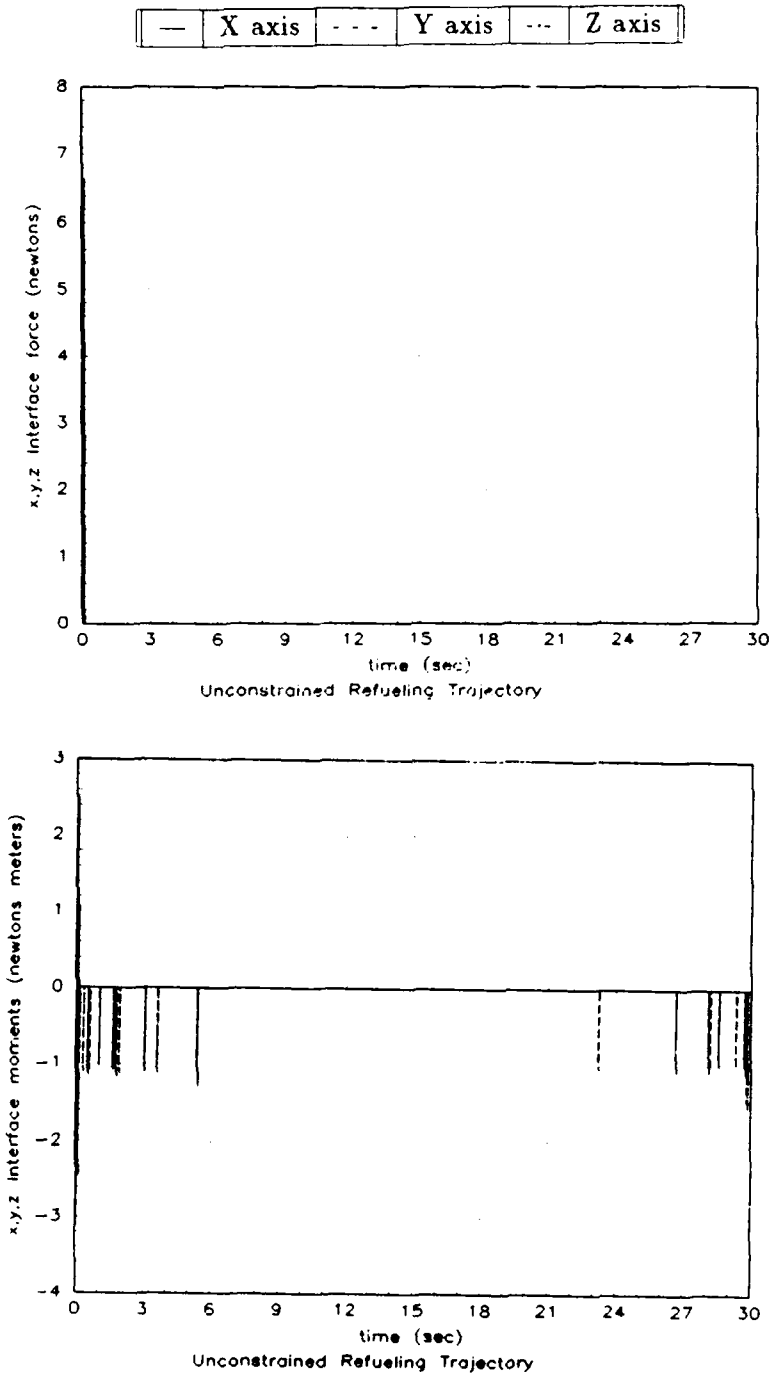

Figure A.9. Unconstrained Refueling Trajectory
Top: Interface Forces
Bottom: Interface Moments

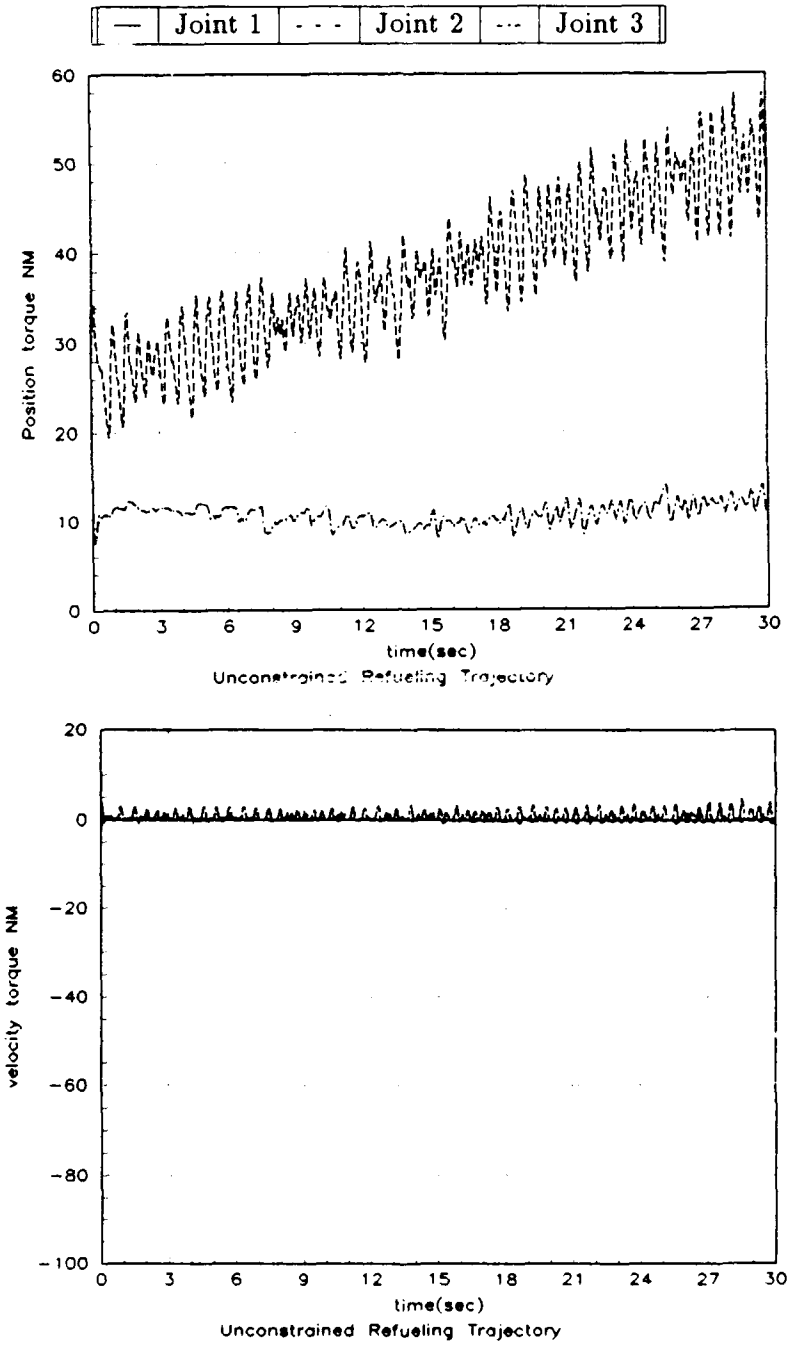

Figure A.10. Unconstrained Refueling Trajectory
Top: Position torques
Bottom: Velocity torques

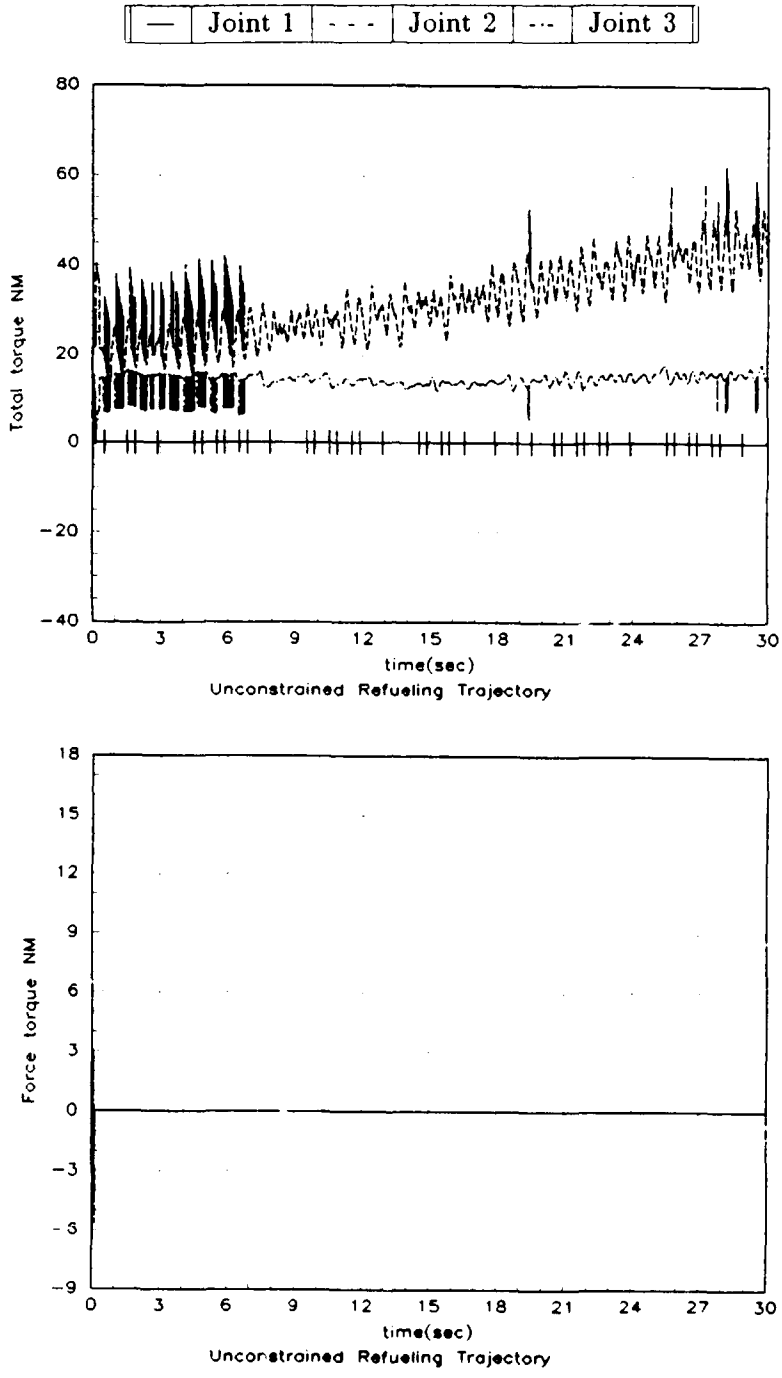

Figure A.11. Unconstrained Refueling Trajectory
Top: Total torques
Bottom: Force torques

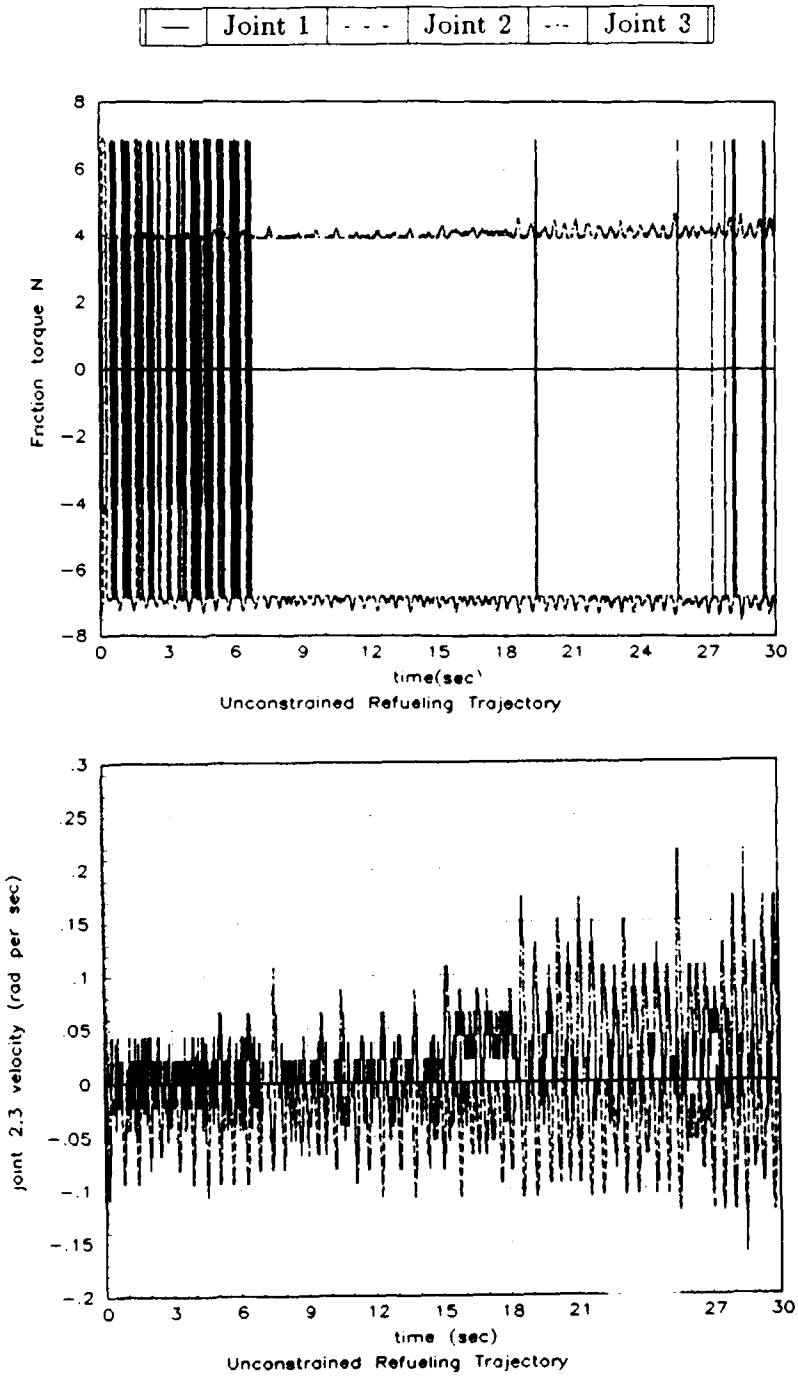

Figure A.12. Unconstrained Refueling Trajectory
Top: Friction torques
Bottom: Joint velocities

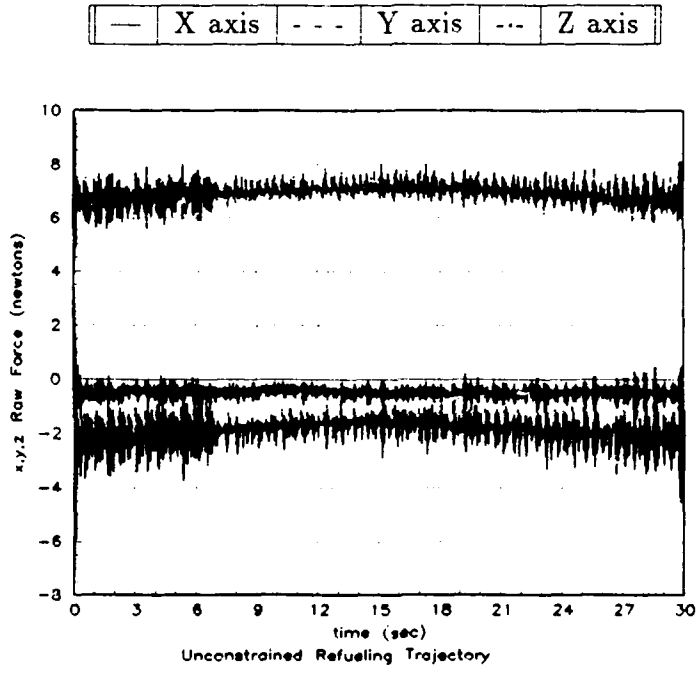

Figure A.13. Unconstrained Refueling Trajectory, Raw Force Readings

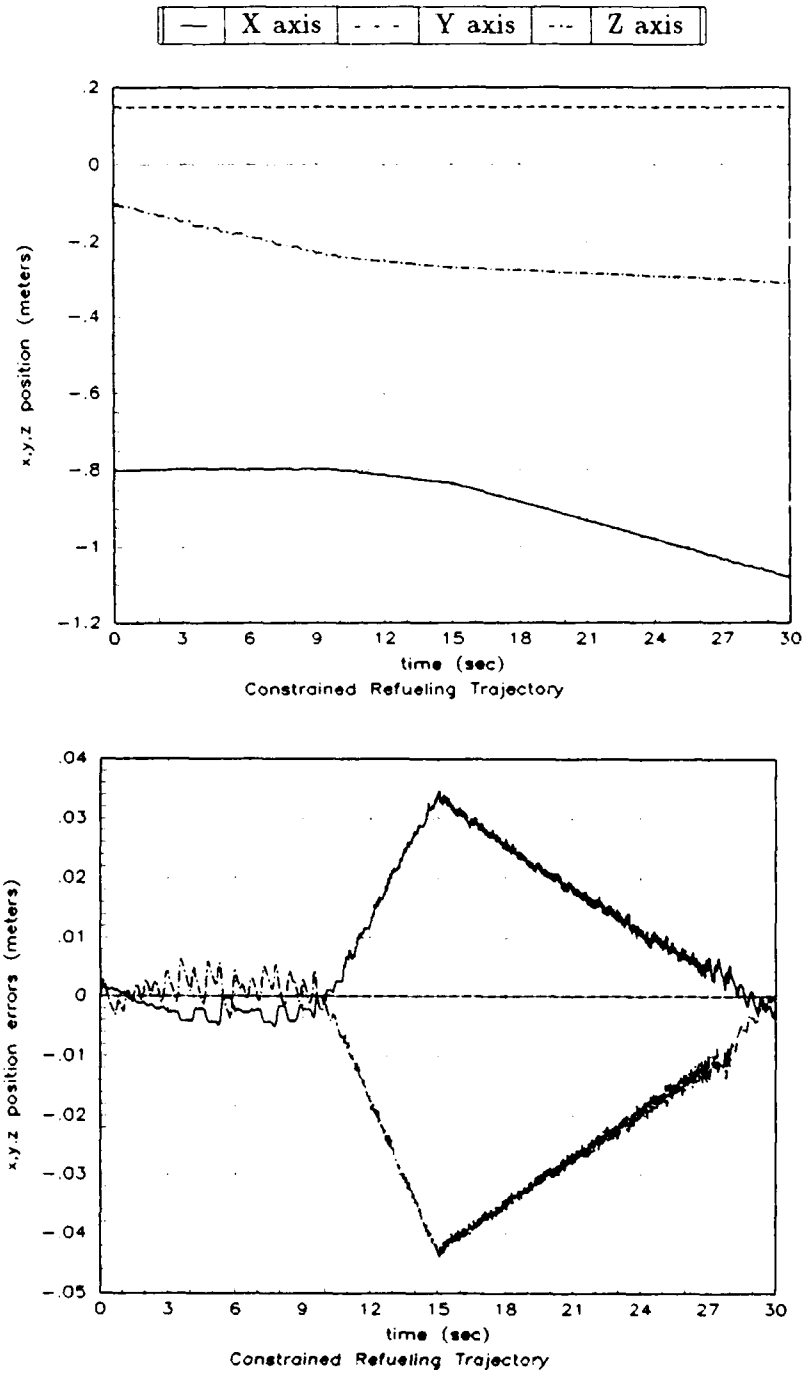

Figure A.14. Constrained Refueling Trajectory
Top:Cartesian Position
Bottom: Cartesian Position Error

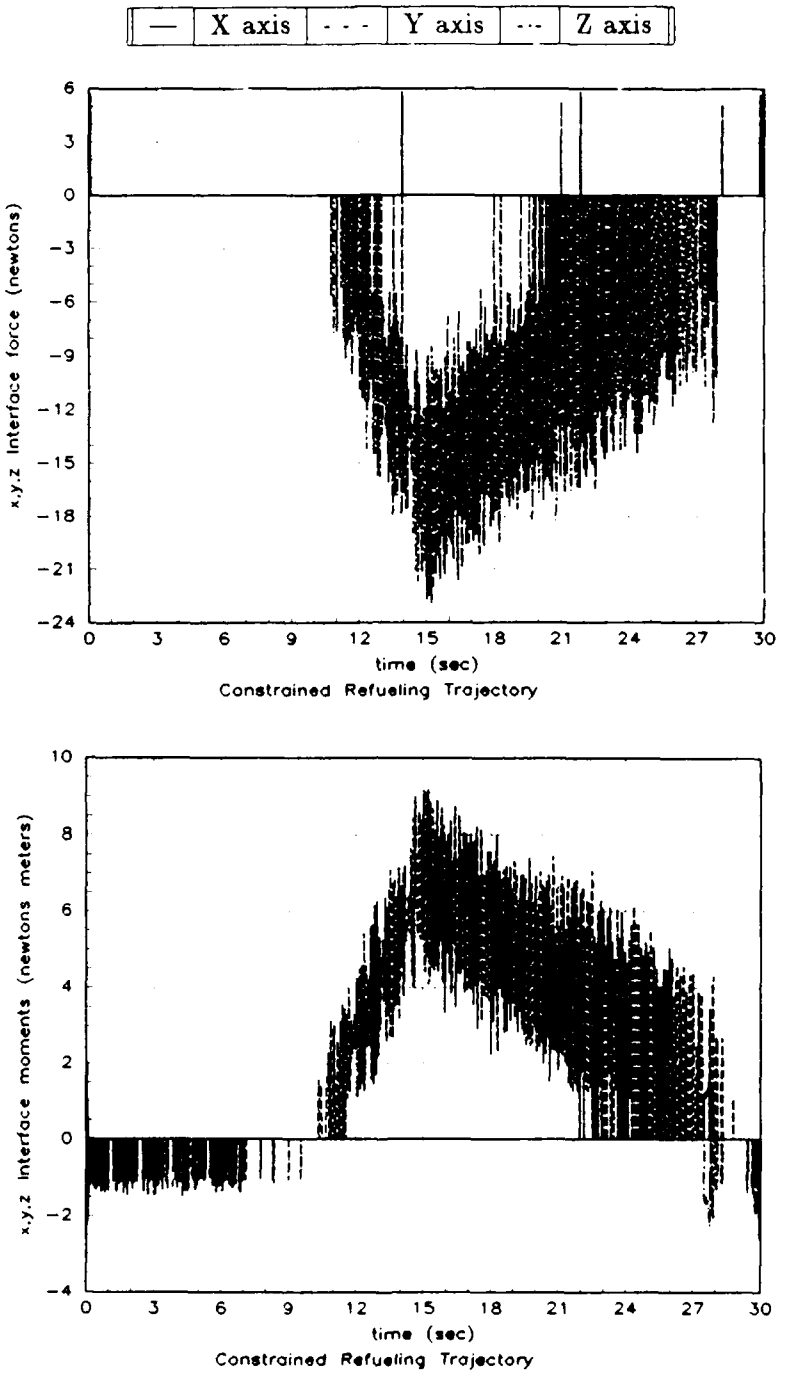

Figure A.15. Constrained Refueling Trajectory
Top: Interface Forces
Bottom: Interface Moments

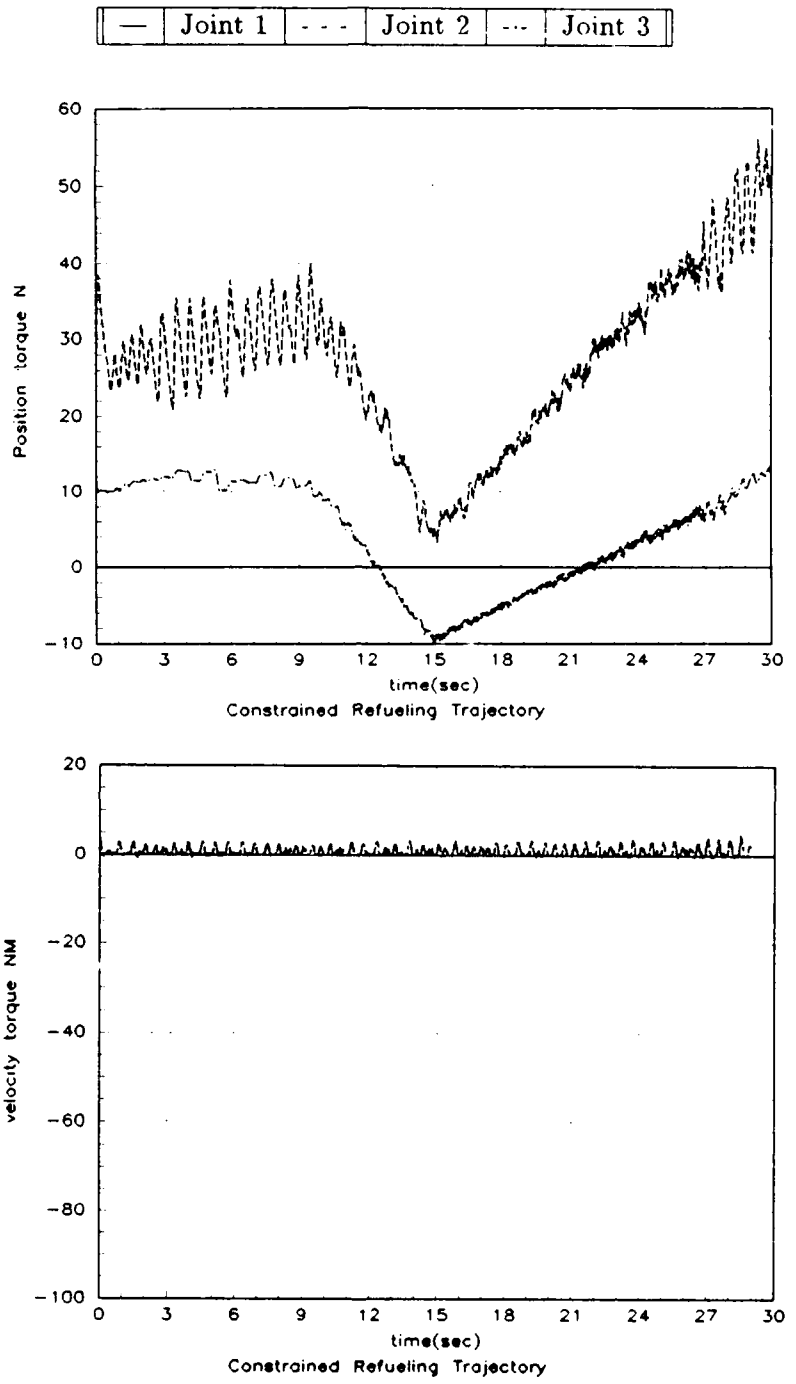

Figure A.16. Constrained Refueling Trajectory
Top: Position torques
Bottom: Velocity torques

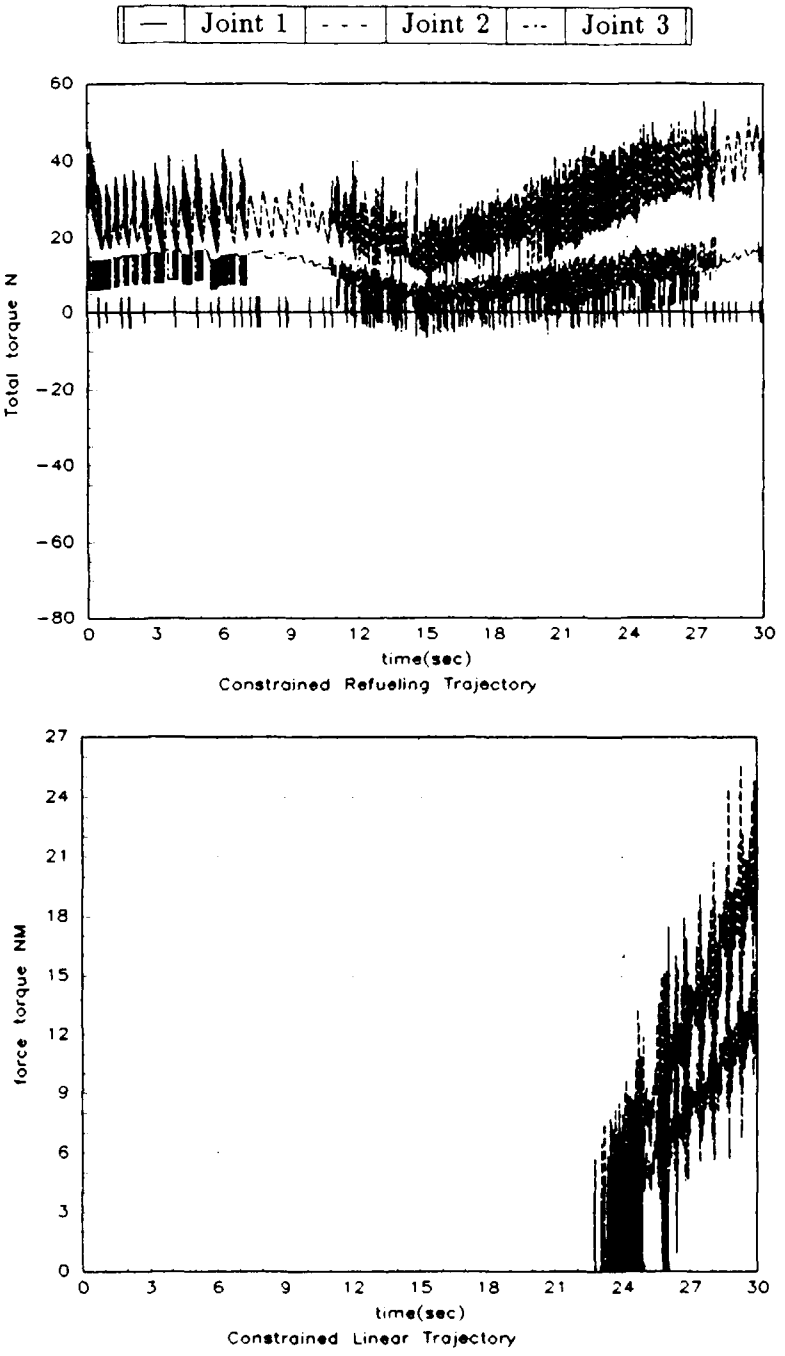

Figure A.17. Constrained Refueling Trajectory
Top: Total torques
Bottom: Force torques

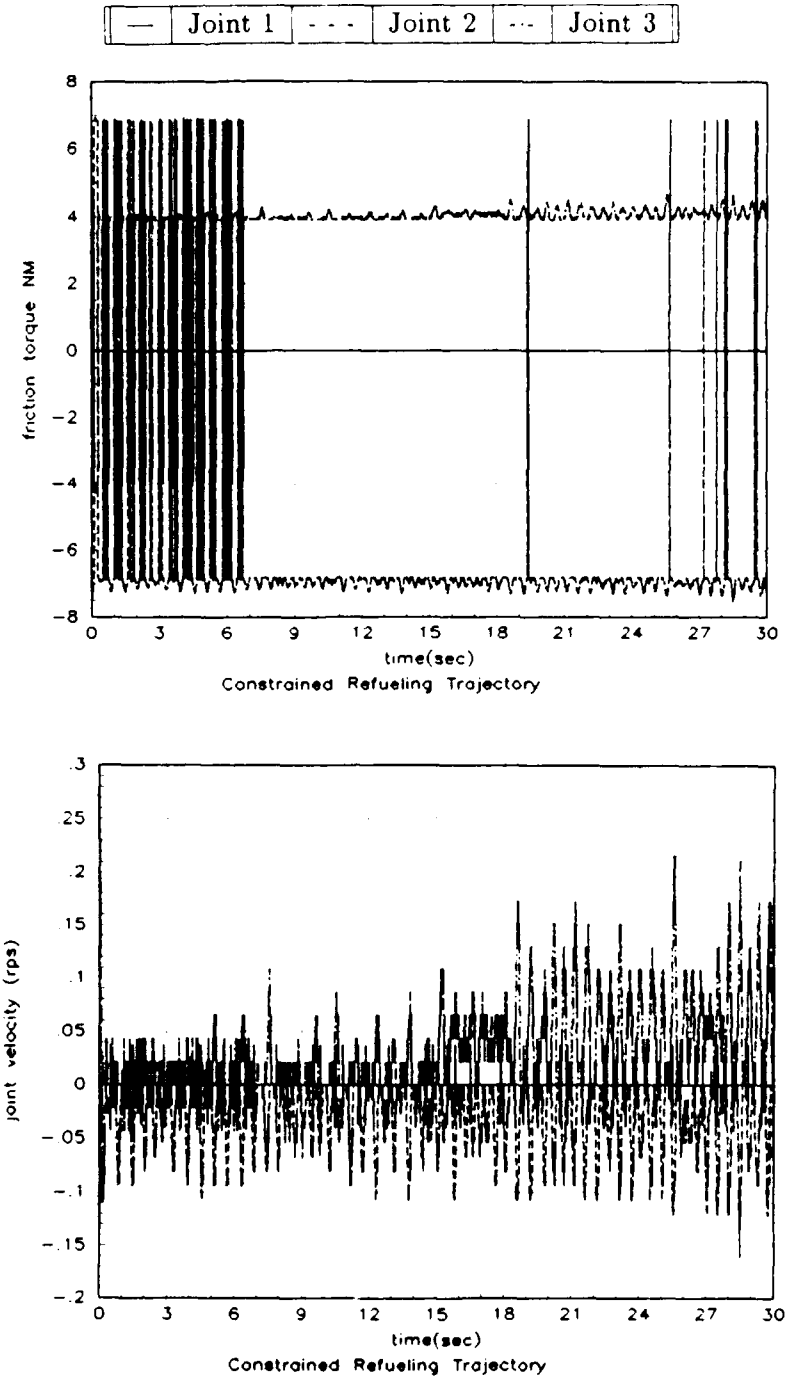

Figure A.18. Constrained Refueling Trajectory
Top: Friction torques
Bottom: Joint velocities

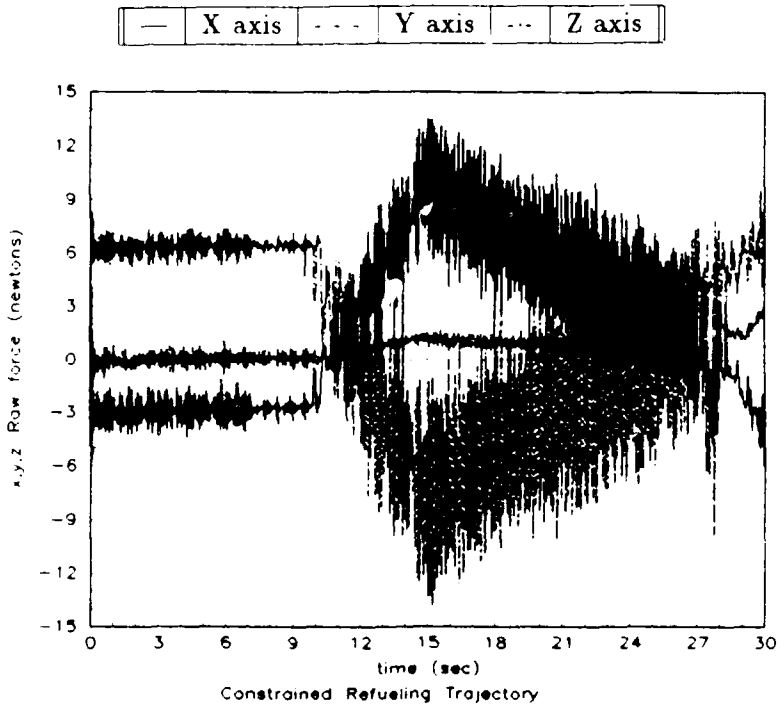

Figure A.19. Constrained Refueling Trajectory, Raw Force Readings

Bibliography

1. An, C.H. and J.M. Hollerbach. "Dynamic Stability Issues in Force Control of Manipulators,"*Proceedings of the 1987 IEEE International Conference on Robotics and Automation.* Vol 2, pp.890-896,1987.
2. An, C.H. and J.M. Hollerbach. "Kinematic Stability Issues in force control of manipulators," *Proc. IEEE Int. Conf. Robotics and Automation*, Raleigh, March 30-April 3, 1987.
3. Anderson R. J. and M. W. Spong, "Hybrid Impedance Control of Robotic Manipulators", *IFEE Journal of Robotics and Automation*, Vol. 4, No. 5, pp 549-556, October 1988.
4. Armstrong, B., "Friction: Experimental Determination, Modeling and Compensation," *Proceedings of the 1988 IEEE International Conference on Robotics and Automation*, Vol 3, pp. 1422-1427, 1988.
5. Battelle Corp., *Concept Development for Robotic Aircraft Turnaround: Final Task II Report*, Columbus OH: Battelle Columbus Laboratories, 1989.
6. Canadus, C., K.J. Astrom and K. Braun(1986) "Adaptive Friction Compensation in DC Motor Drives", *IEEE Journal of Robotics and Automation*, vol. RA-3, no. 6, Dec 1987
7. Canudas De Wit, C., et.al., "Adaptive Friction Compensation in Robot Manipulators: Low-Velocities", *proceedings of the 1989 IEEE International Conference on Robotics and Automation*, Vol 3, pp.1352-1357, 1989.
8. D'Azzo, J.J., and C.H. Houpis. *Linear Control System Analysis and Design, Conventional and Modern.* New York:McGraw-Hill Book Company, 1981.
9. De. Schutter, J. "Improved Force Control Laws for Advanced Tracking Applications," *Proceedings of the 1988 IEEE International Conference on Decision and Control.* Vol 2, pp. 1497-1502, 1988.
10. Duvall, D.J. *Robotic Compliant Motion Control for Aircraft Refueling Applications.* AFIT/GA/ENG/88D-1 Air Force Institute of Technology, Air University, December 1988.
11. Duvall, D.J. *Source Code Listing for Initial Implementation of a Compliant Motion Control Enviroment and Impedance Controller.* Internal Report AFSRL No. 3. AFIT Robotic Systems Laboratory, Dept. of Electrical Engineering, Air Force Institute of Technology, Wright-Patterson AFB OH, December 1988.
12. Fu,King-Sun,R.C. Gonzalez, and C.S.G. Lee. *Robotics: Control, Sensing, Vision, and Intelligence.* New York: McGraw-Hill Book Company, 1987.
13. Gilbart J.W. and G.C. Winston. "Adaptive Compensation for an Optical Tracking Telescope"/ Automatica, Vol.10, pp , 125-131,1974

14. Gogoussis, A. and M.Donath, "Coulomb Friction Joint and Drive Effects in Robot Mechanisms," *Proc. of the 1987 Inter. Conf. on Robotics and Automation*, Raleigh: IEEE, 1987(March 31-April 3).

15. Hogan, N. "Impedance Control: An Approach to Manipulation. Part I - Theory," *ASME Journal of Dynamic Systems, Measurement, and Control*, Vol 107, pp. 1-7, March 1985.

16. Hogan, N. "Impedance Control: An Approach to Manipulation, Part II - Implementation," *ASME Journal of Dynamic Systems, Measurement, and Control*, Vol 107 pp. 8-16, March 1985.

17. Hogan, N. "Impedance Control: An Approach to Manipulation, Part III - Applications," *ASME Journal of Dynamic Systems, Measurement, and Control*, Vol 107 pp. 17-24, March 1985.

18. Hogan, N., "Stable Execution of Contact Tasks Using Impedance Control," *Proceedings of the 1987 IEEE International Conference on Robotics and Automation*. Vol 2, pp.1047-1054, 1987.

19. Houpis, C.H. and G.B. Lamont. *Digital Control Systems*. New York:McGraw-Hill Book Company, 1985.

20. Ishikawa, H., et.al. "Stable Compliance and Its Implementation for a 6 D.O.F. Manipulator," *Proceedings of the 1989 IEEE International Conference on Robotics and Automation*. Vol 1, pp. 98-103, 1989.

21. JR3 Inc. *Universal Force-Moment Sensor System Operation Manual*. JR3,Inc, Woodland,CA, July 1988.

22. Kelly, R., et.al., "On Adaptive Impedance Control of Robot Manipulator", *1989 IEEE Conference on Robotics and Automation*, Vol. 1, pp 572-577,1989.

23. Lawrence, D.A., "Actuator Limitations on Achievable Manipulator Impedance," *1989 IEEE Conference on Robotics and Automation*, Vol. 1 pp. 560-565

24. Leahy, M.B. Jr. *Performance Characterization of a PUMA 600 Robot*. Internal Report No. RAL-56. Robotics and Automation Laboratory, Dept of Elecrical, Computer and Systems Engineering, Rensselaer Polytechnic Institute, Troy NY, May 1985.

25. Leahy, M.B. Jr. *The RAL Hierarchial Control System User's Guide, Version 1.0*. Internal Report No. RAL-67. Robotics and Automation Laboratory, Dept of Electrical, Computer and Systems Engineering, Rensselarer Polytechnic Institute, Troy NY, April, 1986.

26. Leahy, M.B. Jr., *Private Communications*, AFIT, April, 1989.

Department of Electrical and Computer Engineering, Air Force Institute of Technology, Wright-Patterson AFB, OH., July 1989.

28. Leahy, M.B. and G.N.Saridis, "Compensation of Industrial Manipulator Dynamics" *The International Journal of Robotics Research*,Vol 8, No. 4, pp. 73-84,August 1989.

29. Leahy, M.B. Jr. and K. P. Valvanis, *Dynamics Based Control of Robotic Manipulators* Unpublished paper provided in class notes of EENG 534, Fall 1989. Air Force Institute of Technology.

30. Leahy, M.B. Jr., *The RAL Real-Time Robotic Algorithm Exerciser User's Guide, Version 1.0.* Internal Report No. RAL-61. Robotics and Automation Laboratory, Dept of Electrical, Computer and Systems Engineering, Rensselaer Polytechnic Institute, Troy NY, November 1985.

31. Mei-Hua Liu, et.al., "Dynamic and Adaptive Force Controllers for Robotic Manipulators", *Proceedings of the 1988 IEEE International Conference on Decision and Control.* Vol 2, pp 1478-1483, 1988.

32. Niemeyer, G. and Slotine,J.J.E., *1989 IEEE Conference on Robotics and Automation*, Vol. 1 pp 566-571, 1989

33. Paul, R.P. "Problems and Research Issues Associated with the Hybrid Control of Force and Displacement," *Proceedings of the 1987 IEEE International Conference on Robotics and Automation.* Vol 3, pp. 1966 1971, 1987.

34. Raibert, M. H. and J. J. Craig. "Hybrid Position/Force Control of Manipulators," *ASME Journal of Dynamic Systems, Measurement and Control*, Vol. 102, pp. 126-133, June 1981.

35. Salisbury, J.K.,Jr. "Active Stiffness Control of a Manipulator in Cartesian Coordinates," *Proceedings of the 19th IEEE Conference on Decision and Control*, Vol 1, pp. 95-100, 1980.

36. Sharon, A., N. Hogan, D.E. Hardt, *1989 IEEE Conference on Robotics and Automation*, Vol. 1 pp 552-559, 1989

37. Shipman, R. P., *Visual Servoing for Autonomous Aircraft Refueling.* AFIT/GE/ENG/89D-48 Air Force Institute of Technology, Air University, December 1989.

38. Townsend, W.T. and J.K. Salisbury. "The Effect of Coulomb Friction and Stiction on Force Control" *Proceedings of the 1987 IEEE International Conference on Robotics and Automation*, Vol 2, pp. 883-889, 1987.

39. Tustin, A., "The Effects of Backlash and of Speed-Dependent Friction on the Stability of Closed-Cycle Control Systems." *Journal of the Institution of Electrical Engineers*, 94(2A):143-51, 1947.

40. Walrath, C.D. "Adaptive Bearing Friction Compensation Based on Recent Knowledge of Dynamic Friction". Automatica, Vol. 20,No. 6, pp.717-727, 1984.

41. Whitney, D.E. "Historical Perspective and State of the Art in Robot Force Control," *The International Journal of Robotics Research*, Vol 6, No. 1, pp. 3–13 (Spring 1987).

42 Wlassich J J., "Nonlinear Force Feedback Impedance Control", Master of Science Thesis, M.I.T., Mechanical Engineering Department, February 1986.

Vita

Capt Vernon W. Milholen [redacted]

He grew up near Hot Springs Arkansas, and graduated from Lake Hamilton High School in 1970. He entered the United States Air Force in 1972 and served his country with pride in many different locations. In December 1984, he graduated from the University of Arkansas with a Bachelor of Science degree in Electrical Engineering. On 27 April 1985, after attending Officer Training School, he was commissioned in the United States Air Force and assigned to Holloman AFB, NM as an instrumentation design engineer for the Central Inertial Guidance Test Facility. In May 1988, he entered AFIT enrolled in the School of Engineering, Department of Electrical and Computer Engineering. In Februray 1973 he married Vivian Lynn Hignight. They now have two children, Matthew and Traci.

[redacted]